TÉCNICO LISBOA

Understanding NH_3 emissions over a three-way catalyst in lean/rich conditions.

Tiago Casinhas Ribeiro

Thesis to obtain the Master of Science Degree in

Chemical Engineering

Supervisor(s): Dr. David Berthout (IFPEN)
Prof. Maria Filipa Gomes Ribeiro (IST)

Examination Committee

Chairperson: Prof. Sebastião Manuel Tavares Silva Alves (IST)

Supervisor: Prof. Maria Filipa Gomes Ribeiro (IST)

Member of the Committee: Prof. Carlos Manuel Faria de Barros Henriques (IST)

December 2015

This work was performed in collaboration with

"*The results of these labours will, I trust, be useful to the cause of science, by proving that even the most apparently abstract philosophical truths may be connected with applications to the common wants and purposes of life.*

The gratification of the love of knowledge is delightful to every refined mind; but a much higher motive is offered in indulging it, when that knowledge is felt to be practical power, and when that power may be applied to lessen the miseries or increase the comforts of our fellow-creatures."

Sir Humphry Davy

Acknowledgments

The work here present was not possible without the help and support of many people to whom I would like to leave a word of acknowledgement.

I would like to express my deep appreciation to Dr. David Berthout, for his expert advice, constant guidance and very much needed help. Under his supervision I learned a lot during the length of my entire internship and I hope to be able to carry that with me. I also wish to leave a word of thanks to all the people of R10-05 department, at IFPEN, for their warm reception.

I would also like to give a special thanks to Prof. Filipa Ribeiro, first for providing the link that made this internship possible and secondly for her constant advice and technical supervision of this work.

A kind thanks to Joana Fernandes, Vitor Costa and Luís Oliveira for their logistic support and their help in solving my most diverse problems.

To my fellow Portuguese interns, I could have not chosen better people with whom I would have liked to share this adventure, thank you for everything. I will deeply cherish our moments together. Also, to all my friends in Lyon, the old and the new ones, thank you for making this city a home in my heart.

Finally, I would like to say thanks to all my family and friends, who always support and help me despite the amount of mistakes I make, without you nothing of this would have been possible. In particularly, a special thanks to my mother for giving me the best role model I could hope for and make me always aspire to be better than my yesterday's self.

Resumo

Os actuais sistemas de escape dos motores a gasolina encontram-se a atingir o máximo das suas potencialidades e é expectável que, com futuras regulamentações, o actual sistema não seja capaz de cumprir os padrões exigidos. Motores de ignição por faísca com injecção directa, operados em condições pobres, têm um potencial significativo para aumentar a eficiência do motor e reduzir as emissões dos gases de estufa. Contudo, a redução dos NO_x em condições pobres ainda apresenta sérios desafios. Actualmente, o objectivo é adicionar aos veículos a gasolina tecnologia já utilizada em sistemas de escape de veículos a diesel.

Para compreender o papel que o catalisador de três-vias pode ter em sistemas de escape foi utilizada modelação matemática para descrever a cinética das reacções e o transporte de fenómenos. Uma primeira abordagem foi apresentada para aplicações em controlo e simulações em tempo real, onde um modelo com poucas dimensões, desenvolvido pelo IFPEN, foi usado como base para melhorar o esquema cinético. Este modelo foi, posteriormente, calibrado com resultados experimentais. Em seguida, uma segunda abordagem foi tomada para construir um modelo que pudesse incorporar a resistência à transferência de massa da fase gasosa para o catalisador. Apesar da modelação de reactores monolíticos que negligenciam a difusão de massa obter resultados satisfatórios, ainda existe interesse nestes fenómenos visto permitir a optimização na arquitectura destes dispositivos.

Os modelos foram capazes de prever os resultados experimentais. Contudo, a necessidade de validar as funcionalidades acrescidas não pode ser esquecida e deve ser realizada subsequentemente.

Palavras-chave: Catalisador de Três-Vias, Amoníaco, Catálise, Modelação, Transporte de Fenómenos, Cinética de Reacções

Abstract

Current gasoline burn engines' exhaust systems are reaching their full potential and it is expected that, with future regulations, the current design will not be able to meet with the required standards. Lean burn spark ignition direct injection (SIDI) engines offers significant potential for improving engine efficiency and reducing greenhouse gas emissions. However, NO_x reduction in lean burn SIDI engines still presents serious challenges. Current drive is to add, to gasoline burn vehicles, technology already applied in diesel burn engines' exhaust system (as lean NO_x traps (LNT) or selective catalytic reductions (SCR)).

To have a better understanding on the, current and future, role that the three-way catalyst (TWC) might have in the exhaust systems, mathematical modelling was performed on two topics: reaction kinetics and transport phenomena. A first approach was presented with use for control and real time simulations, where a low-dimension model, developed by IFPEN, was taken as base to add complexity to the kinetic scheme. Afterwards, this model was tuned with experimental data. Following that, a second approach was carried out to build a model that might incorporate mass resistance transfer, from the gas phase to and inside the washcoat. While modelling monolithic exhaust after-treatment reactors neglecting mass diffusion has achieved satisfactory results, interest in these phenomena still exists since enables optimization in the exhaust devices architecture.

These models were able to predict the experimental data available. Nonetheless, the need to validate added functionalities with empirical tests cannot be obviated and should be subsequently performed.

Keywords: Three-Way Catalyst, Ammonia, Catalysis, Modelling, Phenomena Transport, Reaction Kinetics

Contents

List of Tables

List of Figures

Nomenclature

Roman symbols

$\dot{m}$	mass flow rate
$\vec{a}$	acceleration vector
A	pre-exponential factor
C	species molar concentration
c_p	thermal capacity at constant pressure
c_v	thermal capacity at constant volume
D	diffusion coefficient
d	hydraulic diameter of a monolith cell
$E(t)$	residence time distribution
Ea	activation energy
$F(t)$	cumulative distribution function
G	inhibition term
Gz	Graetz number
h	transfer coefficient
h'	specific enthalpy
I	identity matrix
K	inhibition constants
k	rate constant of a chemical reaction
M	molar mass
m	mass
N	number of CSTR in series

Nu	Nusselt number
P	static pressure
Pr	Prandtl number
Q	heat
q	heat flow rate
R	ideal gas constant
r	space coordinate (radial direction)
Re	Reynolds number
S	catalytic surface area-to-volume ratio
Sc	Schmidt number
Sh	Sherwood number
T	temperature
t	time
u	internal energy per mass unit
V	volume
x	species gas molar fraction
y	species gas mass fraction
z	space coordinate (axial direction)
(A/F)	air-to-fuel ratio
GHSV	gas hourly space velocity

Greek symbols

ΔH	standard enthalpy
δ	thickness
κ	thermal conductivity
μ	dynamic viscosity
ν	stoichiometric coefficient
ω	reaction rate constant
ρ	density

τ mean residence time

τ stress tensor

θ active site surface coverage

$\vec{v}$ velocity vector

λ stoichiometric air-to-fuel ratio, $\frac{(A/F)_{real}}{(A/F)_{stoich.}}$

Subscripts

0 initial

app apparent

cat catalyst

i ith species

in inlet

j jth species

n nth reaction

out outlet

WGS water-gas shift

z space coordinate (axial direction)

Superscripts

f formation

g bulk gas phase

h heat

m mass

n nth washcoat node

r reaction

s solid phase (washcoat + substrate)

w interface between bulk gas and washcoat phases

wc washcoat phase

Chapter 1

Introduction

1.1 Motivation

Air pollution is not a problem that arose recently and while, through many decades, mankind was oblivious to its effects, from the first part of the 20th century onwards concerns and actions about this matter have been raised.[1] Heat engines have been put to practical use to improve society's life style for over than 250 years.[2] In the early years, the steam engine revolutionized the transportation sector by bringing the railway locomotives to reality. It was not until the 1860s that internal combustion engines came to be a feasible solution and due to their lightness and efficiency they brought another revolution with their great appeal for transport applications. Motor vehicles have since became a common reality in many societies and, since 1940, the air pollution generated by this source has become an apparent problem.[2] It became clear that the engines operated in these vehicles were a major contributor to hydrocarbons (HC), nitrogen oxides (NO_x) and carbon monoxide (CO) atmospheric levels, particularly in urban areas.[2] Carbon monoxide is a direct poison to humans, whereas hydrocarbons and oxides of nitrogen undergo photochemical reactions in the sunlight to generate smog and ozone.[1] Compression ignition engines also expel to the atmosphere soot and smoke particles.[2] As a result of these problems and as a way to ensure a quality air to populations, emission standards for motor vehicles were first introduced in California, and then nationwide in the United States at the beginning of the 1960s.[4] Europe and Japan shortly followed United States policies and ever since, all

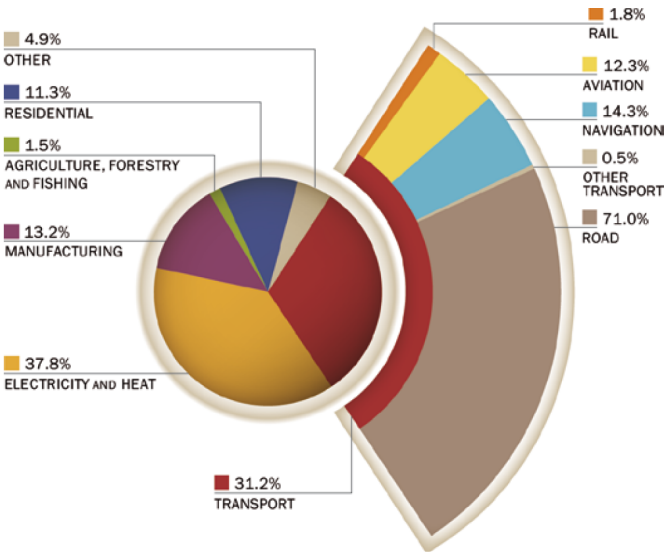

Figure 1.1: CO_2 emissions from Europe in 2009.[3]

around the world, restrictions regarding vehicle pollutions have become increasingly stricter.[2] Table 1.1 presents the evolution of passenger car emissions standards, over the years, for the United States of America and Europe.

Table 1.1: Emissions standard regulations from passenger car sources in United States of America and Europe.[5,6]

Europe (g/km)						
Compounds	Euro 1 (1993)	Euro 2 (1996)	Euro 3 (2000)	Euro 4 (2005)	Euro 5 (2009)	Euro 6 (2014)
CO	2.72	2.20	2.30	1.00	1.00	1.00
HC	-	-	0.20	0.10	0.10	0.10
NO_x	-	-	0.15	0.08	0.06	0.06
HC + NO_x	0.97	0.50	-	-	-	-
PM	-	-	-	-	0.005	0.0045
United States of America (g/mi)						
Compounds	Tier 1 (1991)		Tier 2 (1999)		Tier 3 (2013)	
CO	4.2		4.2		4.2	
NMHC	0.31		0.156		-	
NMOG	-		0.125		-	
NO_x	0.6		0.2		-	
NMOG + NO_x	-		-		0.16	
PM	-		0.02		0.003	

These emission control requirements have led to significant changes of how internal combustion engines are operated and designed.[2] A vital development in the mission of reducing Green-House Gases (GHG) emissions was the implementation of catalysts in the exhaust line.[1] However, nowadays, despite great developments in engine design and catalytic technology, the transport sector can be responsible for more than 30% of CO_2 emissions to the atmosphere, as it is shown by the case of Europe in Figure 1.1.[3] And from this share of emissions more than 70% come from road vehicles, as shown in Figure 1.2.[3] This proves how demanding these problems are and how they still require a lot of attention in optimizing fuel efficiency.

Recently, new design approaches have been proposed for the exhaust line of spark ignition direct injection engines (SIDI).[7] Until now, SIDI engines have always been operated under stoichiometric conditions, since, under these conditions, was verified to be the best way to lower, at a significant extent and simultaneously, the three main pollutants' emissions (CO, HC, NO_x), from the engine outlet.[8] But it was raised the question: "What if it was possible to take advantage of the potential of these engines to improve fuel economy and reduce GHG?".[9] Stoichiometric operation has a lower fuel efficiency which results in higher levels of CO, HC and CO_2, besides an economic penalty for the consumer.[7,10] This problem would be mitigated with an operation in lean conditions, that would allow to maximize the fuel efficiency.[10] Nonetheless, currently, it is used the traditional three-way catalyst (TWC) to mitigate the pollutants concentration on the exhaust gases emitted to the atmosphere and with this present

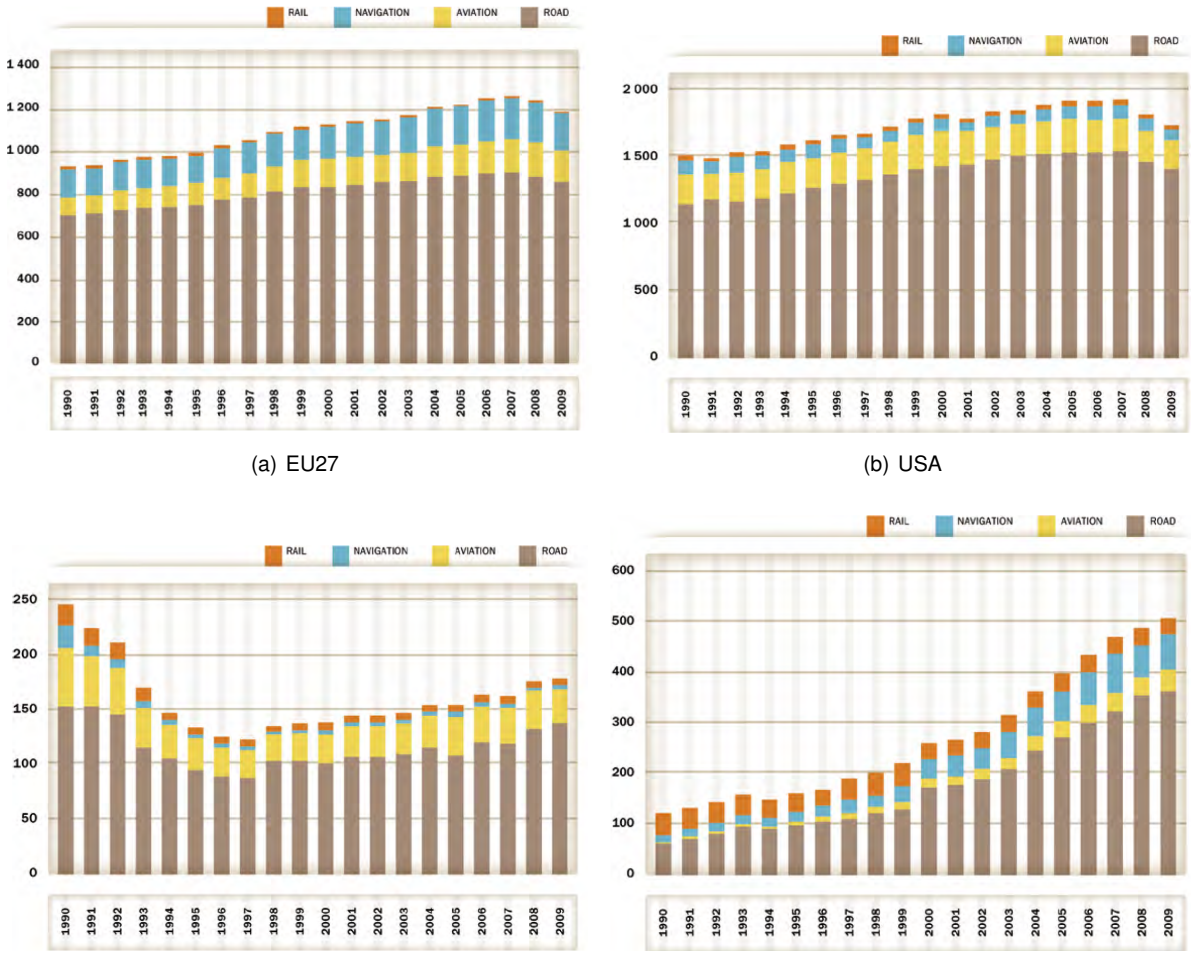

(a) EU27

(b) USA

(c) Russia

(d) China

Figure 1.2: Transportation's sector CO_2 emissions from 1990 to 2009.[3]

technology, if the inlet conditions to the engine were to be changed to lean, this would also mean that NO_x would not be abated in the TWC to levels considered acceptable.[7] So while providing an answer for one important question, this new approach also raises another one: "Is it possible to reduce NO_x in another fashion?". It is an answer to this question that the new exhaust line designs proposed are hoping to provide a solution. If secondary devices (such as a downstream passive ammonia-SCR or a lean NO_x trap) are added to the design of the exhaust line, it may be possible to operate the engine in a cycle operation between lean and rich conditions.[7,10,11] It would mainly operate in lean conditions with periodic short incursions to rich operation, to provide enough ammonia (NH_3) to these secondary devices which were then to be used to reduce NO_x in a lean operation.[7,10,11] However, to have an answer to this question, a better understanding of which conditions optimize the generation of NH_3 over the TWC and how other by-products forms from NO_x reductions is necessary, and is in the scope of this claim that this study hopes to provide an insight.

1.2 Objectives

The thesis objective was, through mathematical modelling of the kinetic reactions and mass diffusion transport in monolithic reactors, being able of providing solid tools that help solve future emissions control challenges and that might help in design optimization of monoliths' washcoats.

1.3 Thesis Outline

This document is structured as followed. The first chapter contains the motivation and goal set for the work. The literature review is presented in the chapter 2 "State of the Art", to explain the general concepts behind the technology of the three-way catalyst and behind the modelling of monolithic converters. In chapter 3 "Methodology" the experimental data procedures and analysis is described as well as the initial approach to the modelling work. In the 4th chapter, the modelling results are given and interpreted. To finalise, the last chapter comprises the conclusions and suggestions for future work.

Chapter 2

State of the Art

2.1 Technology

The quantity of pollutants emitted from an engine depends on a variety of conditions, but is predominantly influenced by the air-to-fuel ratio.[4] Gasoline burn engines usually operate around stoichiometric conditions (λ=1, (A/F)$\simeq$15).[2] Figure 2.1 shows the pollutant formation in a gasoline engine as a function of the air-to-fuel ratio fed to that engine.

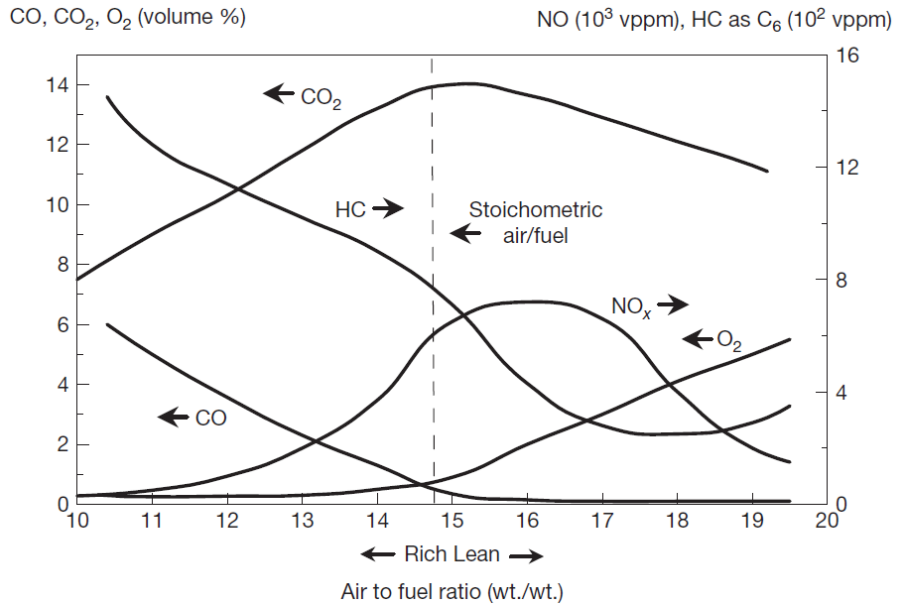

Figure 2.1: Pollutant formation in function of the air-to-fuel ratio at the inlet of a gasoline engine.[1]

When an engine operates in rich conditions (λ<1), CO and HC emissions increase in comparison with stoichiometric operation and NO_x emissions decrease.[1,4] This occurs since complete burning of the gasoline is impossible with deficiency of O_2 in the engine, which results directly in the increase of HC and CO emissions.[1,4] The oxidation of the nitrogen (N_2) does not occur ate low temperatures but only at high temperatures, as the ones felt inside a internal combustion engine.[1,4] Since the partial combustion leads to a lower temperature inside the combustion chamber and the environment inside the chamber is

with deficiency of oxygen (O_2), it also results in a lowering of the oxidation rate of N_2. When the engine is made to operate in lean conditions (λ>1), complete combustion dominates, which leads to almost full conversion of CO and HC and also a lowering of NO_x emissions, compared to stoichiometric values.[1,4] In this case, the lowering of NO_x emissions has only a direct relation with the temperature present in the combustion chamber, since a bigger air-to-fuel ratio origins in a lower operating temperature, a decrease on the formation of NO_x can be seen.[1] Figure 2.1 graphically shows these dynamics.

Catalysis has proven to be the most effective way of dealing with car emissions and achieving the goals set by the increasing regulations over the years.[1]

2.1.1 First Catalytic Converters

During the mid-70s, the first generation of car catalysts emerged and had as main goal to oxidise only HC and CO.[1,4] To avoid formation of NO_x during the combustion, the engine was operated in conditions just slightly richer than the stoichiometric.[1] This however would lead to the necessity of pumping a secondary air into the exhaust air to provide sufficient O_2 for the catalytic oxidation of HC and CO in the catalyst.[1]

During this first generation of car catalysts, several studies were performed in order to find an answer to many unknown issues that the use of catalysts in passenger vehicles could bring.[1] Many studies were performed to reply to the following questions: How to house the catalyst in the exhaust line? Which catalysts were better for this application? How would the presence of the catalyst in the exhaust line increase the back pressure? How would the catalyst conserve its properties in a high temperature oxidative environment with high water content? How much weight would the catalyst add to the vehicle? Would the heat balance in the catalyst change the overall heat balance of the vehicle? Was the catalyst able to be efficient in highly transient environment? All these problems were necessary to solve to come up with a reliable and efficient solution to provide the costumers with a vehicle that would meet the regulations.[1]

Gamma-alumina ($\gamma-Al_2O_3$) was the best material to provide a support for the active sites, due to its high surface area.[4,8,11,12] There were two major options to house the catalyst in the exhaust. A beaded catalyst, which was attractive because of their previous use in petroleum and petrochemical industries and so the structures to manufacture, in mass production, this type of catalyst were already available.[1] On the other end, this types of catalysts would experience many mechanical stresses that would decrease their durability, as the vibration of the vehicle would ground the particles into smaller sizes and they would settle causing the flow to bypass the catalyst.[1] An honeycomb catalyst (or washcoated monolith) was an alternative solution.[1] It had an advantage to the beaded catalyst because of a lower pressure drop, due to the high open frontal area, and the sufficient strength and resistance requirements came to be found achievable after some modifications from ceramic companies to their monolith structures.[1,13,14] The support $\gamma-Al_2O_3$ was washcoated on the walls of the monolith.[1,8] Nowadays the monolith technology is used exclusively worldwide, and several developments were obtained to allow the catalysts, to have thinner washcoats to decrease the mass diffusions resistance, and have bigger

number of active sites per surface area (through the decrease of the wall thickness, as well), to allow smaller volumes of catalyst to treat the exhaust air.[1]

Catalyst screening was also heavily performed during the first generation of catalysts. Platinum (Pt) and palladium (Pd) were known optimum oxidation catalysts, however, the cost and supply of this materials was troublesome.[1] This stimulated investigation to find alternatives to these materials and other alternatives as copper (Cu), chromium (Cr), nickel (Ni), manganese (Mn) and more were studied regarding their capability to oxidise CO and HC.[1] It came to be realized that this non-precious metals had lower activities and they would require a reactor volume larger to have the same efficiency, which was not viable since space was not something easily free in a passenger vehicle.[1] Also these metals did not solve any of the deactivation problems, since they also showed to be susceptible to sulphur poisoning.[1,15] Lead (Pb) was also a major contributor to the poisoning of the catalysts.[1,15] It was proved that Pt had a better resistance to poisoning from lead than Pd and its presence on the catalyst helped to improving the resistance to this type of deactivation.[1] This eventually led to a bigger use of Pt than Pd in the earlier catalysts, despite the better activity showed by Pd to oxidise car pollutants.[1,16] Eventually regulations mandated that the lead was removed from gasoline, since environmental studies showed the severe effect lead could have on humans if present in the environment.[1]

2.1.2 Three Way Catalysts

After the successful implantation of catalysts for controlling CO and HC emissions, in 1979, the reduction of NO_x emissions had to be addressed.[1] There were earlier attempts to abate NO_x emissions, but they were deemed as unacceptable due to fuel penalties and complicated engine control strategies.[4] NO_x reduction is most effective in the absence of oxygen, while the oxidation reactions require O_2.[1] With this, first approaches to eliminate all three pollutants consisted of a first upstream catalyst to reduce NO_x in rich conditions, followed in the stream line by an air injection system to provide enough oxygen for the exhaust flow to go through an oxidizing catalyst.[1] With this arrangement oxygen nitrates could first be reduced by CO, HC and H_2 and the amount that would remain from this reaction could be oxidized in the second catalyst.[1] Rhodium (Rh) was found to be a great NO_x reduction catalyst and had less ammonia (NH_3) than Pd or Pt.[1,8] In 1980, a new revolutionary catalyst was introduced, the three-way catalyst (TWC), that permitted, simultaneously, the conversion of the three main pollutants with only one device, provided the engine was controlled to operate in the stoichiometric air-to-fuel ratio.[4,17] The natural oscillation on the air-to-fuel ratio meant that the catalyst would see alternatively slightly conditions of rich and lean operation (see Figure 2.2).[1] As a way to damper these effects an oxygen-storage component (OSC) was also added to absorb oxygen, when the operation was in lean conditions, and to provide it, when the exhaust was fuel rich.[4] The water-gas shift equilibrium is also promoted to the side of CO_2 production by the presence of this component on the catalyst.[18] Cerium oxide (CeO_2) was found to have a proper redox response and became the most used O_2 storage component in modern TWC.[1] In addition, ceria also helps maintaining the noble metal dispersion on the TWC as well as providing thermal stability for the gamma-alumina phase.[18]

Equations 2.1-2.3 describe the reactions over a cerium oxide under lean conditions.[18]

$$Ce_2O_3 + 0.5\,O_2 \rightleftarrows 2\,CeO_2 \tag{2.1}$$

$$Ce_2O_3 + NO \rightleftarrows 2\,CeO_2 + 0.5\,N_2 \tag{2.2}$$

$$Ce_2O_3 + H_2O \rightleftarrows 2\,CeO_2 + H_2 \tag{2.3}$$

Equations 2.4-2.6 describe the reactions over a cerium oxide under rich conditions.[18]

$$2\,CeO_2 + CO \longrightarrow Ce_2O_3 + CO_2 \tag{2.4}$$

$$12\,CeO_2 + C_3H_6 \longrightarrow 6\,Ce_2O_3 + 3\,CO + 3\,H_2O \tag{2.5}$$

$$2\,CeO_2 + H_2 \longrightarrow Ce_2O_3 + H_2O \tag{2.6}$$

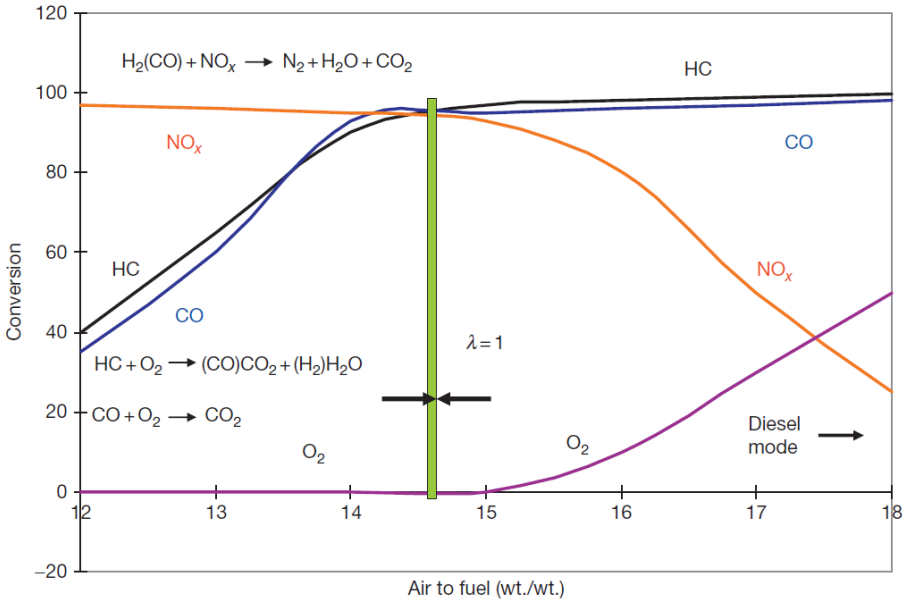

Figure 2.2: Conversion profile of a TWC in function of the air-to-fuel ratio at the inlet of the engine.[4]

Catalysts technology continued to evolve during the following years. Studies regarding the interaction of the metals present in the catalyst was done and possible set-ups with commercial applications were proposed (e.g. double-layer catalysts).[1] Also the use of Pd as a replacement of Pt and/or Rh had been desired for some years since its price was lower than both and had a better activity in oxidizing CO and HC and also showed potential in reducing NO_x.[1,19,20] By mid-90s the increase in the fuel's quality over the previous years, due to stricter regulations, made that the lead's concentration in gasoline was at levels that did not threat the use of palladium.[1] As a way to meet new regulations an earlier obtainment of the light-off temperature was required, which led to catalyst being positioned closer to the engine to reduce the heat-up time.[1,4] This also increased the desire of using Pd instead of Pt, since the former one has a better thermal resistance.[15,19] All this reasons listed above led to a fast rise and advance of Pd technology in the TWC and its use in commercial vehicles.[1] At the end of the twentieth century,

however, this high-demand from palladium made its price shift to higher values since mine sources could not supply all that was demanded.[1] So once again, the TWC saw a change of the metals used in its composition and it was obvious that from that point on forward any future shifts in the composition of this catalyst technology was going to be heavily governed by the shifts in the price/supply of these precious metals.[1,4]

2.1.3 New Catalytic Approaches for Gasoline Burn Engines' Exhaust Systems

A growing consciousness of exhaust gases' environmental impacts and the requirement of having a more efficient combustion, in SIDI engines, have led to a currently common effort to find an alternative design for the combustion and after-treatment systems of gasoline vehicles.[1] Potential in improving fuel economics and reducing exhaust emissions was always recognized in these engines, while being able to maintain the power output, if engine operational conditions were to be changed from stoichiometric to lean.[21] Nevertheless, lean-burn SIDI engine technology continues to be a major technical hurdle as NO_x reduction, with current after-treatment systems, continues to be hard to achieve with satisfactory results that meet with the current levels of nitrogen oxides standard regulations.[22] This occurs as a result of the aforementioned problem of current TWC technology having difficulties in being efficient outside stoichiometric operation, specially in reducing NO_x emissions in excess oxygen environments.[1,20] To modify this, several after-treatment set-ups were proposed. Between those, two of them were lean NO_x control catalyst technologies that have been already successfully employed in diesel vehicles to meet stringent regulations: lean NO_x trap (LNT) and urea selective catalyst reduction (NH_3-SCR).[7]

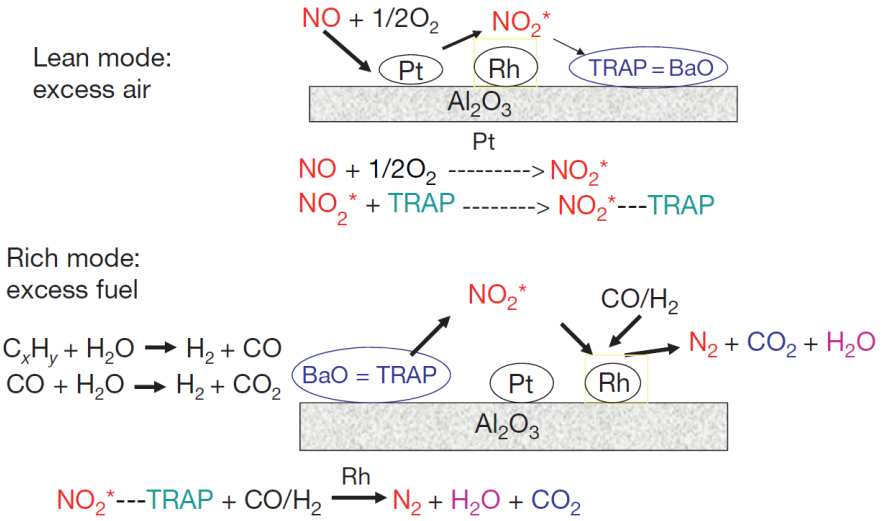

Figure 2.3: Reaction's scheme over a LNT catalyst.[4]

LNT catalysts typically comprise the traditional TWC design and an added alkali or alkaline earth metal storage component (most commonly barium oxide (BaO)).[11,22] They are designed to operate periodically in lean and rich environments.[12,22] During lean periods, NO is oxidized to NO_2 over the precious metals of the catalyst (viz. Pt, Pd, Rh) and subsequently is stored in the form of nitrites and nitrates on the storage component (e.g. BaO).[12] From the different precious metals available, has been

shown that platinum has a better performance than palladium in NO oxidation and the influence of Pt is essential not only to facilitate NO_x storage, through spillover of NO_2 from Pt to BaO, but also to facilitate NO_x reduction during rich operation.[11,19] Hence Pt and BaO close proximity is required to achieve both efficient storage and reduction of NO_x during the lean-rich cycle.[11,19] When the storage component is saturated with nitrogen compounds, operation must be switched to rich conditions for a brief period to convert the stored NO_x to N_2 (NH_3 and N_2O can also be by-products of the NO_x reduction, but the desirable one is the nitrogen molecule) over rhodium and renew the storage capacity of the catalyst.[12] Figure 2.3 presents a schematic view behind this device's operation. LNT technology can be able to achieve up to 90% of reduction of NO_x in the exhaust.[1] Regardless of this, LNT application, in gasoline operated systems, is still thwarted by four key problems: high-cost of the catalyst, poor thermal stability, sulphur poisoning and active SO_x regeneration requirements.[22,23] Catalyst's high cost is derived from the need of high concentration of platinum group metals (PGM) sites and sulphur poisoning occurs since the storage component as an higher affinity for sulphur trioxide (SO_3) and forms $BaSO_4$, which is much more stable than the corresponding nitrates and cannot be removed during rich purging conditions.[7,10,11,21]

Inversely, NH_3-SCR technology does not rely on a cyclic strategy, but instead operates through the selective reaction of NO_x with NH_3 to N_2, in the excess presence of oxygen.[12] It requires a downstream catalyst in an underfloor position (as shown in Figure 2.4) to perform the reduction of NO_x, while the oxidation of the other two main pollutants continue to be performed on the close-coupled TWC, in lean conditions.[22,23] The reaction's reductant is the absorbed NH_3 on the SCR and the reaction will generate N_2 and H_2O, compounds with no impact for the atmosphere.[4] Yet this solution is far from providing an economic and efficient answer for the NO_x reduction, despite being less expensive than the LNT technology. With this system, it is essential to have a source of ammonia for the underfloor catalyst and what have been applied for diesel applications is the addition of an aqueous urea tank (gaseous ammonia is impractical to handle in mobile applications due to volume constrains, so a surrogate, as aqueous urea, is used) and an urea injecting system to the exhaust line.[22,23] This carries relevant concerns, as an extensive urea infrastructure to supply ammonia is required (and it is currently absent), higher NO_x emissions from a lean-burn gasoline engines than from its diesel counterpart (which lead to bigger storage tanks), urea high freezing point (-12°C) and long-term stability issues, all need to be solved so this application can be efficiently used, in gasoline burn vehicles.[12,23] Also an added urea injection system in the exhaust line will increase the system's complexity, which will lead to a more sophisticated control to avoid, for example, NH_3 slips from the exhaust line.[4,12,23] This solution came to be more feasible applied to heavy-duty diesel vehicles since had less the space constrains than in light-duty vehicles, which, in their turn, saw a favoured application of the LNT catalyst.[12]

The reactions desired to accomplish the NO_x reduction in lean conditions, over the SCR, usually have three common reactional pathways and those are presented in Equations 2.7-2.9.[24]

$$4\,NH_3 + 4\,NO + O_2 \longrightarrow 4\,N_2 + 6\,H_2O \tag{2.7}$$

$$2\,NH_3 + NO + NO_2 \longrightarrow 2\,N_2 + 3\,H_2O \tag{2.8}$$

$$8\,NH_3 + 6\,NO_2 \longrightarrow 7\,N_2 + 12\,H_2O \tag{2.9}$$

Equation 2.7 is the typically called standard SCR.[24] When NO_2 is present in the catalyst feed, an equimolar reaction, Equation 2.8, occurs and is usually termed as fast SCR, due to being faster than the standard one.[24] If the molar presence of NO_2 is bigger than the NO then the NO_2 also reacts via an alternative route, as in Equation 2.9.[24] However, despite a full conversion of NO_x is possible to obtain over this catalyst, still some undesirable reactions can occur (e.g. wasting ammonia in a oxidation with only O_2, formation of N_2O, formation of NO).[1]

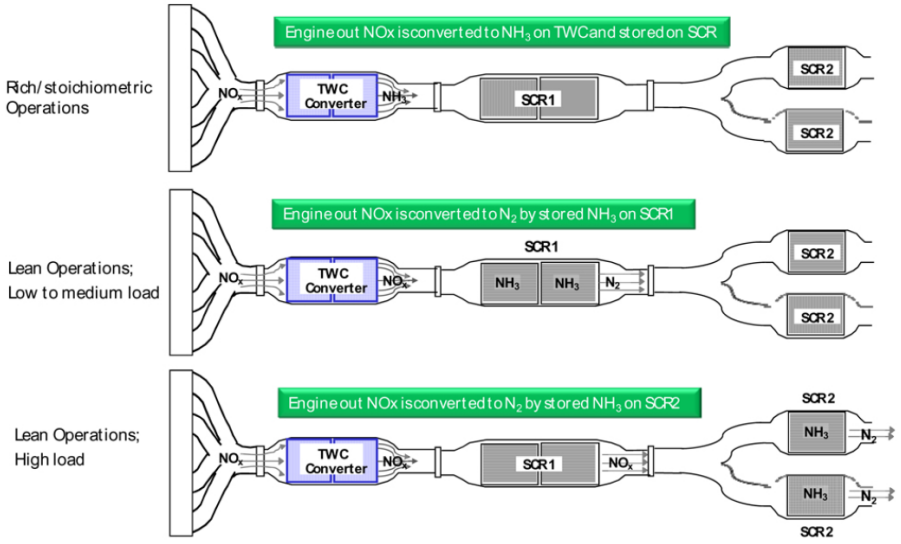

Figure 2.4: Scheme of the after-treatment system with the TWC and SCR in their respective position.[23]

So despite showing some promise in solving the NO_x reduction problem, it was clear that both applications needed to see some modifications to be applied in gasoline vehicles. Recently, researchers at General Motors have proposed a new technology referred as urealess or passive-ammonia SCR.[12,22] Briefly, as in the case of the LNT systems, this technology requires the periodic lean-rich periodic operation, but does not include a LNT catalyst.[12] Instead, this approach attempts to take advantage of the NH_3 formation's potential in rich conditions over the TWC, to provide enough ammonia to store on an underfloor SCR catalyst.[12] After the catalyst storage capacity has been filled, the operation is switched back to lean conditions and thus use this stored ammonia to reduce the NO_x slips from the TWC in lean conditions.[12] As so, to reach a successful application that can allow its commercial use, this new proposal relies heavily on the understanding of some factors. It is necessary to have a selective and robust NH_3 formation over the TWC, a significant storage capacity on the SCR, an efficient utilization of the stored NH_3 to reduce NO_x, and an optimization of the required lean-rich engine timing that permits to meet stringent NO_x regulations while optimizing fuel efficiency.[12] From these factors it can be reasoned that, currently, the understanding of how NH_3 generation's selectivity fluctuates over the TWC, presents the biggest hurdle of this solution providing a reliable alternative for gasoline vehicle's exhaust systems.[12] Ammonia potential formation over TWC is well known, but up until today research efforts

were focused on avoiding NH_3 formation, since NH_3 slips from the TWC were seen unfavourable, in the traditional application.[12] But a change of paradigm is compulsory, and understanding which conditions can optimize NH_3 and sustain a stable formation of NH3 on the TWC is essential for this new application to find its success.[12] As potential has been shown, a growing number of studies is being conducted to comprehend and prove the feasibility of this new exhaust system set-up has in commercial passenger vehicles.[23] In Figure 2.4, a schematic passive-ammonia SCR system is show. The second SCR in the exhaust line scheme is to avoid NH_3 slip at high temperatures, since above $\sim$400°C a breakthrough of stored NH_3 is expected.[23]

Another drawback that is rising more concern over the last few years is the formation of nitrous oxide (N_2O), over the exhaust line catalysts. N_2O is a GHG with a large global warming potential (310 times higher than the one from CO_2) and despite its formation does not occur inside the combustion chamber, small slips are observed, as a result of being a side-product of the catalytic NO_x reductions.[21,25] This has led to the beginning of some regulations over this species, and led research to focus on addressing this problem. It has been enlighten up that the outcome of NO_x reduction is highly influenced by temperature and NO_x/H_2 ratio.[26] In particular, recent studies suggest that the impact of N_2O formation at low temperature values is significant and cold start emissions can be a substantial source for this pollutant atmospheric concentration.[27]

2.2 Catalyst Modelling

Modelling and simulation of dynamical systems has become an essential device to help us understand empirical phenomena and the development of computer machines has allowed modelling to have a fast proliferation in the scientific areas.[14,28] Modelling allows to represent through simulation how a system will respond to a definite set of conditions, without having the need to perform that experimental set-up.[14,17] And although complete precise representation might be impossible, various degrees of precision can be obtained depending on the range of the modeller's needs. Simulation offers a lot of advantages over experimental investigation.[28,29] It is often more cost and time efficient and often allows the investigation scenarios which might be too dangerous to perform experimentally.[17,28] However, simulation does not obviate the necessity of experimentation and they should be symbiotically used for a complete process development.[28] The development of efficient complex models requires the expertise in many fields and a deep understanding how dynamic systems interact. It is indispensable to have a critic approach and understand when complexity development is required to improve the precision of the model predictions or when simplifying assumptions are needed to improve computational times or to adjust to software/hardware limitations. It is an arrangement between these two conditions that can evaluate the proficiency of a model.

Catalytic combustion reactors are heterogeneous reactors because there are two phases: a gas phase (reactants and products) and a solid catalyst.[28] For the model development of such reactors it is essential to have a knowledge in the three following topics: thermodynamics, reaction kinetics and transport phenomena.[28] Thermodynamics is essential to determine the thermodynamic state of a sys-

tem (through variables such as temperature, pressure, volume, energy, enthalpy, entropy, etc.).[28] It is through this state definition that thermodynamics is concerned to characterize where a system is before and after a change, and how much it as changed.[28] Nonetheless, it does not allow us to determine how it changes and that is where the other two topics come in handy. The internal change of the system and the change due to interactions between the system and its surroundings are quantified by the reaction kinetics and transport phenomena, respectively.[28] These enables us to describe the direction and the velocity of the change and, with these, have a proper description of how a flow varies inside a catalytic combustion reactor.[28] Subsequently, it will only be focused the latter two topics (reaction kinetics and transport phenomena) since, with nowadays computer power, thermodynamic states are easy to compute and what brings value to a model is to have a good description of how a system interacts with itself and with the systems surrounding.

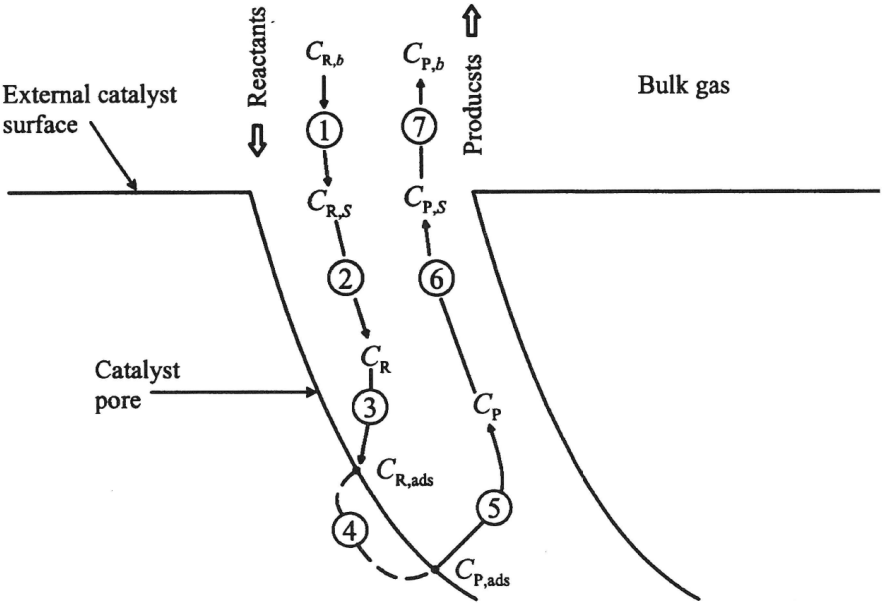

Figure 2.5: Sequence of steps during a solid catalysed reaction.[28]

As aforementioned in the section 2.1 “Technology”, nowadays catalytic combustion chamber are exclusively monolithic reactors. A honeycomb monolith consists of a number of parallel channels, through which the gas flows.[13,14,29] Monoliths can have channels with multiple various cross-sectional shapes.[13,14,29,30] To reduce numerical calculations volume, a first general assumption can be made. If it is assumed that all the channels behave the same way, then a model of a single channel can be representative of the entire reactor.[28] This is called the single channel model and it has been widely used to interpret results from monolithic reactors.[13,28,29] To validate this simplification one must consider that the velocity distribution is uniform among the channels, that the catalyst is equally distributed, that the species concentrations are uniformly distributed, and that there is no radial heat loss.[8,13,14,28] If these criteria are not met, channel interactions may be added to the model and each channel will have its own single channel model that combined together will reproduce the behaviour of a multichannel honeycomb catalyst.[28]

2.2.1 Reaction Kinetics

Modelling of the reaction kinetics can be often a challenging work, drawing upon empirical knowledge as well as theoretical.[28] The model of a reaction mechanism is expressed in the form of a rate expression, as shown in Equation 2.11. It is important to understand that a reaction can be a single elementary step or a complex arrangement of several elementary steps. On the case of an elementary step reaction presents itself it is easy to perceive, through experimentation, that the exponents m and n, from Equation 2.11, are equal to the stoichiometric factors α and β, respectively. However, more common is that it is faced a mechanism with an agglomeration of steps, before reactants can be fully turned into the final products.[28] As in the case present here, with heterogeneous catalysis, this is the usual case where species undergo a series of intermediary steps (viz. adsorption on the metal site, molecular dissociation, desorption, intermediary species) to reach the final products (see Figure 2.5).[31] As so, a simple rate expression, like the Equation 2.11, to model such reaction is not adequate. Hence, it is necessary to resort to fundamental theories of reaction rates to describe each reaction step that explains the reaction behaviour, to complete the pathway between reactants and products.[28] However theory cannot provide us with knowledge to predict reaction rates and such knowledge must be extracted empirically for each case.[28] Adding to that, it is also very difficult to determine exactly what steps are occurring during a chemical reaction, especially in fast combustion reactions.[28] Furthermore, the mechanism may be so complex that rate expression based on it may be too cumbersome to be efficient.[28] Simplifying assumptions becomes then attractive to make the result tractable.[28]

$$\alpha\mathrm{A} + \beta\mathrm{B} \longrightarrow \gamma\mathrm{C} \tag{2.10}$$

$$\omega = -\alpha \cdot \frac{\mathrm{d}A}{\mathrm{d}t} = -\beta \cdot \frac{\mathrm{d}B}{\mathrm{d}t} = \gamma \cdot \frac{\mathrm{d}C}{\mathrm{d}t} = k \cdot C_A^m \cdot C_B^n \tag{2.11}$$

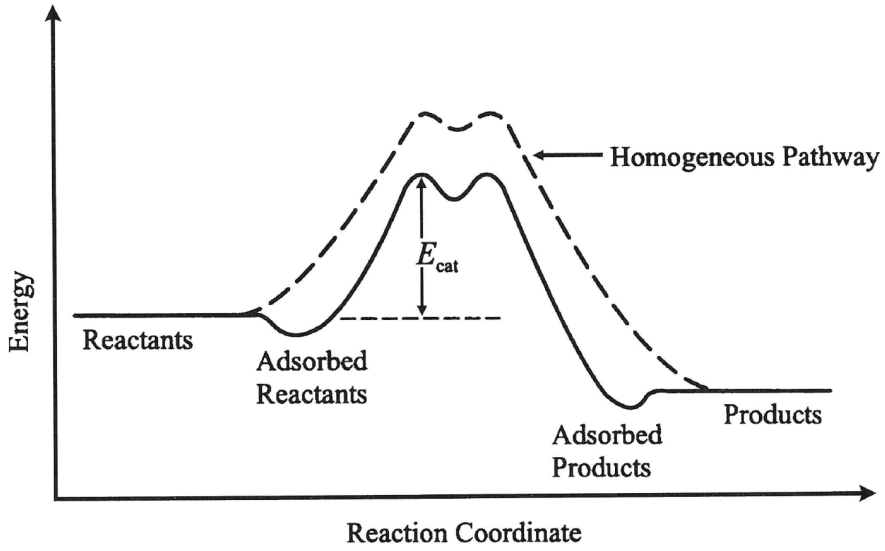

Figure 2.6: Difference between activation energies of a homogeneous reaction and catalysed one.[28]

The role of a catalyst is to provide an alternative reactional pathway that lowers the activation energy, as shown in Figure 2.6.[28] In heterogeneous catalysis, the activation energy for the absorbed species

must be lower than the one for the species in the bulk gas. Activation energy is the minimum energy that allows the start of any reaction by making some chemical bonds rearrangements in the reagents.[28] In the previous paragraph was described how a complex reaction scheme can be considered as a gathering of various elementary reaction steps. Each elementary step has its own activation energy and its own reaction rate. From Equation 2.11 one can see that the reaction rate constant (k) must be a function of temperature, an objective measure of the system's energy. That relation is expressed through the Arrhenius Equation, as in Equation 2.12.

$$k = A \cdot \exp\left(-\frac{Ea}{R \cdot T}\right) \tag{2.12}$$

Chemical kinetics modelling can have various grades of description, and can be divided in two groups: macrokinetics (also known as global parameter kinetics) and microkinetics. Microkinetics tries to describe every reaction step, while macrokinetics tries to present a simpler model that has the phenomena concealed in a fewer number of parameters.[32] Microkinetics, due to taking into account every reaction's intermediary step, are usually computationally intensive and, hence, are not easily used in models for control applications.[31] Besides this, this type of models require a lot of time (years) to develop, due to demanding a great amount of theoretical work coupled with experimental tests to determine the model parameters.[31] In addition, in after-treatment devices, the chemical reactions are a function of an immeasurable number of parameters (viz. catalyst formulations, washcoat material and its aging, etc.) and sometimes it is not even possible to determine the kinetic parameters in each individual step.[8,31–33] This has led that over the years, to predict kinetic rates, a macrokinetic model being used and one of the most commonly approaches used to achieve this, for heterogeneous catalysis, is the Langmuir-Hinshelwood-Hougen-Watson mechanism (LHHW).[28,31,34,35] The models reached from this mechanism usually have a good predictive capability and are helpful in rapid design evaluations or control algorithms.[21,31,36] The basics assumptions of this mechanism are: all active sites are the same, heat of adsorption is not a function of coverage, the rate of adsorption is proportional to the fraction of empty sites, the rate of desorption is proportional to the number of molecules adsorbed, and there is one rate determining step that is slower than the other steps of the mechanism.[28,34] Although this success, these models are best suited to model a steady-state operation, and are generally incapable of capturing the fine details of the operation of a TWC, such as the amount of adsorbed species at a given time.[33]

Table 2.1: Kinetic models extracted from the literature and their expression rates.

Author	Reactions	Model
Voltz et al.(1973)[37]	$\mathrm{CO}+0.5\mathrm{O_2}\longrightarrow\mathrm{CO_2}$	$\omega_1 = \frac{k_1 \cdot C_{\mathrm{CO}} \cdot C_{\mathrm{O_2}}}{G}$
	$\mathrm{C_3H_6}+4.5\mathrm{O_2}\longrightarrow 3\mathrm{CO_2}+3\mathrm{H_2O}$	$\omega_2 = \frac{k_2 \cdot C_{\mathrm{C_3H_6}} \cdot C_{\mathrm{O_2}}}{G}$
	Inhibition term	$G=\left(1+K_1 \cdot C_{\mathrm{CO}}+K_2 \cdot C_{\mathrm{C_3H_6}}\right)^2 \cdot \left(1+K_3 \cdot \left(C_{\mathrm{CO}} \cdot C_{\mathrm{C_3H_6}}\right)^2\right) \cdot \left(1+K_4 \cdot C_{\mathrm{NO}}^{0.7}\right)$

Author	Reactions	Model
Subramaniam and Varma(1985)[38]	$CO+0.5O_2 \longrightarrow CO_2$	$\omega_1 = \frac{k_1 \cdot C_{CO} \cdot C_{O_2}}{(1+K_1 \cdot CO+K_2 \cdot NO)^2}$
	$CO+NO \longrightarrow CO_2+0.5N_2$	$\omega_2 = \frac{k_2 \cdot C_{CO}^{1.4} \cdot C_{NO}^{0.13} \cdot C_{O_2}^{0.3}}{(1+K_3 \cdot CO)^2}$
	$2.5\,CO+NO+1.5\,H_2O \longrightarrow NH_3+2.5\,CO_2$	$\omega_3 = \frac{k_3 \cdot C_{CO}^{1.5} \cdot C_{NO}^{0.4} \cdot C_{O_2}^{0.7}}{(1+K_4 \cdot CO)^2 \cdot \left(1+K_5 \cdot O_2\right)^2}$
Koltsakis et al.(1997)[39]	$CO+0.5O_2 \longrightarrow CO_2$	$\omega_1 = \frac{k_1 \cdot C_{CO} \cdot C_{O_2}}{G}$
	$H_2+0.5O_2 \longrightarrow H_2O$	$\omega_2 = \frac{k_2 \cdot C_{H_2} \cdot C_{O_2}}{G}$
	$C_xH_y+(x+\frac{y}{4})O_2 \longrightarrow xCO_2+\frac{y}{2}H_2O$	$\omega_3 = \frac{k_3 \cdot C_{C_xH_y} \cdot C_{O_2}}{G}$
	$C_xH_y+xH_2O \longrightarrow xCO+(x+\frac{y}{2})H_2$	$\omega_4 = \frac{k_4 \cdot C_{C_xH_y} \cdot C_{H_2O}}{G}$
	$2\,CO+2\,NO \longrightarrow 2\,CO_2+H_2$	$\omega_5 = \frac{k_5 \cdot C_{H_2}^m \cdot C_{O_2}^{0.5}}{G} \cdot \left(1 - \frac{C_{s,CO}^x \cdot C_{s,H_2}^{x+0.5y}}{C_{C_xH_y}^x \cdot C_{H_2O}^x \cdot k_{SR}}\right)$
	Inhibition term	$G=T^w \cdot \left(1+K_1 \cdot C_{CO}+K_2 \cdot C_{C_3H_6}\right)^2 \cdot \left(1+K_3 \cdot \left(C_{CO} \cdot C_{C_3H_6}\right)^2\right) \cdot \left(1+K_4 \cdot C_{NO}^{0.7}\right)$
Matthess et al.(2001)[36]	$CO+0.5O_2 \longrightarrow CO_2$	$\omega_1 = \frac{k_1 \cdot x_{CO} \cdot x_{O_2}}{G_1}$
	$C_3H_6+4.5O_2 \longrightarrow 3\,CO_2+3H_2O$	$\omega_2 = \frac{k_2 \cdot x_{C_3H_6} \cdot x_{O_2}}{G_1}$
	$CO+NO \longrightarrow CO_2+0.5\,N_2$	$\omega_3 = \frac{k_3 \cdot x_{CO} \cdot x_{NO}}{G_2}$
	$0.5\,CO+NO+0.5\,H_2O \longrightarrow CO_2+NH_3$	$\omega_4 = \frac{k_4 \cdot x_{CO} \cdot x_{NO}}{G_2}$
	$C_3H_6+9\,NO \longrightarrow 3\,CO_2+3\,H_2O+4.5\,N_2$	$\omega_5 = \frac{k_5 \cdot x_{C_3H_6} \cdot x_{NO}}{G_1}$
	$C_3H_6+3\,H_2O \rightleftarrows 3\,CO+6\,H_2$	$\omega_6 = \frac{k_6 \cdot x_{C_3H_6} \cdot x_{H_2O}}{G_1}$
	$CO+H_2O \rightleftarrows CO_2+H_2$	$\omega_7 = \frac{k_7 \cdot x_{H_2O} \cdot x_{H_2O}}{G_1}$
	Inhibition terms	G_1, same as in Voltz et al.[37] $G_2=(1+K_1 \cdot x_{CO})^2 \cdot (1+K_2 \cdot x_{NO})^2$
Ramanathan et al.(2012)[9,31]	$CO+0.5O_2 \longrightarrow CO_2$	$\omega_1 = \frac{k_1 \cdot C_{CO} \cdot C_{O_2}}{G}$
	$C_3H_6+4.5O_2 \longrightarrow 3\,CO_2+3H_2O$	$\omega_2 = \frac{k_2 \cdot C_{C_3H_6} \cdot C_{O_2}}{G}$
	$C_3H_8+5O_2 \longrightarrow 3\,CO_2+3H_2O$	$\omega_3 = \frac{k_3 \cdot C_{C_3H_8} \cdot C_{O_2}}{G}$
	$H_2+0.5O_2 \longrightarrow H_2O$	$\omega_4 = \frac{k_4 \cdot C_{H_2} \cdot C_{O_2}}{G}$
	$CO+NO \longrightarrow CO_2+0.5\,N_2$	$\omega_5 = \frac{k_5 \cdot C_{CO} \cdot C_{NO}}{G}$
	$C_3H_6+9\,NO \longrightarrow 3\,CO_2+3\,H_2O+4.5\,N_2$	$\omega_6 = \frac{k_6 \cdot C_{C_3H_6} \cdot C_{NO}}{G}$
	$H_2+NO \longrightarrow H_2O+0.5\,N_2$	$\omega_7 = \frac{k_7 \cdot C_{H_2} \cdot C_{NO}}{G}$
	$CO+H_2O \rightleftarrows CO_2+H_2$	$\omega_8 = \frac{k_8 \cdot \left(C_{CO} \cdot C_{H_2O} - \frac{C_{CO_2} \cdot C_{H_2}}{k_{WGS}}\right)}{G}$
	$C_3H_6+3\,H_2O \longrightarrow 3\,CO+6\,H_2$	$\omega_9 = \frac{k_9 \cdot C_{C_3H_6} \cdot C_{H_2O}}{G}$

Author	Reactions	Model
Ramanathan et al.(2012)[9,31]	$2\,Ce_2O_3+O_2 \longrightarrow 4\,CeO_2$	$\omega_{10} = k_{10} \cdot C_{O_2} \cdot (1-\theta)$
	$Ce_2O_3+NO \longrightarrow 2\,CeO_2+0.5\,N_2$	$\omega_{11} = k_{11} \cdot C_{NO} \cdot (1-\theta)$
	$CO+2\,CeO_2 \longrightarrow Ce_2O_3+CO_2$	$\omega_{12} = k_{12} \cdot C_{CO} \cdot \theta$
	$C_3H_6+12\,CeO_2 \longrightarrow 6\,Ce_2O_3+3\,CO+3\,H_2O$	$\omega_{13} = k_{13} \cdot C_{C_3H_6} \cdot \theta$
	$C_3H_8+14\,CeO_2 \longrightarrow 7\,Ce_2O_3+3\,CO+4\,H_2O$	$\omega_{14} = k_{14} \cdot C_{C_3H_8} \cdot \theta$
	$H_2+2\,CeO_2 \longrightarrow Ce_2O_3+H_2O$	$\omega_{15} = k_{15} \cdot C_{H_2} \cdot \theta$
	$NH_3+1.25\,O_2 \longrightarrow NO+1.5\,H_2O$	$\omega_{16} = \frac{k_{16} \cdot C_{NH_3} \cdot C_{O_2}}{G}$
	$NO+2.5\,H_2 \longrightarrow NH_3+H_2O$	$\omega_{17} = \frac{k_{17} \cdot C_{H_2} \cdot C_{NO}}{G}$
	$NH_3+1.5\,NO \longrightarrow 1.25\,N_2+1.5\,H_2O$	$\omega_{18} = \frac{k_{18} \cdot C_{NH_3} \cdot C_{NO}}{G}$
	Inhibition term	$G = \left(1+K_1 \cdot C_{CO}+K_2 \cdot C_{C_3H_6}\right)^2 \cdot \left(1+K_3 \cdot \left(C_{CO} \cdot C_{C_3H_6}\right)^2\right) \cdot \left(1+K_4 \cdot C_{NO}\right)$

In Table 2.1 is exposed a brief summary of some kinetic modelling studies performed in the past. Voltz et al.(1973) studied the catalytic oxidation of carbon monoxide and propylene over platinum packed beds and validated their work for real engine exhausts.[37] Subramaniam and Varma(1985) proposed a kinetic rate expression for the NO reduction, over a commercial three-way catalyst.[38] Koltsakis et al.(1997) proposed a 6 reaction scheme which described the TWC behaviour, with sufficient accuracy, for usual gasoline operating conditions.[39] Also, a new feature was added which was the inclusion of the steam-reforming reaction in the catalytic reaction scheme.[39] Matthess et al.(2001) proposed a new approach to obtain reliable kinetic data from light-off temperatures from simple mixtures.[36] Ramanathan et al.(2011) proposed a new global reaction scheme with the purpose of building a model for control algorithms, taking in considerations the new demands for lean-burn SIDI engines (viz. NH_3 kinetics).[9,31]

Other studies have been performed, along the years, to improve macrokinetic modelling of this type of systems, ranging from more mechanistic to more empirical ones.[21,32,34,35] In the last 20 years, microkinetic models have started to appear as well.[33,40]

2.2.2 Transport Phenomena

The behaviour of any flow system can be described by transport balance of mass, momentum and energy.[28] These three quantities are collectively referred as transport phenomena and they postulate how the local values of temperature, pressure and composition change, depending on the interactions with their surroundings.[28] The transport mechanisms for mass, momentum and energy consist of diffusion or advection. Broadly speaking, the diffusion phenomena relates with the molecular level phenomena

and advection with the macroscopic flow motion. The combined transport of phenomena through both these mechanisms is referred as convection.[28] The modelling of any fluid phenomena can be a really hard endeavour. The Navier-Stokes equations are a set of differential equations that model the phenomena transport inside a finite volume.[29,41] They follow the conservation laws for mass, momentum and energy.[29,42] The world, that we live in, is described by three spatial dimensions and one time dimension and as it can be seen, in Equations 2.13–2.16, these equations describe the flow in these four dimensions and all the dependent variables of the system(i.e. density, pressure, and temperature) are a function of their position.[43] From analysing the Navier-Stokes equations, it can be recognized the several meanings of its terms. As shown in Equations 2.13–2.16, in the left side of the equal signal the Navier-Stokes equations are comprised of two terms, which are the a transient or accumulation term, which describes the variations of the phenomena inside the volume, and the advective terms, which describes the phenomena going in and out of the volume, due to the macroscopic fluid movement, and is defined by the velocity vector field. At the right side of the equal signal, the terms present represent the other forms of phenomena transport (viz. diffusion, conduction, external forces, stresses, etc.) and sinks or sources of phenomena that might exist in the system (e.g. chemical reactions).

$$\frac{\partial \rho}{\partial t} + \nabla \cdot (\rho \cdot \vec{v}) = 0 \tag{2.13}$$

$$\frac{\partial \rho \cdot y_j}{\partial t} + \nabla \cdot (\rho \cdot y_j \cdot \vec{v}) = -\nabla \cdot (-D_j \cdot \nabla (\rho \cdot y_j)) + \omega_j \tag{2.14}$$
$$\omega_j = M_j \cdot \sum_n \left(\nu_{j,n} \cdot k_n \prod_i C_i^{\alpha_i} \right)$$

$$\frac{\partial \rho \cdot \vec{v}}{\partial t} + \nabla \cdot (\rho \cdot \vec{v}\vec{v}) = -\nabla P + \nabla \cdot \tau + \rho \cdot \vec{a} \tag{2.15}$$
$$\tau = \mu \cdot \left(\nabla \vec{v} + (\nabla \vec{v})^T \right) - \frac{2}{3} \cdot \mu \cdot (\nabla \cdot \vec{v} \cdot I)$$

$$\frac{\partial \rho \cdot c_p \cdot T}{\partial t} + \nabla (\rho \cdot c_p \cdot T \cdot \vec{v}) = -\nabla \cdot (-\kappa \cdot \nabla T) - \nabla \cdot \left(\sum_j -D_j \cdot \nabla (\rho \cdot y_j) \cdot h_j' \right) - \nabla \cdot (P \cdot \vec{v}) + \nabla \cdot (\vec{\tau}\vec{v}) + \sum_j \omega_j \cdot \Delta H_j^f \tag{2.16}$$

Despite the aid of computer calculations, even with nowadays high-speed computers, these equations still present a hard challenge to solve and in most of the scenarios (viz. real time simulations, reactor control and optimization) it is wise to make use of some assumptions or simplifications.[13] The same way as described on the section 2.1 “Reaction Kinetics”, with the microkinetics and macrokinetics models, the transport phenomena models can also be divided with regard to their detail. A more detailed model takes into account all the spatial and time variations of the properties of the system, and a more lumped one makes use of average parameters to describe some or all of those variations.[28]

The decision of which modelling detail to obtain for a system, can vary from a different number of factors (viz. system, computational power, extent of the problem, etc.).[13] Usually a good rule of thumbs when it comes to choose a model is to choose the least sophisticated model that can obtain satisfactory results. Sometimes, even if possible, a model that rigorously takes into account all the phenomena can be too onerous to be a practicable option.[13,28,44]

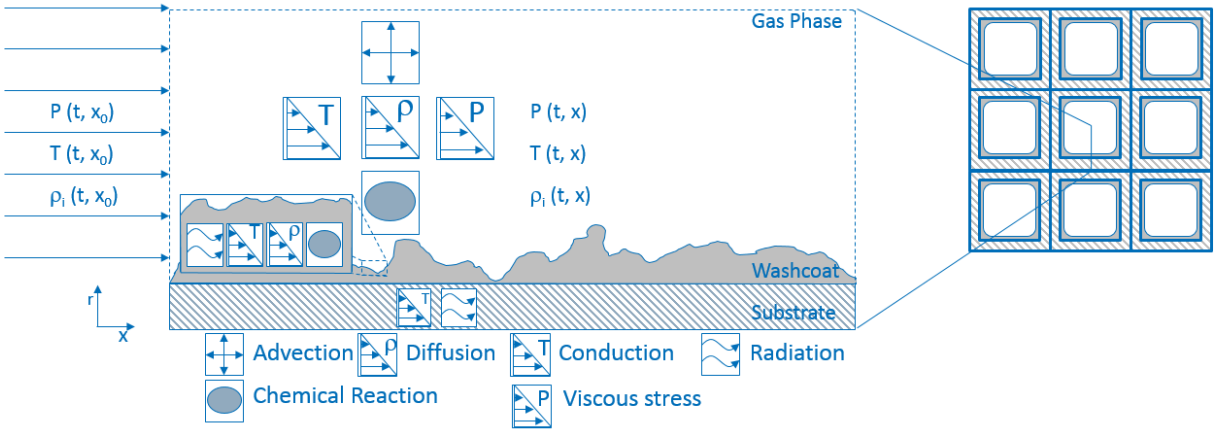

Figure 2.7: Graphic summary of all existing phenomena inside a monolithic channel.[1]

The phenomena present in a flow inside a monolith chamber can be summarized in the Figure 2.7. By observing the scheme is quite evident that each channel is composed by three distinct phases (gas phase, washcoat phase and substrate phase) and either their phenomena as their interactions are vital to be well understood, if a good description is to be achieved by the model. From empirical knowledge it is known that some phenomena have an higher influence on the system than other and, relying on that, it is possible to make assumptions and simplifications, with some level of security that the final output of the model will be accurate with the results produced by the dynamical system.

To model the gas phase in monolithic converters, one of the most common assumptions is the plug flow assumption.[29] Equations 2.13–2.16 model the gas phase in the three spatial dimensions. The plug flow assumption represents a simplification assuming that radial and angular phenomena can be neglected and, as so, all variables become independent of these two spatial dimensions and can be expressed only in function of their axial position in the channel.[29] This is a very useful assumption since by neglecting two spatial dimensions, enables the reduction of computational effort required.[29] Further on, all the models that use this plug flow assumption will also be refereed as 1D models. It can be seen, from Figure 2.8, that neither for laminar or turbulent flow this assumption is precisely true. The contrast between the model and the reality occur near the wall of the channel, where a velocity gradient is seen. This profile arises from the drag force exerted on the surface of the fluid by the wall, which causes the fluid velocity to decrease in its vicinity.[28] This is an important feature that needs to be taken into account in heterogeneous catalysis since this boundary layer affects the flow of the species from the bulk flow to the catalyst surface and therefore affect the reaction rate, but this will be addressed later on. Despite the fact that the turbulent flow profile resembles more the velocity profile assumption made

[1] Figure 2.7 is inspired in a sketch done by Holder et al.(2006).[32]

in the plug flow model, specially in the region closer to the centre of the channel, it is known that the flow profile in monolithic catalysts is the laminar one (Re<2000).[8,30] However, it has been common practice to apply this assumption to this type of converters, for a long time, with proven results.[30] For modelling a gas flow through a monolithic converter, neglecting terms, such as diffusion (D), tension (τ) and heat conduction (κ) in the axial direction, has also been a commonplace, since their impact in this type of systems has been empirically proved to be smaller than others, with a degree which assures a level of security in the final model's results.[8,32,42]

The Equations 2.17–2.21 show how the Navier-Stokes equation look after applying the plug flow model hypothesis to the Equations 2.13–2.16.

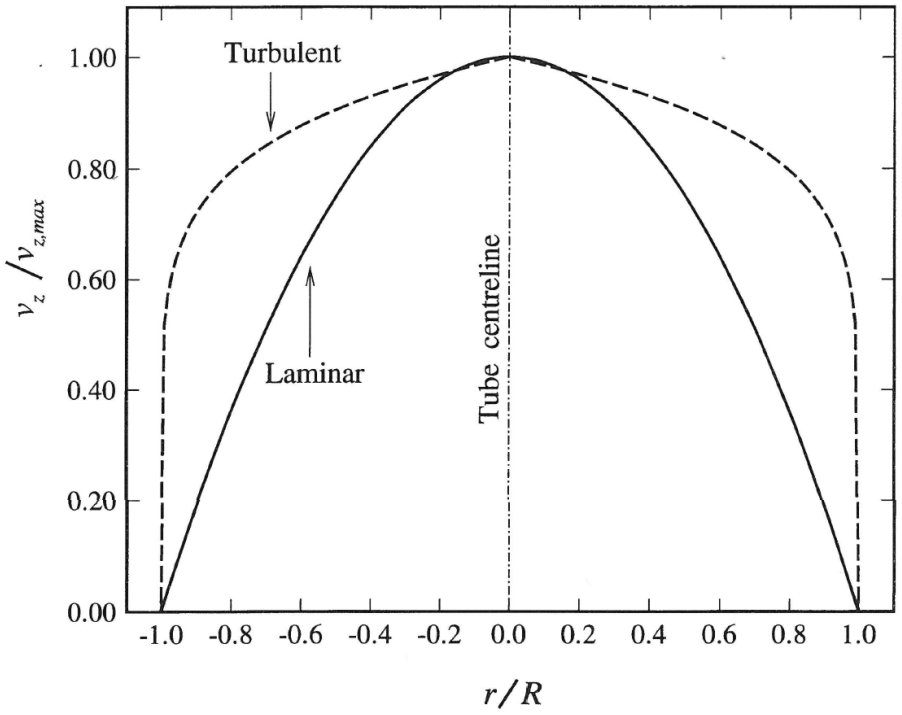

Figure 2.8: Typical velocity profiles in a circular duct of laminar and turbulent flows.[28]

$$\frac{\partial \rho}{\partial t} + \frac{\partial \rho \cdot v_z}{\partial z} = 0 \tag{2.17}$$

$$\frac{\partial \rho \cdot y_j}{\partial t} + \frac{\partial \rho \cdot y_j \cdot v_z}{\partial z} = \omega_j \tag{2.18}$$

(2.19)

$$\frac{\partial \rho \cdot v_z}{\partial t} + \frac{\partial \rho \cdot v_z^2}{\partial z} = -\frac{\partial P}{\partial z} + \rho \cdot a_z \tag{2.20}$$

$$\frac{\partial \rho \cdot c_p \cdot T}{\partial t} + \cdot \frac{\partial \rho \cdot c_p \cdot T \cdot v_z}{\partial z} = -\frac{\partial P \cdot v_z}{\partial z} + \sum_j \omega_j \cdot \Delta H_j^f \tag{2.21}$$

Momentum equation (Equation 2.20) is also often neglected, since the pressure (P) through a catalyst is often constant, and with no external sources (i.e. accelaration (a_z)), the velocity (v_z) can be

considered constant, hence, reducing the computational effort required by the model.[8,32]

The equations that have been discussed are only for the modelling of the bulk gas phase and, from Figure 2.7, one can recall that other phases exist in the monolith besides this one. Commonly, despite homogeneous gas phase reactions may happen in reality, they are usually neglected in the model, due to limited temperatures and small residence times of the gas stream within the monolith, for typical operating conditions in automotive applications.[32] As so, the heterogeneous reactions are usually the only ones considered. In this type of convection-diffusion-reaction problems, one-dimensional models are adequate to model the gas phase but are not able to depict the washcoat phase neither their interaction. To avoid the calculations that considering another phase might bring, the Equations 2.17–2.21 might be used to model the catalyst. This is called the pseudo-homogeneous model.[28] Due to neglecting all the phenomena transport between phases, this model is limited, specially, at low temperatures, since the assumption, that the species concentration is equal in the washcoat as in the bulk gas phase, is only achieved when the reaction rate is slower and limits all the other phenomena transport rate.[13]

From many possible options, some phenomena that can be better described is the mass and heat diffusion to the wall and the reaction in the washcoat. While still avoiding the heavy load of calculations that a two spatial dimensions model might entice another approach can be used, that is referred as the heterogeneous plug flow model.[13,32] This are the most commonly 1D models and require two-phase modelling.[13,45] In this approach, the differences of the wall species concentration and temperature are taken into account in the model.[28] And both phases are coupled using transport coefficients for convective heat and mass transfer.[32,45] To attain this, two sets of equations are used to describe the two distinct phases.[28]

Equations 2.22–2.23 state the model equations for the gas phase.

$$\frac{\partial \rho \cdot y_j^g}{\partial t} + \upsilon_z \cdot \frac{\partial \rho \cdot y_j^g}{\partial z} = h_j^m \cdot \rho \cdot S \cdot \left(y_j^w - y_j^g\right) \tag{2.22}$$

$$\frac{\partial \rho \cdot c_p \cdot T^g}{\partial t} + \upsilon_z \cdot \frac{\partial \rho \cdot c_p \cdot T^g}{\partial z} = h^h \cdot S \cdot (T^w - T^g) \tag{2.23}$$

Equations 2.24–2.25 state the model equations for the washcoat phase.

$$\frac{\partial \rho \cdot y_j^{wc}}{\partial t} = -\frac{1}{r} \cdot \frac{\partial - r \cdot D_j \cdot \frac{\partial \rho \cdot y_j^{wc}}{\partial r}}{\partial r} + \omega_j \tag{2.24}$$

$$\frac{\partial \rho \cdot c_p \cdot T^{wc}}{\partial t} = -\frac{1}{r} \cdot \frac{\partial - r \cdot \kappa \cdot \frac{\partial T^{wc}}{\partial r}}{\partial r} + \sum_j \omega_j \cdot H_j^f \tag{2.25}$$

The boundary conditions, for the set of Equations 2.22–2.23, are defined bellow.

$$y_j^g = y_{j,t=0}^g, \quad \text{at t=0 for any z} \tag{2.26}$$

$$T^g = T_{t=0}^g, \quad \text{at t=0 for any z} \tag{2.27}$$

$$y_j^g = y_{j,z=0}^g, \quad \text{at z=0 for any t} \tag{2.28}$$

$$T^g = T_{z=0}^g, \quad \text{at z=0 for any t} \tag{2.29}$$

The boundary conditions for the set of Equations 2.24–2.25, defined bellow.

$$y_j^{wc} = y_{j,t=0}^{wc}, \quad \text{at t=0 for any r} \tag{2.30}$$

$$T^{wc} = T_{t=0}^{wc}, \quad \text{at t=0 for any r} \tag{2.31}$$

$$D_j \cdot \frac{\partial \rho \cdot y_j^{wc}}{\partial r} = h_j^m \cdot \rho \cdot \left(y_j^w - y_j^g\right), \quad \text{at r=}\delta_{wc}\text{ for any t} \tag{2.32}$$

$$D_j \cdot \frac{\partial \rho \cdot y_j^{wc}}{\partial r} = 0, \quad \text{at r=0 for any t} \tag{2.33}$$

$$k^h \cdot \frac{\partial T^{wc}}{\partial r} = h^h \cdot \left(T^w - T^g\right), \quad \text{at r=}\delta_{wc}\text{ for any t} \tag{2.34}$$

$$k^h \cdot \frac{\partial T^{wc}}{\partial r} = 0, \quad \text{at r=0 for any t} \tag{2.35}$$

The link between both phase's equations are done through their shared boundary conditions.

$$y_j^w = y_j^{wc}, \quad \text{at r=}\delta_{wc}\text{ for any t and z} \tag{2.36}$$

$$T^w = T^{wc}, \quad \text{at r=}\delta_{wc}\text{ for any t and z} \tag{2.37}$$

Inside the two-phases heterogeneous model, several approaches might be taken to model the monolithic catalyst. One can consider reaction only at a catalytic wall, consider just the solid phase for the energy balance, steady-state for the reaction-diffusion problem, etc.[8,13]

Going further into the reduction of computational effort, it is possible to neglect the only space dimension considered in the previous gas phase model. Further on these will be referred as 0D models. It has been proved that these models can be really rapidly computed and despite some loss of accuracy are still able to attain a good predictability of the system's behaviour. This is really valuable, specially for models applied in control applications, since fast responses are mandatory to have a proper control. The neglection of any spatial dimension thwarts the description of the flow along the catalyst length and, with this model, the flow is considered completely mixed within the total volume considered, resembling a continuous stirred-tank reactor (CSTR). To overcome this situation, drawing upon the knowledge that a series of CSTRs is able to approximate to the flow description of a plug flow reactor (PFR), it is possible with a fixed number of tanks have a flow description with 0D models.[8]Equations 2.38–2.41 represent the equations for the gas phase 0D models for both pseudo-homogeneous and heterogeneous hypotheses.

Pseudo-Homogeneous Model

$$\frac{\partial \rho \cdot y_j}{\partial t} + \frac{\upsilon_z \cdot \rho \cdot y_j}{\Delta z}\Big|_{outlet} - \frac{\rho \cdot y_j \cdot \upsilon_z}{\Delta z}\Big|_{inlet} = \omega_j \tag{2.38}$$

$$\omega_j = M_j \cdot \sum_n \left(\nu_{j,n} \cdot k_n \prod_i C_i^{\alpha_i}\right)$$

$$\frac{\partial \rho \cdot c_p \cdot T}{\partial t} + \left.\frac{v_z \cdot \rho \cdot c_p \cdot T}{\Delta z}\right|_{outlet} - \left.\frac{v_z \cdot \rho \cdot T}{\Delta z}\right|_{inlet} = \sum_j \omega_j \cdot H_j^f \tag{2.39}$$

Heterogeneous Model

$$\frac{\partial \rho \cdot y_j^g}{\partial t} + \left.\frac{v_z \cdot \rho \cdot y_j^g}{\Delta z}\right|_{outlet} - \left.\frac{v_z \cdot \rho \cdot y_j^g}{\Delta z}\right|_{inlet} = h_j^m \cdot \rho \cdot S \cdot \left(y_j^w - y_j^g\right) \tag{2.40}$$

$$\frac{\partial \rho \cdot c_p \cdot T^g}{\partial t} + \left.\frac{v_z \cdot \rho \cdot c_p \cdot T^g}{\Delta z}\right|_{outlet} - \left.\frac{v_z \cdot y_j \cdot \rho \cdot T^g}{\Delta z}\right|_{inlet} = h^h \cdot S \cdot (T^w - T^g) \tag{2.41}$$

To solve any of these previous equations, besides the inlet and boundary conditions, the model parameters are necessary to be known. These parameters can be empirically obtained and usually are bounded to some certain conditions and assumptions. For example, recalling Equation 2.12, to obtain the pre-exponential factor (A_0) and activation energy (Ea) one must admit a reaction order that predicts the experimental rate and interpolate the function to find the approximate parameters. To predict mass transfer (h_j^m) and heat transfer (h^h) coefficients for the heterogeneous model, average values for some fixed length are usually used to quantify the local transverse gradients at each axial position.[13] For boundary layer problems, such as the one presented here, it is common to use to the concept of dimensionless gradients to account for these gradients in each phase.[13,45] The dimensionless temperature gradient and concentration gradient are known as the ratio between convective and conductive heat transfer (Nusselt number) and the ratio between mass transfer rate and diffusion rate (Sherwood number), respectively. They are both defined in Equations 2.42–2.43.

$$Nu = \frac{h^h \cdot d}{\kappa} \tag{2.42}$$

$$Sh = \frac{h_j^m \cdot d}{D_j} \tag{2.43}$$

Since both scenarios are analogous, only the treatment for heat transfer will be focused, further on, and it can be deduced that for the mass transfer scenario the same conclusions can be applied. For the classical heat transfer problems, for incompressible Newtonian fluids, it is accepted that, for a circle cross-section, the Nusselt number takes values of 3.66 for fully developed region with a constant wall temperature and 4.364 for a constant wall flux.[32,46] For non-reacting fluids, the correlations for constant wall temperature (Nu_T) and constant wall flux (Nu_H) are expressed in Equations 2.44–2.45.[46]

It was stated that, in this type of reactors, the region up to the point of the reactor where the light-off was verified the constant wall flux condition should be used, while after that point onwards the condition to be used was the constant wall temperature.[46]

$$Nu_T = 3.655 + 6.8741 \cdot \left(\frac{Gz}{1000}\right)^{0.488} \cdot \exp\left(-\frac{57.2}{Gz}\right) \tag{2.44}$$

$$Nu_H = 4.364 + 8.68 \cdot \left(\frac{Gz}{1000}\right)^{0.506} \cdot \exp\left(-\frac{41.0}{Gz}\right) \tag{2.45}$$

$$Gz = \frac{d}{x} \cdot Re \cdot Pr \tag{2.46}$$

$$Re = \frac{\rho \cdot v \cdot d}{\mu} \tag{2.47}$$

$$Pr = \frac{c_p \cdot \mu}{\kappa} \tag{2.48}$$

To calculate the Graetz number (Gz) for the mass problem, in Equation 2.46, the Prandtl number (Pr) should be replaced by the Schmidt number (Sc).

$$Sc = \frac{\mu}{\rho \cdot D_j} \tag{2.49}$$

This concept of transfer coefficients reduce the local degrees of freedom and provide a low-dimension description of the transport process in terms of macro-scale averaged variables.[44] The simple explanation presented here, however, is the usual correlations derived for the heat problem analogy, with heat transfer under steady-state and nonreacting conditions (i.e. Graetz-Nusselt problem). The adequacy of these correlations have been studied (and others proposed), and it became evident that the prediction of these coefficients was not straightforward.[46] However, and despite not predicting the same numbers, the order of magnitude was found to be the same and previous applications of these correlations to this type of reactor were already performed.[46]

Chapter 3

Methodology

3.1 Experimental Procedure

The experimental data that are used in this work, for calibration and validation of the models, were obtained at the synthetic gas bench (SGB) of IFPEN. This experimental work was performed in November of 2014. The goal of these experiments was to evaluate the efficiency of a gasoline three-way catalyst (properties in the Table 3.1) in different operating conditions.

Table 3.1: Catalyst properties.

Diameter / in	1.0
Length / in	2.0
Apparent Density / kg/m^3	520
Wall Thickness / thou	3
CPSI	900
Catalyst Loading / g/ft^3	96
PGM (Pt/Pd/Rh)	0/23/1
Ceria Presence	Yes

To see the impact of the temperature on the performance of the catalyst, Light-off tests have been done. They allow to determine at which temperature, this specific catalyst, can promote the conversion of the pollutants. The different tests performed had the same general procedure with variations on concentrations and gas velocity. The changes in the initial conditions, between each tests, are exposed in the Table 3.2.

The unit layout is visible on the Figure 3.1. Before each test the analysers were calibrated for their respective composition ranges. The experimental procedure starts with the flow of a neutral gas (N_2) from the ramp 2, at 50°C, through the catalyst for 120 seconds. During this time, the furnace is electrically heated so that after 120 seconds the temperature on the system, catalyst plus gas flow, can be 100°C. At 120 seconds, the flow from ramp 2 is turned off and simultaneously the flow from ramp

Table 3.2: Initial conditions for each test.

Test	**GHSV**	λ	**Composition**										
			N_2	O_2	CO	CO_2	C_3H_6	NO	NO_2	H_2	N_2O	NH_3	H_2O
	h^{-1}		% (v/v)	% (v/v)	ppm_v	% (v/v)	ppm_vC	ppm_v	ppm_v	% (v/v)	ppm_v	ppm_v	% (v/v)
1	35000	0.95	82.82	2	7000	14	3000	1500	0	2300	0	0	0
2	35000	0.99	83.82	1	7000	14	3000	1500	0	2300	0	0	0
3	35000	1.01	83.32	0.9	11500	14	3000	1500	0	3800	0	0	0
4	35000	1.05	81.74	0.9	23300	14	3000	1500	0	7800	0	0	0
5	35000	–	98.10	1.8	0	0	3000	0	0	0	0	0	0
6	35000	–	97.50	1.8	7000	0	0	0	0	0	0	0	0
7	35000	–	99.15	0	7000	0	0	1500	0	0	0	0	0
8	70000	0.95	82.82	2	7000	14	3000	1500	0	2300	0	0	0
9	70000	0.99	83.82	1	7000	14	3000	1500	0	2300	0	0	0
10	70000	1.01	83.32	0.9	11500	14	3000	1500	0	3800	0	0	0
11	70000	1.05	81.74	0.9	23300	14	3000	1500	0	7800	0	0	0

Table 3.3: Type of analysers used in the experiment.

Analyser Model	Species	Range of Detection
Siemens Ultramat 6	CO	0 - 8 % (v/v)
Siemens Ultramat 6	CO_2	0 - 20 % (v/v)
Siemens Oximat 61	O_2	0 - 25 % (v/v)
Environnement SA GRAPHITE 52M	HC	0 - 10000 ppm_v
Environnement SA TOPAZE 32M	NO_x	0 - 10000 ppm_v
Emmerson NGA 2000	H_2	0 - 5 % (v/v)
Tethys EXM400	NH_3	0 - 700 ppm_v
Emmerson NGA 2000	N_2O	0 - 500 ppm_v

1 is turned on with the composition desired for each test. The flow through the catalyst stabilizes for 280 seconds, so the initial conditions can be properly achieved and after that time an increase of the furnace's temperature will take place, at a rate of 10°C per minute, until the temperature reaches the 450°C. After achieving that temperature, the previous heating rate decreases so that the temperature inside the furnace stabilizes at that temperature. After 3700 seconds from the start of the process, the ramp 1 mixture inlet is closed and a mixture with a composition of O_2 of 10%(v/v) and the rest with N_2 is passed through the catalyst at a temperature of 600°C to make the catalyst's regeneration. After that, the inlet valve of O_2 is closed and the heating turned off so that the furnace temperature can be decreased with a neutral compound (N_2) running through it. A summary of the devices used, for analysing the mixture and their respective properties, is exposed in the Table 3.3.

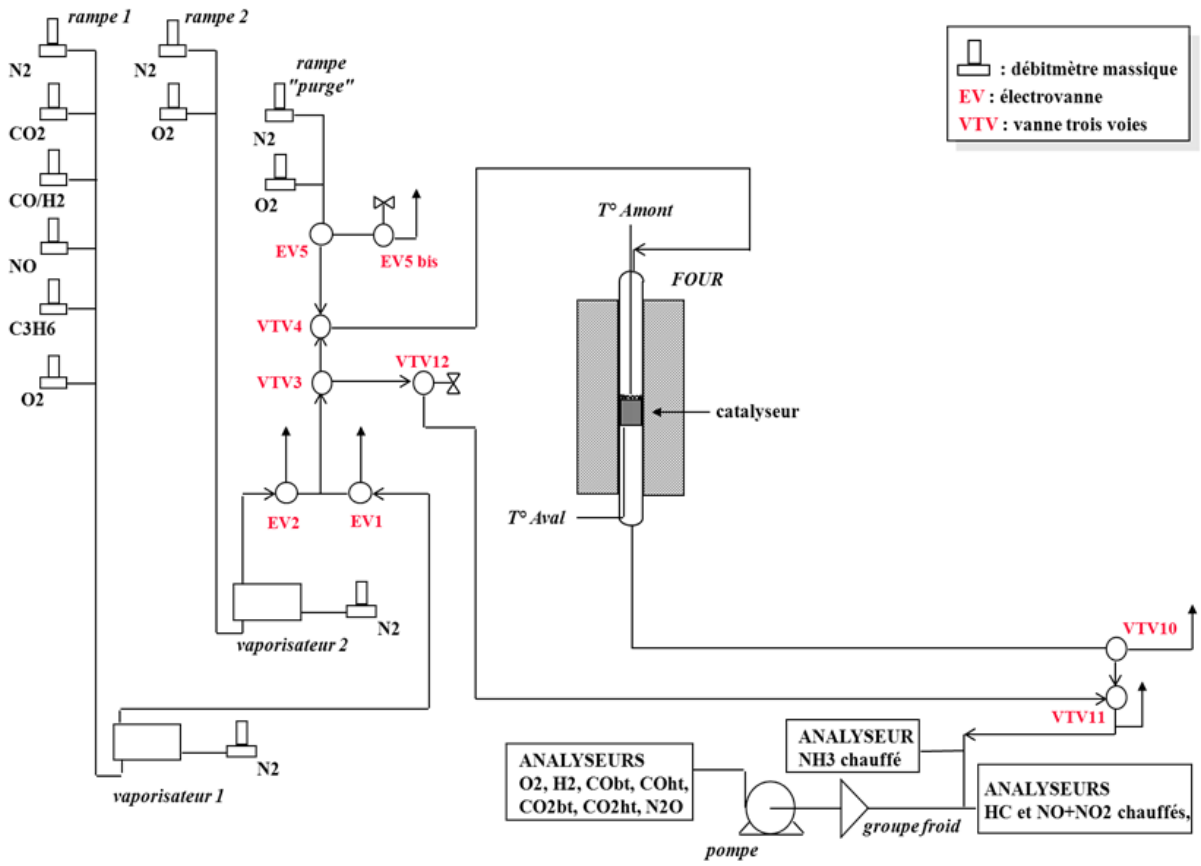

Figure 3.1: Experimental set-up.

3.2 Analysis of Data

From the procedure explained in the section 3.1 “Experimental Procedure”, several data were collected for each of the different 11 tests performed. Tests 1 to 4 emulate the outlet of an engine with different fuel-to-air ratios, to show the impact of this ratio on the TWC’s performance. The tests 8 to 11 have almost exactly the same set-up with the only difference being the increase of the gas flow. The purpose is to show the impact of different flows on the outlet products of the catalyst. The tests 5, 6, and 7, give an important insight on the reaction scheme of the three main reactions (HC oxidation, CO oxidation, and NO_x reduction with CO).

All the results obtained will not be fully analysed since it is not the main goal of the study and only a global view for the following parts, such as the modelling, is required. The results from test 1 and 4 well show the differences between the rich and lean conditions on the TWC operation, and how they need to be reproduced in the model. For both these tests, a trivial analysis of the three main pollutants’ reactions will be performed and the outlet concentration profiles of their reactants and products will be studied. This study has a key importance since, when building a model, it is important to have a good awareness of what happens physically in the system, in order to be able to well translate it to the model. The tests 5 to 7 will also be analysed. The inlet of these experiments was only constituted by simple mixture of two reactants and an inert (N_2), to evaluate each of these reactions separately. From the formation

of products a reaction rate was estimated by numerical differentiation, and from that rate and with the concentrations at each time known, a constant rate was determined and its logarithm graphed against the inverse of the temperature. Equation 3.1 shows this logarithmic relation derived from Equation 2.12. For these tests, a first order reaction was considered for all the three reactions. Since 100% conversion, of the main pollutants, was achieved in all 3 tests, the results displayed were only considered until a 95% conversion was achieved. From this graphic display, it is hoped that a conclusion can be done on the existence of mass transfer limitations, in these reactions, and if they exist what is their type. To confirm the presence of external mass transfer limitation, since mass diffusion and reaction occur in series and the apparent activation energy is controlled by the limiting step, when the kinetic rate starts to reach its high (i.e. at high temperatures), if the mass transfer diffusion hinders the reaction rate this will be revealed by a decrease of the apparent rate slope.

From these 3 experiments other important information can also be withdrawn, to help with a future model calibration.

$$\ln k = \ln A - \frac{Ea}{R \cdot T} \tag{3.1}$$

The experimental results for Tests 5, 6 and 7 are exposed in Appendix A.

3.2.1 Test 1 - Lean Conditions

The results obtained from the 1st test are exposed in the Figure 3.2 and Figure 3.3. From a first global analysis, these results can corroborate what has already been deeply study and proved on this topic. The TWC, in a lean operation, can effectively oxidise all the CO and HC at relatively low temperatures (bellow 250°C, which is relatively low since the TWC is, nowadays, located close to the engine and the temperatures from the outlet of the engine are quite higher). It can also be visualized the major drawback of this catalyst when operating in lean conditions, which is the little reactivity shown by the NO_x.

From the Figure 3.2 it can be seen that the consumption of the CO starts around the same time as the consumption of O_2 and the formation of CO_2. The profile of the CO seems quite simple, and while no other interactions are undervalued (such as impact on the reduction of NO_x or the influence of the water-gas shift) it seems that the consumption of the pollutant is in the majority controlled by the oxidation with O_2. One can also note that the profile of the hydrocarbons moderately resembles the one seen for the CO. The reaction may start a bit later as it is hinted by the profiles of CO_2 and O_2 since, when the consumption of HC starts, the slope of the formation and consumption of each increases. This hints that, probably, this reaction starts a bit later than the oxidation of CO. However, despite starting later the slope of the profile of the HC seems bigger than its counterpart from CO (even after scale corrections). This might indicate a probable faster reaction rate. As in the case of its predecessor, it is essential to have in mind that other reactions might influence the consumption of the HC, despite that, seemingly, the oxidation reaction is the one with the highest influence.

From the Figure 3.3 it is clear that the conditions to reduce the NO_x to NH_3 and N_2O, in lean operation, occur only in a small range of temperatures ($\sim$200-240°C) and are linked to the NO consumption.

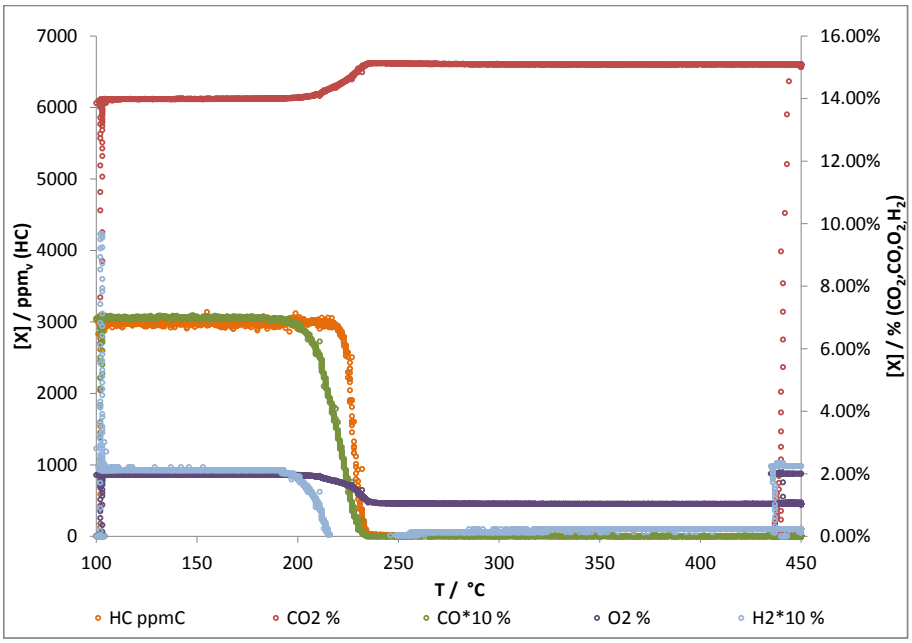

Figure 3.2: Experimental results of Test 1 (λ = 0.95) with the outlet concentrations of CO, HC, CO_2, O_2 and H_2.

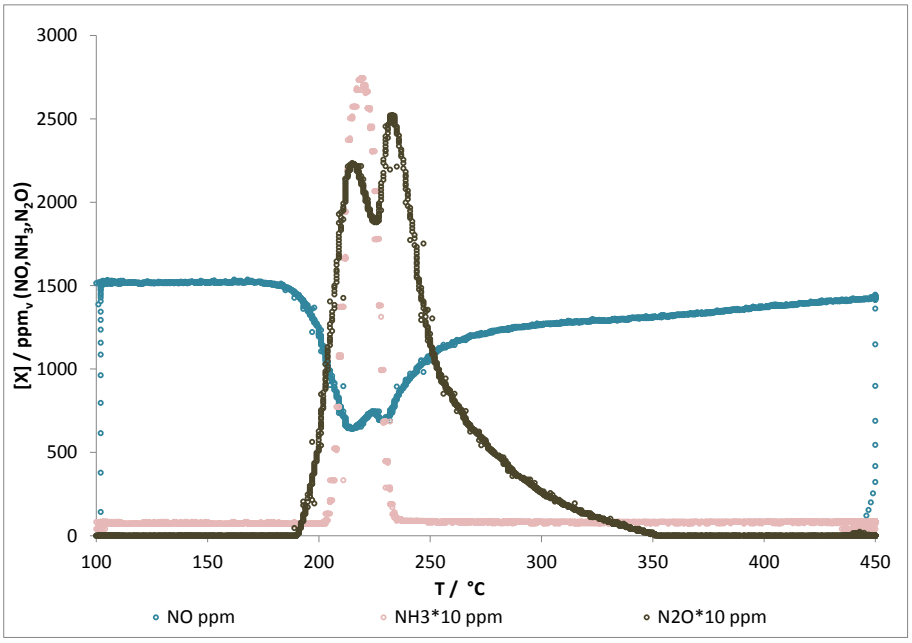

Figure 3.3: Experimental results of Test 1 (λ = 0.95) with the outlet concentrations of NO, NH_3 and N_2O.

3.2.2 Test 4 - Rich Conditions

The impact of the rich operating condition, over a TWC, is shown in the Figure 3.4 and Figure 3.5. Several differences appear with the profiles in the Figure 3.2 and Figure 3.3. The CO consumption is not total at any temperature and the total consumption of the HC is only possible at high temperatures ($\sim$350°C). On the other hand, NOx total consumption is achieved at relatively low temperatures, whereas in the previous case its total consumption was never achiever for all the range of temperatures used on the test. One can also note that after a certain temperature, the formation of NH_3 is stably promoted

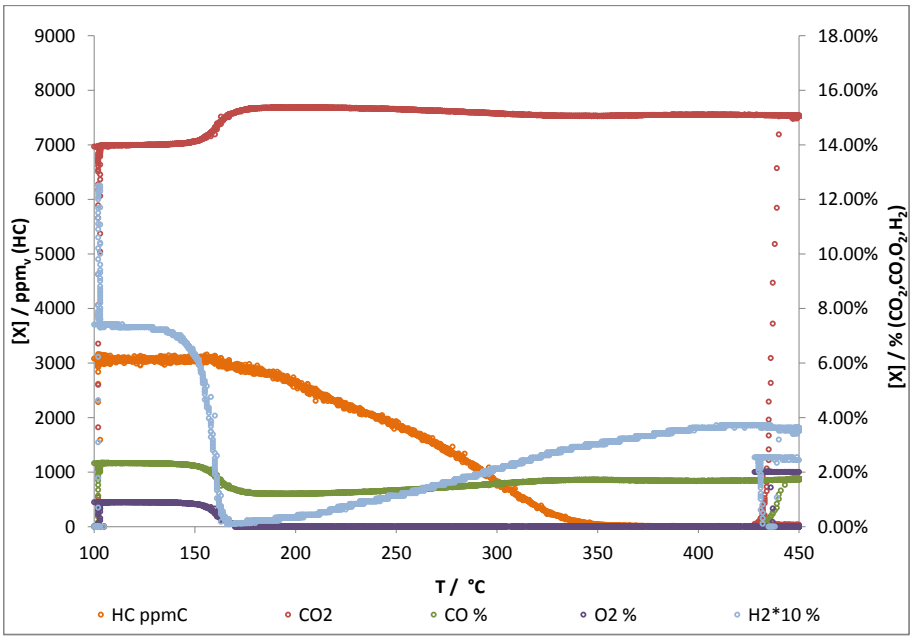

Figure 3.4: Experimental results of Test 4 (λ = 1.05) with the outlet concentrations of CO, HC, CO_2, O_2 and H_2.

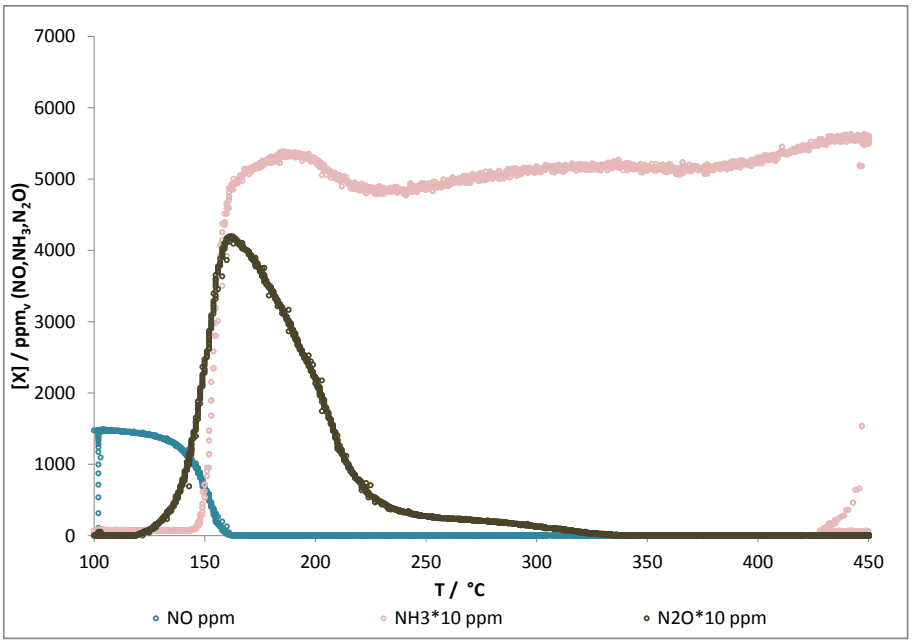

Figure 3.5: Experimental results of Test 1 (λ = 1.05) with the outlet concentrations of NO, NH_3 and N_2O.

and its selectivity from the reagent NO_x despite some small fluctuation does not show a big variation. Nonetheless, N_2O formation appears to still be only promoted in a range of low temperatures, despite that in rich operation this range seems to be bigger than the one show in its counterpart lean experiment.

The oxidation of CO is never fully performed, as can be proved in Figure 3.4. Furthermore, the profile of the CO through all the range of temperatures has some fluctuation. That seems to somehow influence the formation of CO_2, as in its profile the same fluctuations are present but with an inverse direction. This profile can arise from multiples sources and since no further study was done to answer

this particular question, some simple considerations, to try to explain the shape of such profile, will be done. This will help to keep clear in mind some possible external sources of influence, in this reaction. The HC can be one of the sources of this phenomena that influences the CO profile by two ways, either by competitive oxidation with CO for O_2 or by the steam reforming reaction that would generate CO. This last one could also explain the resurgence of H_2 above a certain temperature.The competitive reduction to react with NO_x can also have some influence on the concentration of CO. Another source of impact that can be considered is that, with higher temperatures, and since the concentration of the H_2 on the gas increases, the water-gas shift equilibrium is slightly changed which will directly influence the CO profile. With the data available it was impossible to make further evaluations and test these hypothesis presented. An impact of one of these, or even a combination of all these phenomena, can be behind the shape of the CO profile. Since it is not possible to arrive to an answer from this data, it is just important to retain, from this simple analysis, the information that we are in the presence of a quite complex system and that a lot of interaction between each species happens. So when facing the task of modelling these phenomena, it is important to remember all possible sources of influence and see if a correct description can be achieved.

Figure 3.5 shows that a stable formation of NH_3 is possible through the reduction of NO_x in rich operation, above a certain temperature. The profile shown by NH_3 also displays some fluctuation. One can query if this profile arises from the same sources than the one shown by CO or if other reasons, such as competitiveness of NO_x reduction reactions can be the cause. The N_2O formation continues to be promoted at low temperatures, as was already suggested by several literature.[9,21,25,26]

3.2.3 Test 5 - CO Oxidation

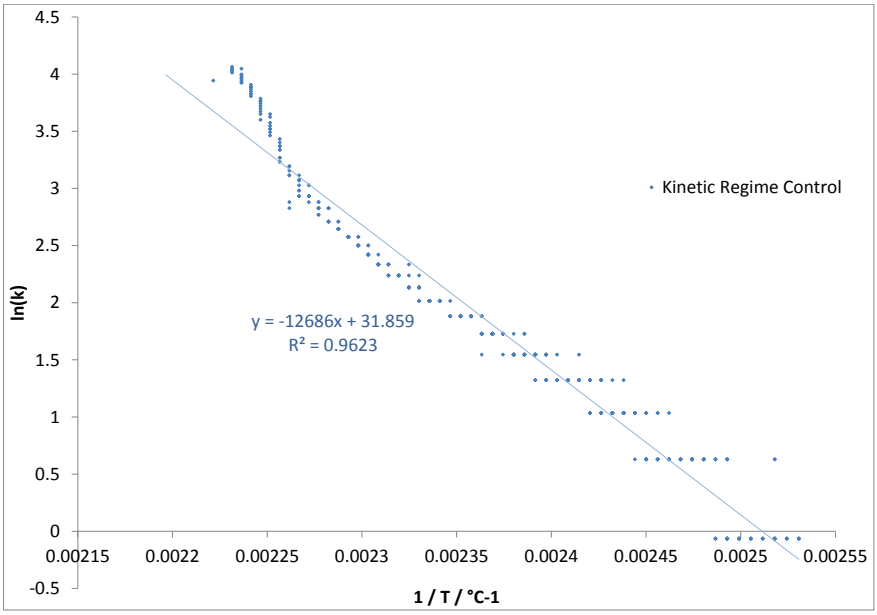

Figure 3.6: Temperature dependence of the observed reaction rate constant for the carbon monoxide oxidation with oxygen.

Table 3.4: Values of the observed rate constant and activation energy for kinetic regime, in test 5.

	Kinetic Regime	Mass Transfer Regime
A_0 / mol/s	6.855×10^{13}	-
Ea / J/mol	105473.65	-

In test 5, the oxidation of CO with only O_2 was performed. In Figure 3.6, the linearised dependency does not show, at first sight, a mass transfer limitation on the reaction rate. However, at higher temperatures a odd profile arises since the slope of the linear dependency seems to increase. A explanation for this phenomenon was not withdrawn.

3.2.4 Test 6 - HC Oxidation

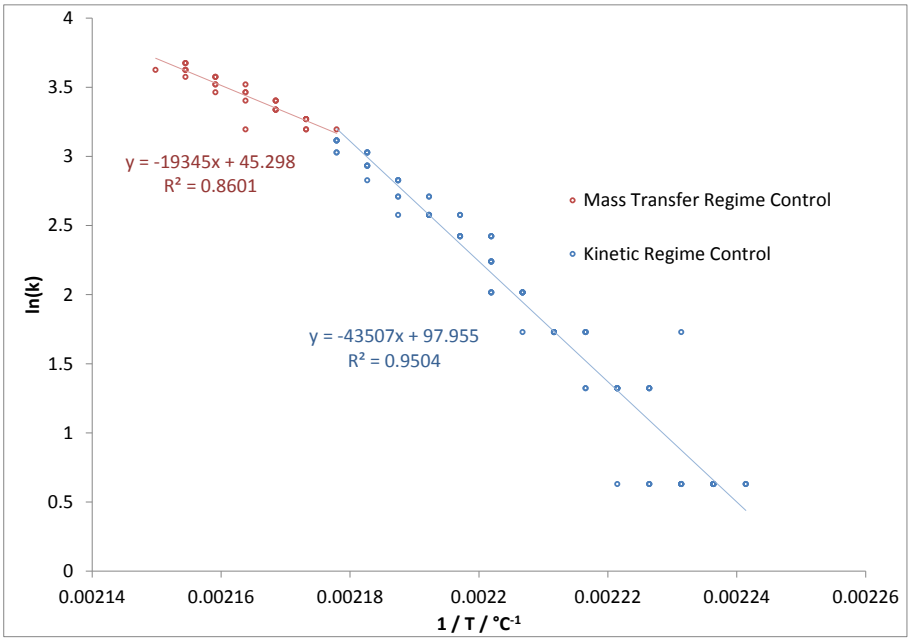

Figure 3.7: Temperature dependence of the observed reaction rate constant for the hydrocarbons oxidation with oxygen.

Table 3.5: Values of the observed rate constant and activation energy for both regimes, in test 6.

	Kinetic Regime	Mass Transfer Regime
A_0 / mol/s	3.476×10^{42}	4.708×10^{19}
Ea / J/mol	361713.70	160833.55

In the test 6, the oxidation of HC with O_2 was performed. The linearised dependency of this constant rate's profile, in function of the temperature's inverse, can be seen to have the two different regions well expressed in Figure 3.7. At low temperatures, the reaction rate is not limited by diffusional resistance and the observed reaction rate is expected to be the true rate of the reaction. At higher temperatures, as

the reaction rate increases, this mass and heat transfer inhibition start to show on the observed reaction rate and a lowering of the slope can be noticed.

The calculated observed constant rate pre-exponential factor and activation energy, for both different regions, are exposed in Table 3.5. A comparison with the values of the previous test, can also indicate, that this reaction has a faster rate than the oxidation of CO, as already suggested before. The values for the activation energy of CO and HC are consistent with the oxidation activity ranking observed in other studies, with CO having a lower activation energy than HC.[15,16]

3.2.5 Test 7 - NO Reduction

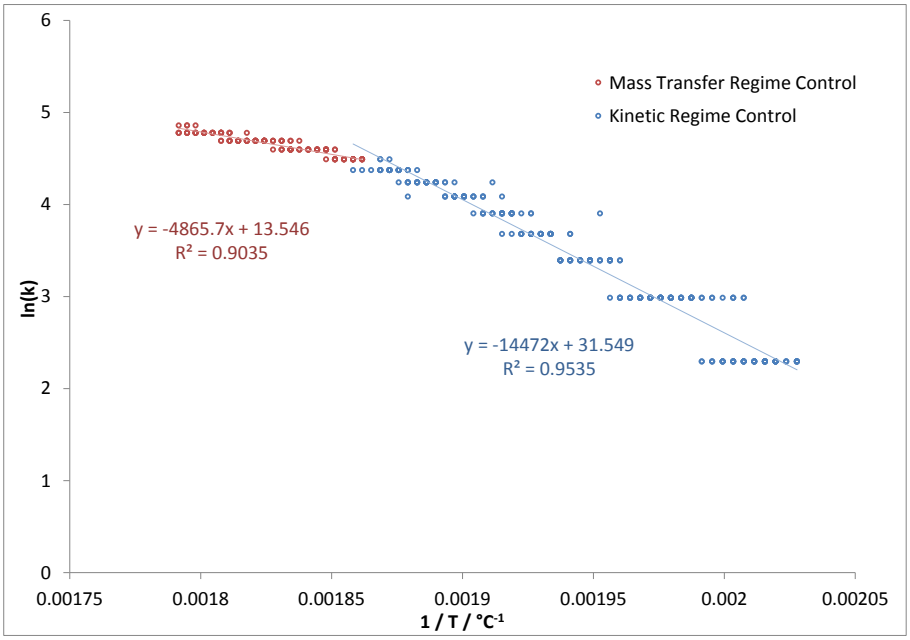

Figure 3.8: Temperature dependence of the observed reaction rate constant for the nitric oxide reduction with carbon monoxide.

Table 3.6: Values of the observed rate constant and activation energy for both regimes, in test 6.

	Kinetic Regime	Mass Transfer Regime
A_0 / mol/s	5.029×10^{11}	7.640×10^{5}
Ea / J/mol	120316.46	40453.18

In the last performed test of this kind, the reaction studied was the reduction of nitric oxide with carbon monoxide. As in the previous test, when also observing the linearised dependency of this constant rate's profile in function of the temperature's inverse, two different regions in the Figure 3.8 can be detected. The same reasoning done for the arise of this type of profiles in the previous test, holds true for this case.

The calculated observed constant rate pre-exponential factor and activation energy for both different regions are exposed in Table 3.6.

3.3 Modelling Approach

Model development and simulation of the exhaust line were done using the software LMS Imagine.Lab Amesim^{TM}. The modelling part was divided in two different approaches with two final different applications.

The first modelling part did not start from scratch, but from an existing model developed by IFP Energies Nouvelles. This model is oriented for control applications, in which not only a reliable output is mandatory but also fast computational times. To achieve the best compromise between these two goals, some assumptions were done. A thorough explanation of the type of assumptions commonly done in the modelling of monolithic catalysts are already described in the section 2.2 “Catalyst Modelling”. As so, in this section will only be summarized which of these assumptions were taken on the original model and which modifications were performed during the realization of this work.

The flow through the channel of a TWC cannot be described with a perfect reactor model. An association of reactor models is needed. In Amesim 0D model, to lower computational effort, the spatial description in all directions is to be neglected and only a time description is taken into account for a fixed volume. This makes the assumption that, in a single volume, the flow is perfectly mixed and the properties are constant in all the volume considered, which corresponds to an ideal continuous flow stirred-tank reactor (CSTR). In this work, it was considered that a series of CSTR could be enough to reproduce the flow with accuracy enough for a control application and with a small computational effort able to meet the demands. To find the optimal values of tanks required to have a sufficient flow description, an analysis of the residence distribution times in the catalyst is required.

Moving onto the kinetic description of this model, originally it took into account 8 kinetic reactions, that will be described in the following chapter. With the evolution of operating conditions of gasoline engines and to be able to address the questions raised by the new exhaust lines designs proposed, it was clear, that the complexity of the model had to be improved in order to take into account, at least, the formation and consumption of NH_3. So, the work was to improve the kinetic part of the model using the conclusions of the bibliographic study. One model was selected to provide the ammonia kinetic equations to the model. This model was extracted from the work of Ramanathan et al.(2012).[9] After adding of the kinetic equations into the code of the existing model, some manual calibrations of the kinetic parameters were performed, for both rich and lean operation, in order to meet the results obtained with experimental tests 1 and 4 performed at IFPEN. Tests 2 and 3 were used to validate the model and see how the model behave on other experimental conditions. It is important to note that ceria reactions were neglected in this modelling work, but this device is present in the catalyst and have an influence on the experimental outlet results. It is expected then, that some deviations between experimental and model results are observed and even some reaction parameters might be calibrated comprising some phenomena that is not intrinsically related with that reaction, but instead with a reaction with a ceria component.

The second direction undertaken was to evaluate the limits of the transport phenomena in the control model and to improve the modelling approach. The work performed in this part has a slightly different

role and purpose than the one performed previously. While on the first part, the goal was a model for control purposes, on the second part, a model to solve design questions regarding the washcoat was built. It has been common practice in modelling of honeycombed catalysts to use either the pseudo-homogeneous assumption or a steady-state heterogeneous assumption.[8,32] The goal was then to see if a transient heterogeneous model would be able to give accurate results, with acceptable calculation times, and bring added information to the models already present in the literature. The model present at IFP Energies Nouvelles was one with a pseudo-homogeneous assumption, in which only one phase is considered, the bulk gas phase. The idea was then to design a complete new component to model all the washcoat phenomena (i.e. diffusion and reaction), to describe the interaction between each phase (bulk gas and solid) and to remove all the phenomena from the bulk gas phase which did not happen there (such as the removal of all the reaction's kinetic treatment of this component).

All the simulations were performed in the same computer, for the sake of performance comparison between models. The computer properties are described in Table 3.7.

Table 3.7: Computer properties.

Computer Model	DELL OPTIPLEX 740MLK SF
CPU	AMD X2 5800 3GHz
RAM memory	4 GB

Chapter 4

Modelling Results

4.1 Approach 1: Control Model

The "control" model available at IFPEN for the TWC did not have the NH_3 dynamics accounted in it. With the current drive in optimizing the operation of SIDI engines, the relevance of studying these reactions has increased. As already explained, a model designed for control applications requires low computational effort, since computational power is not easily available in a vehicle system and fast responses are desired in order to have a proper control action.

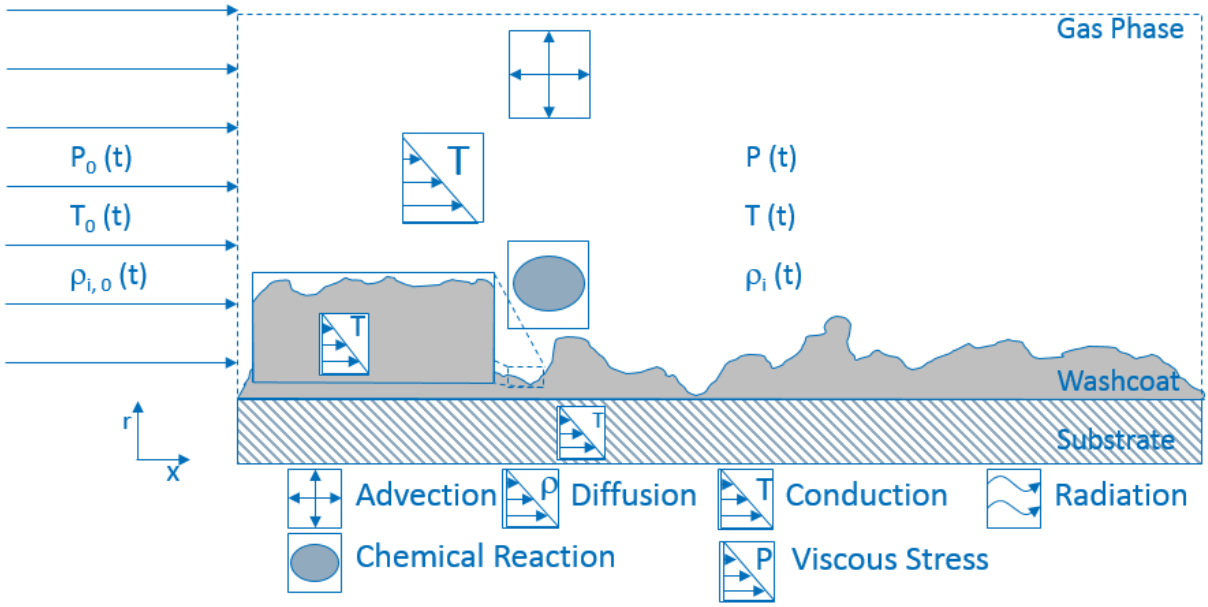

Figure 4.1: Summary of the phenomena considered for the "control" model.

For the phenomena transport treatment, the control model considered a single channel, 0D model, pseudo-homogeneous (only the bulk gas phase), with axial mass and energy transfer, and an enthalpic balance done in the interface between the solid and the gas phases. A summary of the phenomena considered for this model is displayed in Figure 4.1 and the governing equations that describe the phe-

nomena depicted on this figure are exposed in Table 4.1.

Table 4.1: Governing equations for the “control” model.

Bulk Gas Axial Flow Governing Equations	
Mass Balance	$\frac{\mathrm{d}m \cdot y_j}{\mathrm{d}t} = (y_j \cdot \dot{m})\Big\vert_{in} - (y_j \cdot \dot{m})\Big\vert_{out} + \omega_j$
Energy Balance	$m \cdot c_v \cdot \frac{\mathrm{d}T}{\mathrm{d}t} + m \cdot \sum_j \frac{\mathrm{d}y_j}{\mathrm{d}t} \cdot u_j + \frac{\mathrm{d}m}{\mathrm{d}t} \cdot \int c_v \cdot \mathrm{d}T = \sum_j m_j \cdot h'_j + \frac{\mathrm{d}Q}{\mathrm{d}t} - P \cdot \frac{\mathrm{d}V}{\mathrm{d}t}$
Interface Gas-Solid Phases Governing Equations	
Energy Balance	$\rho_{app} \cdot c_p^s \cdot V_{cat} \cdot \frac{\mathrm{d}T^w}{\mathrm{d}t} = h^h \cdot S \cdot (T - T^w) - q\Big\vert_{out} - \sum_n \Delta H_n^r \cdot \omega_n$

4.1.1 Spatial Discretization

As it is evident from the Figure 4.1 and Table 4.1, in this model there is a neglection of all spatial dimensions, and the model behaves like an homogeneous tank. To perform simulations to test this model, a residence time distribution analysis needs to be performed with the catalyst to determine the amount of tanks required to have a proper description of the flow inside the TWC. To study the residence time distribution, standard techniques exist to have a rigorous determination of the flow profile inside the reactor. Unfortunately it was not possible to perform such experiments and, as a way to have an idea of how many tanks were required to have a good compromise between low computational effort and flow description, a more casual approach was undertook. With the inlet mixture for the tests performed, the component with the closest profile to the one of a tracer was the one of CO_2, since at inlet conditions was considered to be inert, stable, not adsorbing in the catalyst, have similar properties to the reactional mixture and not changing the hydrodynamic behaviour of the reactor.[47] It is quite clear that this is not a rigorous analysis, and if a correct one is to be done a experimental set-up needs to be performed with a proper tracer choice and with a correct amount injected at a known time and location. However, since this was not the main scope of the work, the procedure went with the already existing data.

It is possible to determine the mean residence time (τ) in the reactor, through the Equation 4.3.[47]

$$F(t) = C(t)/C_0 \tag{4.1}$$

$$E(t) = \frac{\mathrm{d}F(t)}{\mathrm{d}t} \tag{4.2}$$

$$\tau = \int_0^\infty t \cdot E(t)\mathrm{d}t \tag{4.3}$$

The global residence time distribution for a series of CSTR can be calculated through Equation 4.4, with N being the number of reactors in series.[48]

$$E(t) = \left(\frac{N}{\tau}\right)^N \cdot \frac{t^{N-1} \cdot \exp\left(-\frac{N \cdot t}{\tau}\right)}{(N-1)!} \tag{4.4}$$

With this, it is possible to plot the experimental residence time distribution and contrast it with a series of CSTR and analyse which is the number of reactors required to model the real reactor. This is shown in Figure 4.2.

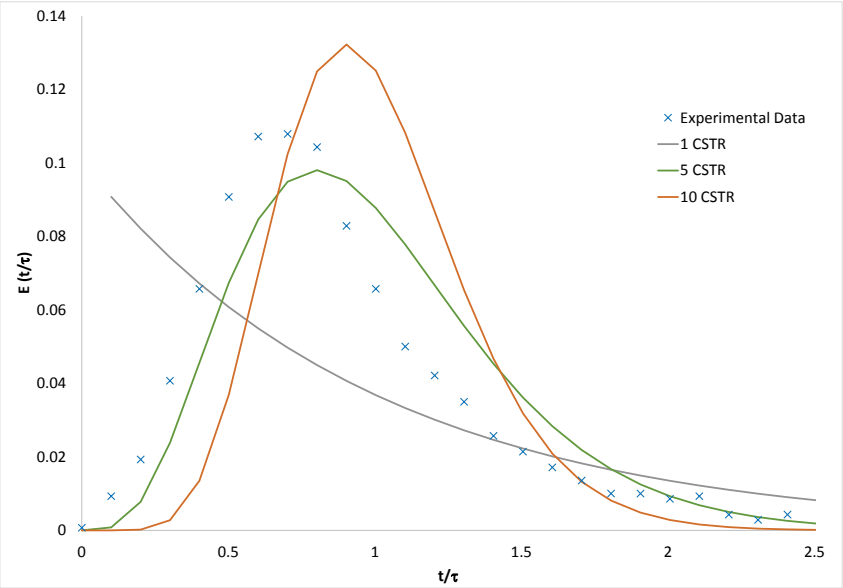

Figure 4.2: Residence time distribution for the experimental data and the 3 different CSTR series.

Table 4.2: Mean distribution time for the experimental data and the 3 different CSTR series.

	Residence Time / s
Experimental Data	9.97
1 Reactor	9.91
5 Reactors	9.97
10 Reactors	9.97

With these results, the choice was to model the real reactor with a series of 5 0D model components (or tanks), since it had the profile which most resembled the one from the experimental data.

4.1.2 Global Kinetic Treatment

The kinetic model available in the TWC component of the IFP-Exhaust library is summarized in the Table 4.3.

The reaction rate constant parameters (k_j) from Table 4.3 are defined with an Arrhenius Law as in Equation 2.12. The equilibrium constant (k_{eq}) is defined as expressed in Equation 4.5. The G_1 and G_2 parameters present in the same table, are adsorption and inhibition parameters. They are expressed in the Equation 4.6 and Equation 4.7.

$$k_{eq} = A_{eq} \cdot \exp\left(\frac{Ea_{eq}}{R \cdot T^w}\right) \tag{4.5}$$

Table 4.3: Original kinetic model for the TWC.

Equation	Kinetic Model
$CO + 0.5O_2 \longrightarrow CO_2$	$\omega_1 = \frac{k_1 \cdot x_{CO} \cdot x_{O_2}}{G_1}$
$C_3H_6 + 4.5O_2 \longrightarrow 3CO_2 + 3H_2O$	$\omega_2 = \frac{k_2 \cdot x_{C_3H_6} \cdot x_{O_2}}{G_1}$
$CO + NO \longrightarrow CO_2 + 0.5N_2$	$\omega_3 = \frac{k_3 \cdot x_{CO} \cdot x_{NO}}{G_2}$
$C_3H_6 + 9\,NO \longrightarrow 3\,CO_2 + 3\,H_2O + 4.5\,N_2$	$\omega_4 = \frac{k_4 \cdot x_{C_3H_6} \cdot x_{NO}}{G_1}$
$C_3H_6 + 3\,H_2O \longrightarrow 3\,CO + 6\,H_2$	$\omega_5 = \frac{k_5 \cdot x_{C_3H_6} \cdot x_{H_2O}}{G_1}$
$CO + H_2O \rightleftarrows CO_2 + H_2$	$\omega_6 = \frac{k_6 \cdot \left(x_{CO} \cdot x_{H_2O} - \frac{x_{CO} \cdot x_{H_2O}}{k_{eq}}\right)}{G_1}$
$H_2 + 0.5O_2 \longrightarrow H_2O$	$\omega_7 = \frac{k_7 \cdot x_{H_2} \cdot x_{O_2}}{G_1}$
$H_2 + NO \longrightarrow H_2O + 0.5N_2$	$\omega_8 = \frac{k_8 \cdot x_{H_2} \cdot x_{NO}}{G_1}$

$$G_1 = T^w \cdot (1 + K_0 \cdot x_{CO} + K_1 \cdot x_{HC})^2 \cdot (1 + K_2 \cdot x_{CO}^2 \cdot x_{HC}^2) \cdot (1 + K_3 \cdot x_{NO}^{0.7}) \tag{4.6}$$

$$G_2 = (1 + K_4 \cdot x_{CO})^2 \cdot (1 + K_5 \cdot x_{NO})^2 \tag{4.7}$$

To improve the kinetic scheme and be able to predict NH3 formation or consumption, three reaction schemes involving NH3, based on the work of Ramanathan et al.(2012)[9], were added to the global kinetic scheme of the model, as shown in Table 4.4.

Table 4.4: Added kinetic reactions to the original model.

Equation	Kinetic Model
$NH_3 + 1.25O_2 \longrightarrow NO + 1.5\,H_2O$	$\omega_9 = \frac{k_9 \cdot C_{NH_3} \cdot C_{O_2}}{G_1}$
$NO + 2.5\,H_2 \longrightarrow NH_3 + H_2O$	$\omega_{10} = \frac{k_{10} \cdot C_{H_2} \cdot C_{NO}}{G_1}$
$NH_3 + 1.5\,NO \longrightarrow 1.25\,N_2 + 1.5\,H_2O$	$\omega_{11} = \frac{k_{11} \cdot C_{NH_3} \cdot C_{NO}}{G_1}$

The inhibition factor was considered to be the same to simplify and reduce the calibration effort. These parameters were maintained constant through all the study, and their formula is exposed in Table 4.5.

Table 4.5: Inhibition parameters.

$K_0 = 65.6 \cdot \exp\left(\frac{961}{T^w}\right)$
$K_1 = 2080 \cdot \exp\left(\frac{361}{T^w}\right)$
$K_2 = 3.98 \cdot \exp\left(\frac{11611}{T^w}\right)$
$K_3 = 479000 \cdot \exp\left(\frac{-3733}{T^w}\right)$
$K_4 = 53 \cdot \exp\left(\frac{1200}{T^w}\right)$
$K_5 = 53 \cdot \exp\left(\frac{1500}{T^w}\right)$

4.1.3 Model Calibration

Calibration of the kinetic parameter of the different reaction rates has been done manually, by trying to fit the model results with the experimental curves. The model was calibrated in lean (λ = 0.95) and rich (λ = 1.05) conditions. The values of the kinetic parameters obtained are given in Table 4.6

Table 4.6: Kinetic model parameters after calibration.

Equation	Lean Operation		Rich Operation	
	A / $mol \cdot K/s$	Ea / J/mol	A / $mol \cdot K/s$	Ea / J/mol
$CO + 0.5O_2 \longrightarrow CO_2$	6.72×10^{12}	72000	2.00×10^{13}	52000
$C_3H_6 + 4.5O_2 \longrightarrow 3CO_2 + 3H_2O$	4.37×10^{13}	99000	4.37×10^{13}	105000
$CO + NO \longrightarrow CO_2 + 0.5N_2$ [1)]	1.60×10^{8}	100100	1.60×10^{8}	99100
$C_3H_6 + 9\,NO \longrightarrow 3\,CO_2 + 3\,H_2O + 4.5\,N_2$	5.47×10^{12}	101600	5.47×10^{11}	121600
$C_3H_6 + 3\,H_2O \longrightarrow 3\,CO + 6\,H_2$	1.04×10^{8}	42900	1.04×10^{8}	48000
$CO + H_2O \rightleftharpoons CO_2 + H_2$ [2)]	5.77×10^{10}	80300	5.77×10^{9}	90300
$H_2 + 0.5O_2 \longrightarrow H_2O$	1.72×10^{18}	117000	1.72×10^{15}	55000
$NO + H_2 \longrightarrow 0.5\,N_2 + H_2O$	1.00×10^{15}	75500	1.50×10^{13}	35000
$NH_3 + 1.25O_2 \longrightarrow NO + 1.5\,H_2O$ [3)]	1.00×10^{5}	110400	1.00×10^{6}	75000
$NO + 2.5\,H_2 \longrightarrow NH_3 + H_2O$ [3)]	2.03×10^{6}	65000	8.00×10^{8}	62000
$NH_3 + 1.5\,NO \longrightarrow 1.25\,N_2 + 1.5\,H_2O$ [3)]	1.00×10^{5}	126400	5.00×10^{6}	70000

1) For this reaction's kinetic rate, the pre-exponential parameter (A) unit is mol/s

2) For this reaction's equilibrium constant, the parameters are: $k_{eq} = 0,0126$ and $Ea_{eq} = 29000\ J/mol$

3) For these reactions' kinetic rate, the pre-exponential parameter (A) unit is $mol \cdot (m^3/mol)/s$

Lean Operating Conditions - λ = 0.95

The catalyst composition outlet results for the model simulations, in lean operation, are plotted against the experimental data obtained in Test 1, in Figure 4.3 and Figure 4.4.

The results' global analysis highlights that the phenomena are quite well described when the system runs in lean conditions. However, some calibration and model improvements can still be done. For example, in Figure 4.3, the model predicts that the hydrocarbons consumption starts only after the full consumption of carbon monoxide. But in the experimental results is clear that the consumption of the HC starts when the CO is still not fully consumed in the system and even has a slower consumption rate than the HC. Also the reaction rates can be slightly improved since the slopes not always have a good description of the profile evidenced by the experimental data. The two peaks observed in the NO experimental profile, in Figure 4.4, are also not reproduced by the model. This is expected since the behaviour behind this profile is probably due to the dynamics of N_2O and this reaction is not taken into account in this model.

Consequently, regarding the performance of the model's enthalpy balance, the predicted outlet tem-

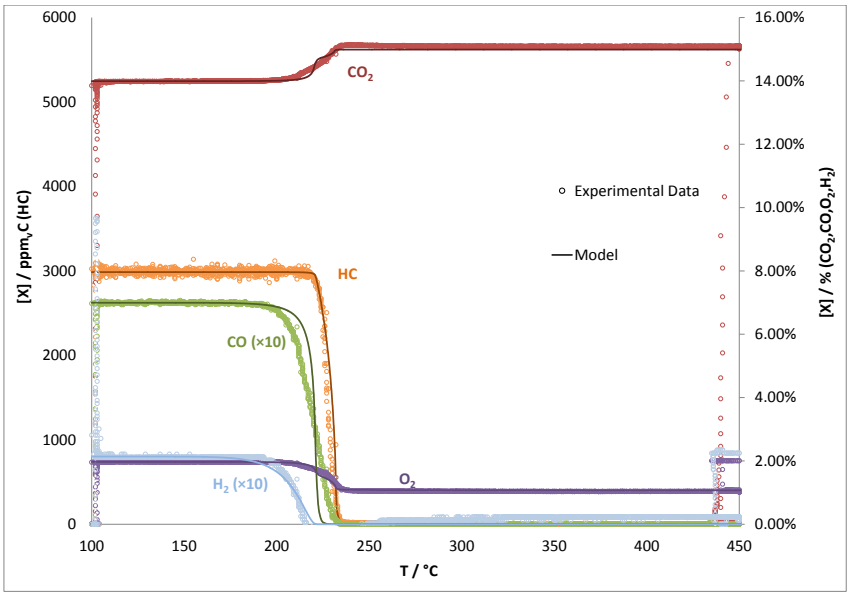

Figure 4.3: "Control" model results for lean conditions (λ = 0.95) with the outlet concentrations of CO, HC, CO_2, O_2 and H_2.

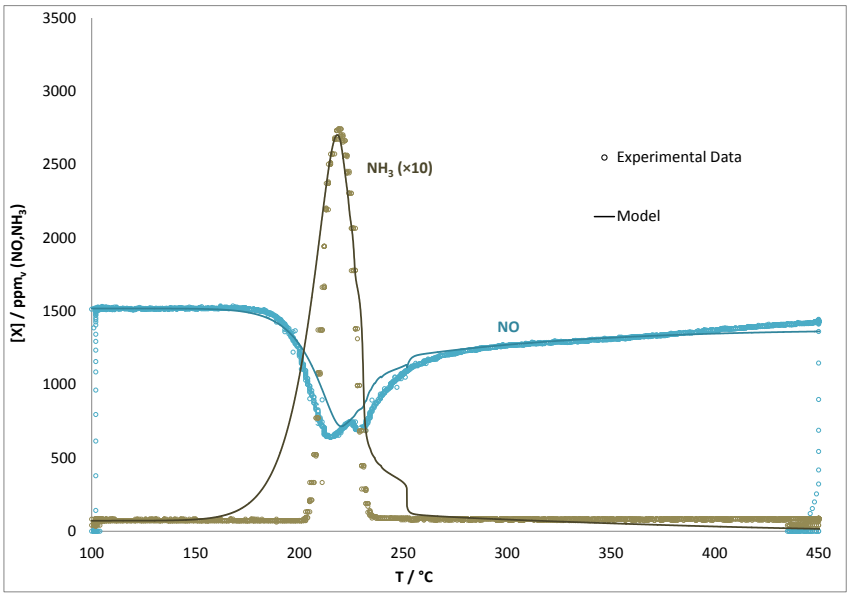

Figure 4.4: "Control" model results for lean conditions (λ = 0.95) with the outlet concentrations of NO and NH_3.

perature increase sooner, in the time scale, than it is physically observed. Also the temperature stabilizes at a higher temperature. Besides the obvious deviation that the mass balance shifts induce in the enthalpy balance, one can also explain this deviation from the fact that an isenthalpic system is being considered, with no radially heat losses being taken into account.

The conversion of the three main pollutants in function of the temperature are graphed in the Figure 4.6. The light-off temperatures for these pollutants, experimentally obtained and predicted by the model, are in Table 4.7.

The CPU time needed to compute these results was 11.047 seconds.

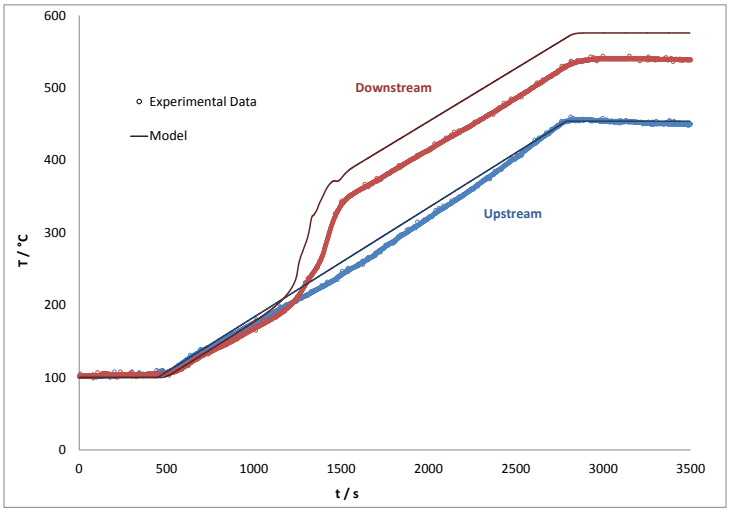

Figure 4.5: "Control" model results for lean conditions (λ = 0.95) with the temperature upstream and downstream of the catalyst.

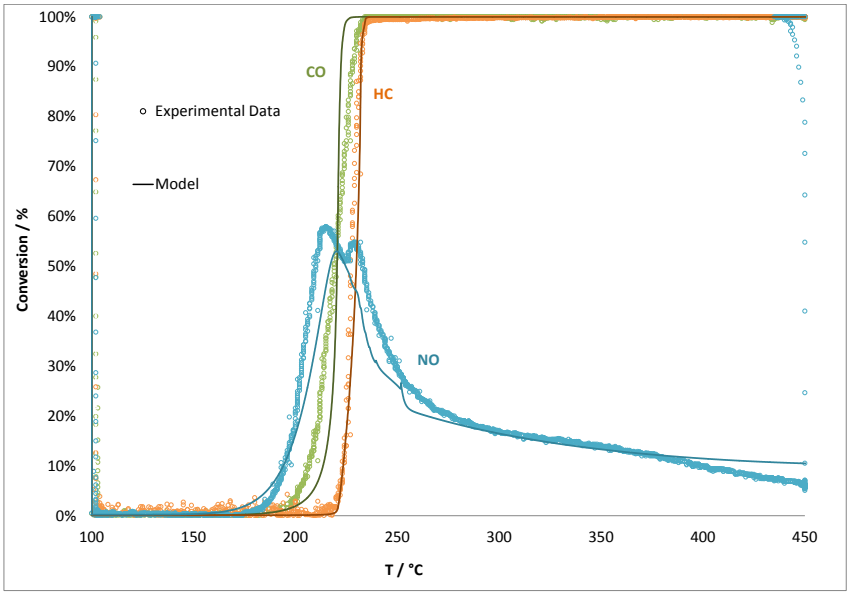

Figure 4.6: Model results for lean conditions (λ = 0.95) with the conversion of the three main pollutants in function of the temperature.

Table 4.7: "Control" model and experimental light-off temperature results in lean conditions (λ = 0.95).

Components	CO	HC	NO_x
Experimental Data	219 ℃	227 ℃	210 ℃
Model	220.4 ℃	229.9 ℃	216.8 ℃
Error	0.64 %	1.26 %	3.22 %

Rich Operating Conditions - λ = 1.05

The catalyst composition outlet results for the model simulations, in rich operation, are plotted against the experimental data obtained in Test 4, in Figure 4.7 and Figure 4.8.

The performance of the model in rich conditions has also a good overall description. Nonetheless,

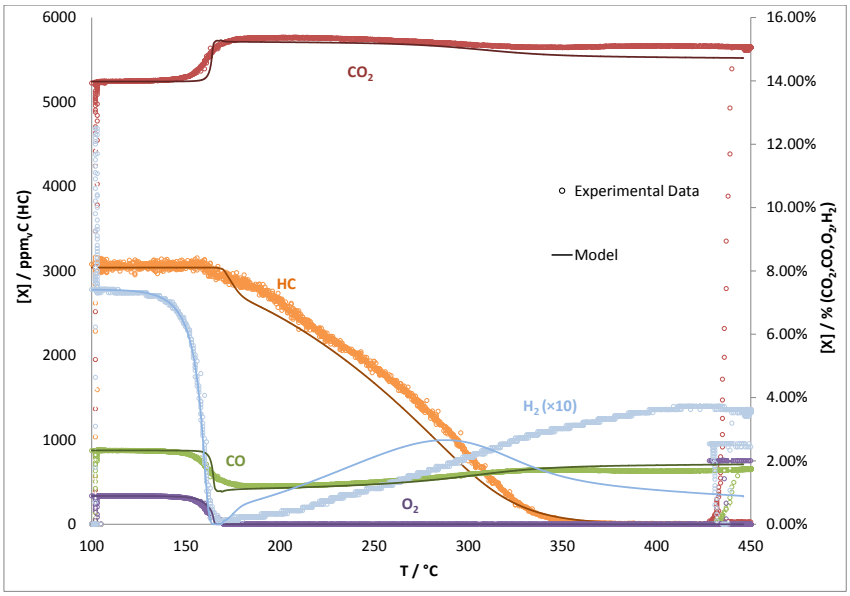

Figure 4.7: "Control" model results for rich conditions (λ = 1.05) with the outlet concentrations of CO, HC, CO_2, O_2 and H_2.

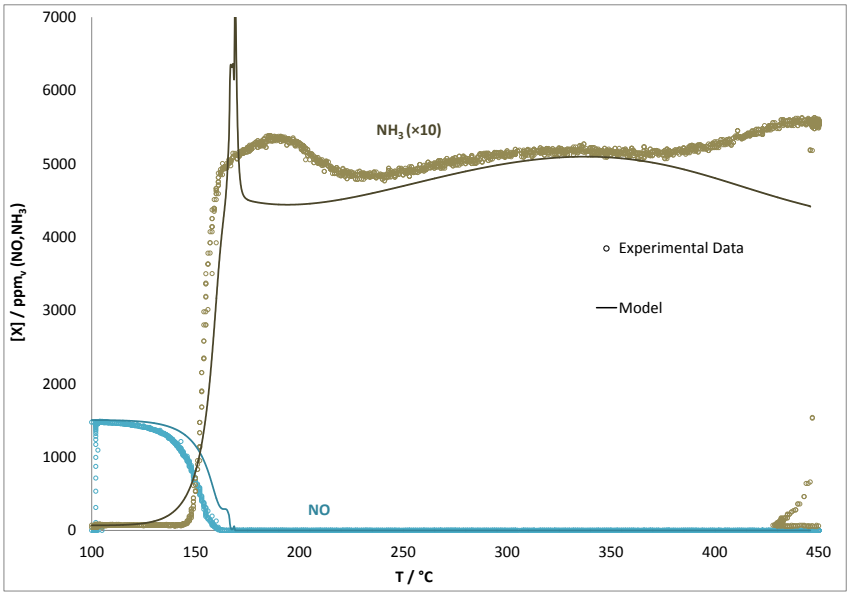

Figure 4.8: "Control" model results for rich conditions (λ = 1.05) with the outlet concentrations of NO and NH_3.

shifts are more pronounced in these conditions. Above 300°C, it needs to be highlighted the inability of the model to predict the correct behaviour of the H_2 profile.

NO_x consumption and NH_3 formation profiles are graphed in Figure 4.8. The highlight of these results is that NH_3 formation can be relatively well predicted with this model. It is important to recall what was explained in section 2.1 "Technology", regarding the new approaches for exhaust line designs. If the periodic operation between rich and lean conditions is proved to be the most efficient way to operate SIDI engines, models like this one prove their value by their fast calculations times and good overall prediction of NH_3 formation. There is, however, some phenomena that can be better described. The first peak of

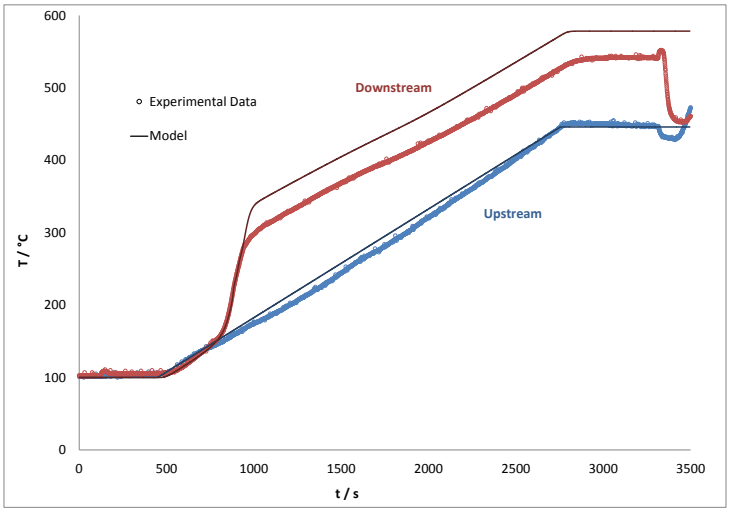

Figure 4.9: "Control" model results for rich conditions (λ = 1.05) with the temperature upstream and downstream of the catalyst.

NH_3 computed does not appear in the experimental data's profile. At around the same temperature of this NH_3 peak ($\sim$160°C), the NO model profile also shows a step formation in its profile. There is a possibility that both these phenomena are linked. A possible explanation could be a bad balance in the kinetic's dynamics of all reactions that may disrupt the smoothness seen in the experimental data's profile.

The temperatures at the positions upstream and downstream of the catalyst is graphed in the Figure 4.9.

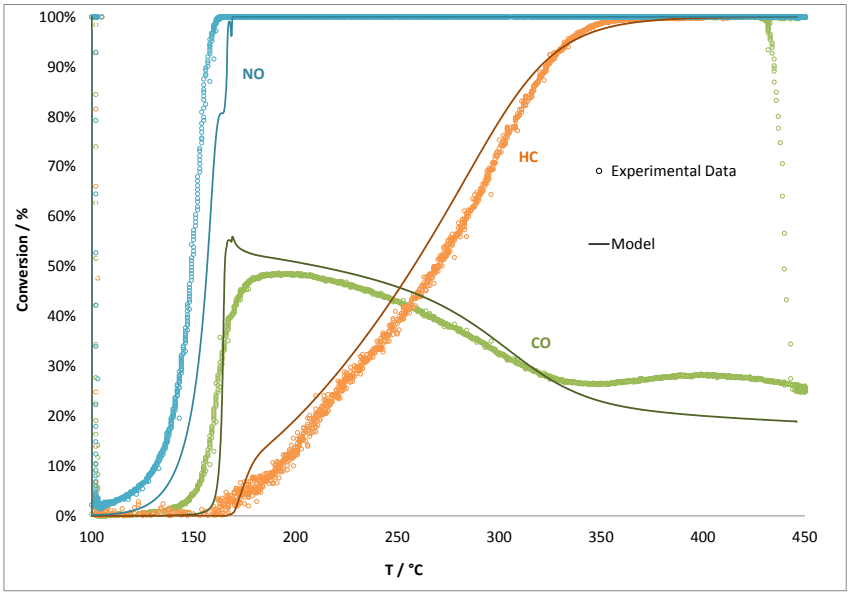

Figure 4.10: Model results for rich conditions (λ = 1.05) with the conversion of the three main pollutants in function of the temperature.

The conversion of the three main pollutants in function of the temperature are graphed in the Figure 4.10. The light-off temperatures for these pollutants, experimentally obtained and predicted by the model, are in Table 4.8.

Table 4.8: "Control" model and experimental light-off temperature results in rich conditions (λ = 1.05).

Components	$CO^{1)}$	HC	NO_x
Experimental Data	167 ℃	269 ℃	149 ℃
Model	164.8 ℃	257.9 ℃	156.6 ℃
Error	1.33 %	4.12 %	5.09 %

1) The light-off temperature for the CO was considered at a conversion of 40%, instead of the traditional 50%, since this value was never achieved by the experimental data.

The CPU time needed to compute these results was 9.006 seconds.

4.1.4 Model Validation

To validate the parameters obtained in the fitting work and to validate the model itself, two simulations were run outside the calibration points, to evaluate how the model would behave. As already mentioned, the air-to-fuel ratio has a great impact on the performance of the TWC and as so this was selected as the changing condition between simulations. Since the TWC is contemplated to work on two different conditions (rich and lean) we require two sets of experimental data to provide the physical validation to the simulations' results. The experimental data obtained in Tests 2 and 3 provide that validation (the conditions can be consulted in Table 3.2) since they have the exact same protocol as the tests used to tune the parameters with their only difference being the air-to-fuel ratio.

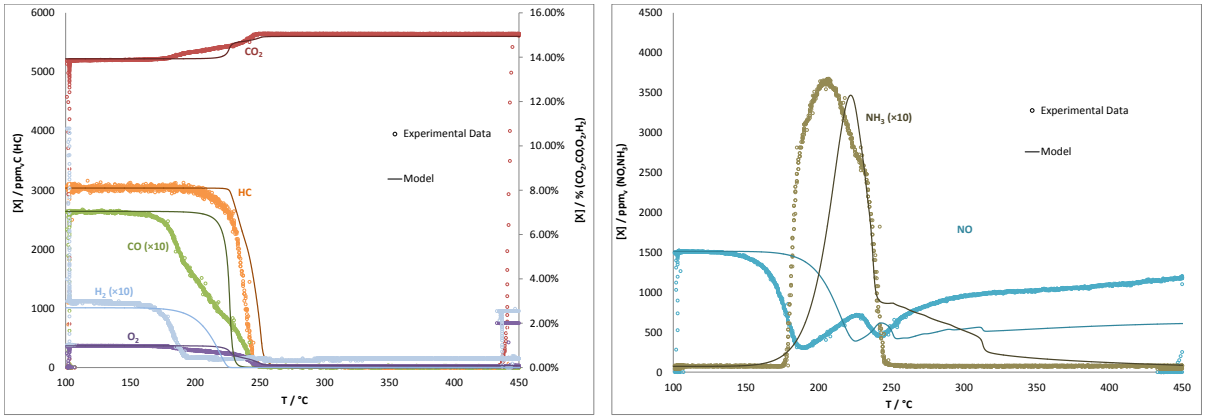

Figure 4.11: Model results for lean conditions (λ = 0.99) with the outlet concentrations of CO, HC, CO_2, O_2, H_2, NO and NH_3.

In Figure 4.11, the lean counterpart results (λ = 0.99) are graphed. It can be seen that the model results deviation from the experimental data is amplified in conditions closer to the stoichiometric. Specially the CO and NO model results have a shift to a higher light-off temperature than the experimental data shows. For the rich operation was not possible to perform the validation since the parameters tuned for this conditions did not translate well the phenomena closer to the stoichiometric point (λ = 1.01). It is important to highlight some points that can prompt these deviations shown in both operations. The al-

ready mentioned phenomena that the model does not take into account (viz. oxygen storage component reactions and N_2O formation), the natural fluctuations in a dynamical system that closer to stoichiometric conditions only enhances an hybrid operation instead of a clear rich or lean operation, and the lumped transport phenomena, are all probable reasons, for the model, not to translate exactly the phenomena seen at the catalyst in different conditions.

4.1.5 Kinetic Overview

One of the benefits of modelling is that some data are immediately available, whereas with experimental tests special measurements and calculations are required. Access to post-processed data such as reaction rates, products formation from each reaction pathway, phenomena's profile on the catalyst, etc. are easily available after a model simulation.

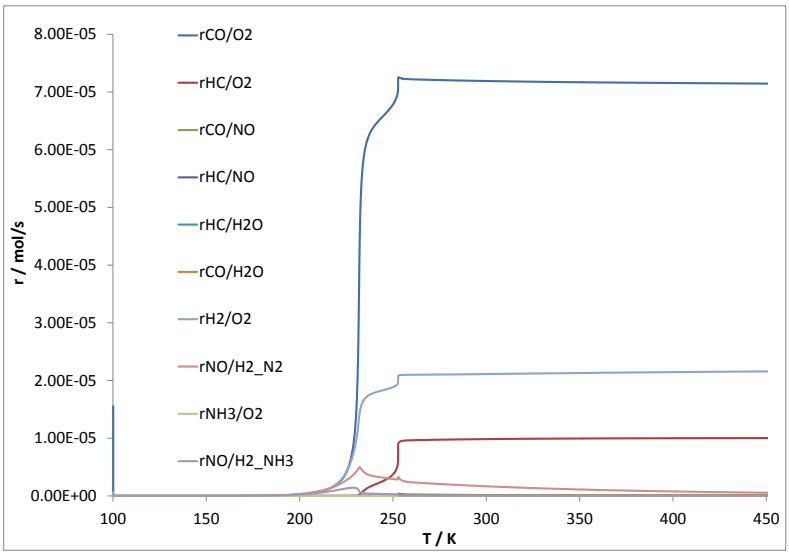

(a) Lean (λ = 0.95)

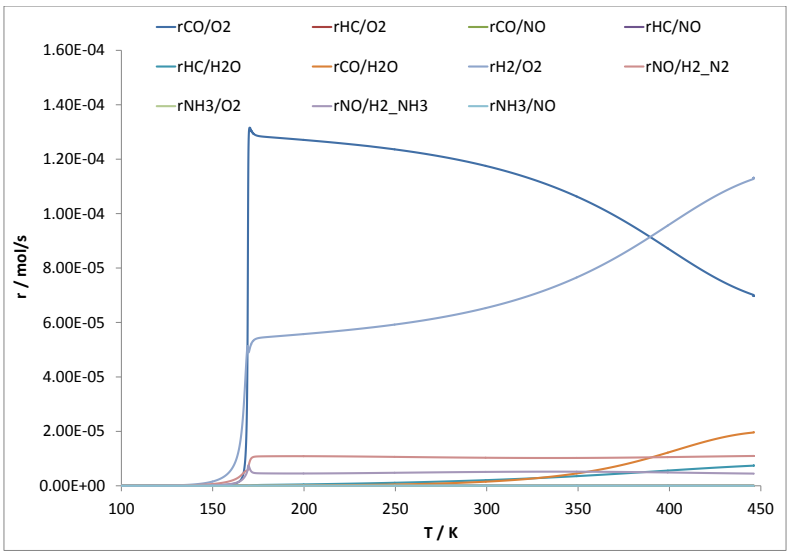

(b) Rich (λ = 1.05)

Figure 4.12: Reaction rates predicted by the model for both conditions.

The analysis of these data can indicate which things are or are not well described on the model. As so, a simple analysis will be done for the results of the simulations run with λ = 0.95 and λ = 1.05.

In Figure 4.12, the reaction rates are plotted as a function of the temperature. The rates in lean conditions are, apparently, quite straightforward. The carbon monoxide oxidation is the fastest reaction and the hydrogen's oxidation has second fastest rate. Around 230°C, when the hydrocarbons oxidation starts, it is possible to see an impact on the former two reaction rates. This is probable due to adsorption inhibition factors. The reduction reactions show a quite low impact as expected. The rates in rich conditions, however, show a bigger dynamics than the lean ones. At lower temperatures the fastest reaction rate is still the oxidation of CO but at higher temperatures, with the increase of H_2 (due to steam reforming and water-gas shift reactions), the oxidation of hydrogen increases. Since oxygen is the limiting reactant, there is a competition between both compounds, which leads to a decline on the CO oxidation rate at higher temperatures.

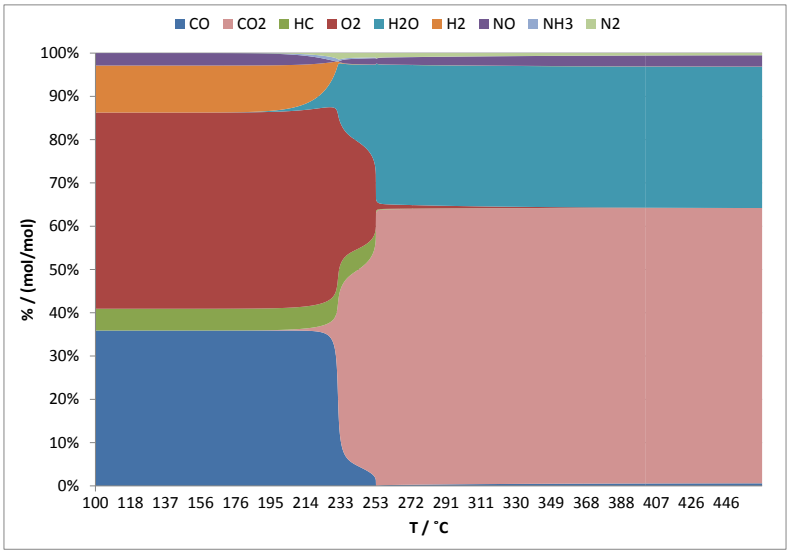

(a) Lean (λ = 0.95)

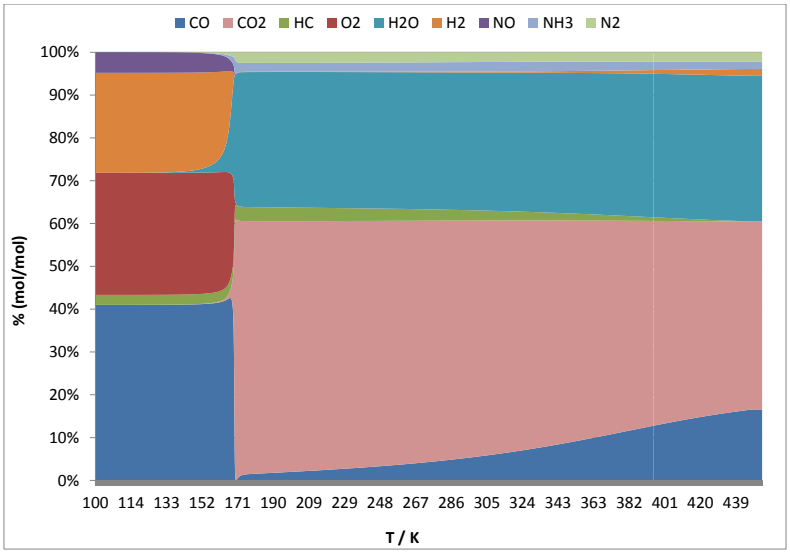

(b) Rich (λ = 1.05)

Figure 4.13: Relative species formation or consumption predict by the model for both conditions.

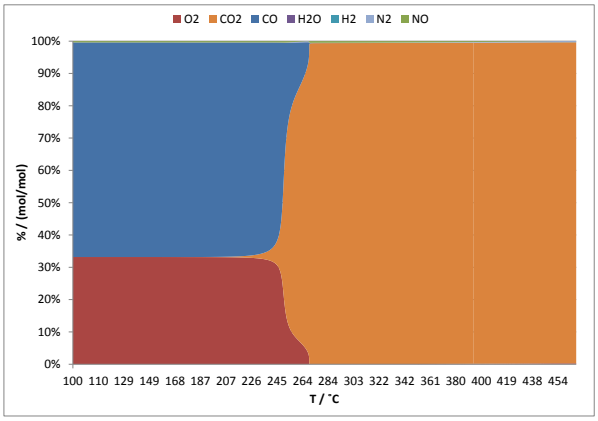

(a) CO oxidation - Lean (λ = 0.95)

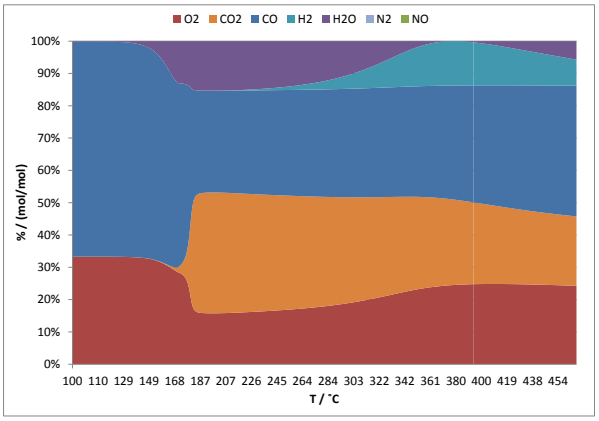

(b) CO oxidation - Rich (λ = 1.05)

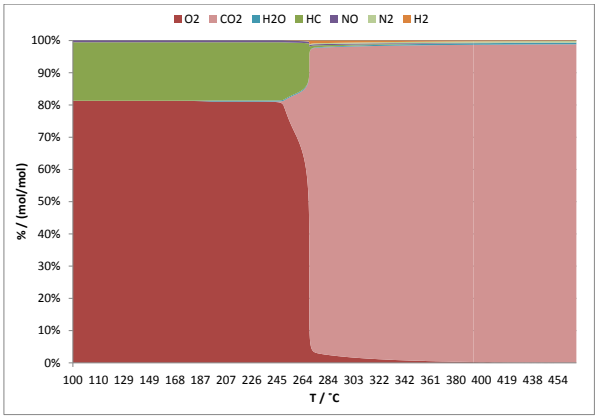

(c) HC oxidation - Lean (λ = 0.95)

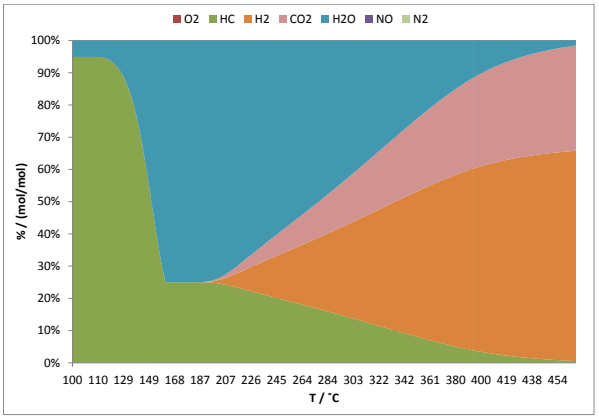

(d) HC oxidation - Rich (λ = 1.05)

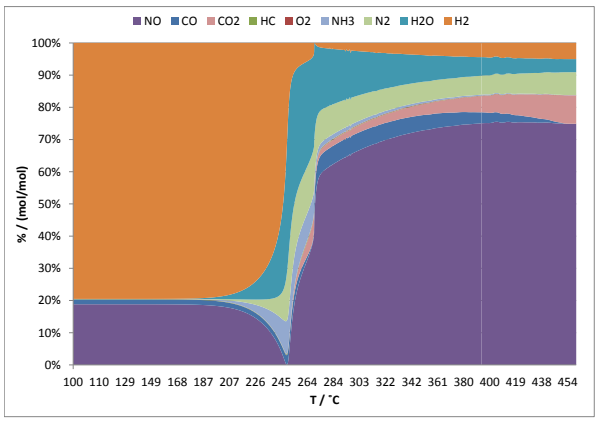

(e) NO reduction - Lean (λ = 0.95)

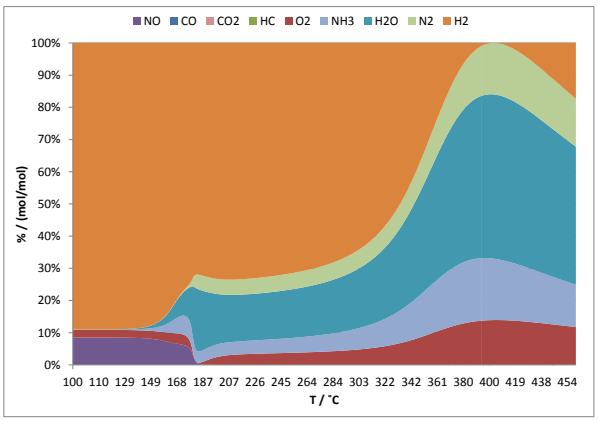

(f) NO reduction - Rich (λ = 1.05)

Figure 4.14: Relative species formation or consumption, discriminated for the three main pollutants, predicted by the model for both conditions.

In Figure 4.13, a relative composition of the chemical species, that are either consumed or formed by the reactions, are plotted in function of the temperature. Since what is displayed is relative compositions, fluctuations on the chemical elements' quantity, across temperatures, does not translate necessarily in an indication of formation or consumption. These plots only have an illustrative purpose, to show how the compositions of active compounds changes. Nonetheless, important information can still be extracted from them. Contrasting Figure 4.13(a) and Figure 4.13(b) several differences for the two operations

can be evidenced. Full conversion of CO and HC, above a certain temperature, is possible in lean operation, while in rich operation is not. The contrary can be seen for the NO case. In both operations the reaction that is enabled at lower temperatures is CO with H_2. While, on the lean operation, NH_3 is disabled by the competition with O_2, in rich operation, the formation of NH_3 is stably promoted above a certain temperature, because O_2 is the limiting reagent for the oxidation of H_2. Also, in rich conditions, as already hypothesised, here is one visual hint of the link between the oxidation of HC with the increase of relative quantity of CO, at higher temperatures.

In the Figure 4.14 the same type of graphic are shown, but this time with the 3 pollutants individually discriminated. The chemical elements shown, in each graphic, is only the active amount of each that interacts with the pollutant in concern. From comparing lean and rich operation results, for each pollutant, valuable and different information can be extracted from the Figure 4.14. For the CO, while in lean conditions, O_2 is the only responsible for the consumption of CO, in the rich case H_2O has an equivalent role as O_2. For HC case, in rich operation, is important to evoke the two hypothesis done in subsection 3.2.2 “Test 4 - Rich Conditions” and see that one of them is attested by these results and the other rejected. Here is clear that the HC only reacts with H_2O, and not with O_2 and that its impact on the fluctuations of CO originates from this source.

4.2 Approach 2: Washcoat Diffusion Modelling

Modelling washcoat diffusion phenomena was not possible with the current “control” model. These phenomena are needed to be modelled, if purpose is to help in the washcoat design. Through a model, a manufacturer can understand what is and what is not essential to achieve a good catalyst performance and, as so, he can optimize his production process to obtain it. To reach this goal a new model had to be built. The previous model will serve as a base of work for this following part.

It is self-explanatory that the “control” model used before is insufficient to describe the phenomena on the washcoat. Even if it has good overall prediction for the TWC performance, it gives no information on the phenomena that happens in the washcoat. This was what led to the necessity of building a new model. A single element was considered insufficient to obtain the goal set to achieve, and, as so, the change from a pseudo-homogeneous model to an heterogeneous one (with two elements to model each phase separately) was done. One element would model the bulk gas phase and the other the washcoat phase. The Figure 4.15 summarizes the phenomena on the channel. In the bulk gas phase both mass and energy exchange was considered in the axial direction with phenomena exchanges in the interface between both phases. In the washcoat phase only the radial direction was considered for both balances. The governing equations for both these elements are in Table 4.9 and Table 4.10. A 0D model was used for both phases. As a reminder, the boundary condition, for the washcoat governing equations (Table 4.10), is similar to the ones provided in section 2.2 “Catalyst Modelling”, where the diffusional flux, in the radial direction at the interface point, is equal to the outlet flux from the bulk gas phase ($\dot{m}_j|_{out}$ and $q|_{out}$).

To deeply validate this new model and its added functionalities there was not enough experimental

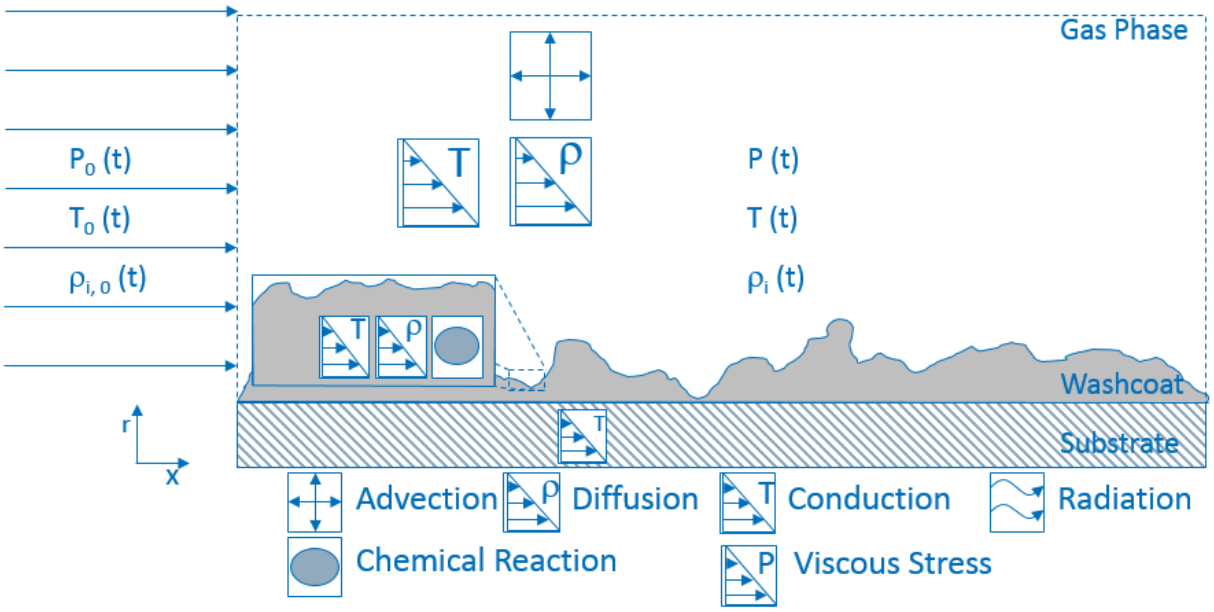

Figure 4.15: Summary of the phenomena considered for the washcoat diffusion treatment.

Table 4.9: Governing equations of the bulk gas phase for the washcoat diffusion treatment.

Bulk Gas Axial Flow Governing Equations	
Mass Balance	$\frac{\mathrm{d}m\cdot y_j}{\mathrm{d}t} = (y_j\cdot\dot{m})\Big\vert_{in} - (y_j\cdot\dot{m})\Big\vert_{out} + h_j^m\cdot S\cdot(\rho_j-\rho_j^w)$
Energy Balance	$m\cdot c_v\cdot\frac{\mathrm{d}T}{\mathrm{d}t} + m\cdot\sum_j\frac{\mathrm{d}y_j}{\mathrm{d}t}\cdot u_j + \frac{\mathrm{d}m}{\mathrm{d}t}\cdot\int c_v\cdot\mathrm{d}T = \sum_j m_j\cdot h_j + \frac{\mathrm{d}Q}{\mathrm{d}t} - P\cdot\frac{\mathrm{d}V}{\mathrm{d}t}$
Interface Gas-Solid Phases Governing Equations	
Mass Balance	$\dot{m}_j\Big\vert_{out} = h_j^m\cdot S\cdot(\rho_j-\rho_j^w)$
Energy Balance	$q\Big\vert_{out} = h^h\cdot S\cdot(T-T^w)$

Table 4.10: Governing equations of the washcoat phase for the washcoat diffusion treatment.

Washcoat Radial Flow Governing Equations	
Mass Balance	$\frac{\mathrm{d}\rho\cdot y_j}{\mathrm{d}t} = \frac{D_j}{r^n}\cdot\frac{r^{n+\frac{1}{2}}\cdot\rho_j^{n+1}-2\cdot r^n\cdot\rho_j^n+r^{n-\frac{1}{2}}\cdot\rho_j^{n-1}}{\Delta r^2} + \omega_j$
Energy Balance	$\rho_{app}\cdot c_p^s\cdot\frac{\mathrm{d}T}{\mathrm{d}t} = \frac{\kappa}{r^n}\cdot\frac{r^{n+\frac{1}{2}}\cdot T^{n+1}-2\cdot r^n\cdot T^n+r^{n-\frac{1}{2}}\cdot T^{n-1}}{\Delta r^2} - \sum_n\Delta H_n^r\cdot\omega_n$

data to support the simulation's results. As so, in a way to test if the model was working as expected, some small exams were done. First, the basic functionalities were tested, to see if they hold true to what the theory behind these type of problems (reaction/mass diffusion problem) stated. Even if the results had no physical meaning it enabled to see if the performance was in the range of expected and if it was theoretically sound. After this, it was tested how the model would predict the performance of the catalyst and compare it with the experimental data and, also, contrast it with the results obtained from the previous model. Following this, with the added functionality of this model, two scenarios were explored. One in which the catalyst had an homogeneous composition, and the active sites that promote oxidation

and reduction reactions were evenly distributed, through the entire length and thickness of the washcoat. The other scenario is admitting that an heterogeneous layer is present in the catalyst. As briefly specified in chapter 1 “Introduction”, double layer TWC are quite common in commercial applications and their optimal design can be something achieved by a type of model as the one present here. As so, this scenario was also considered and a simulation with two layers, one for the oxidation’s reactions and another for the reduction, was performed.

Due to time constrains, only simulations with lean operation conditions were run and no further calibration work, on the kinetic part, was performed.

4.2.1 Element Basic Functionality Tests

Due to the lack of experimental data to support the model, three basic tests were performed to verify its functionality. All the tests performed in this subsection were done with the only reaction considered being the oxidation of CO.

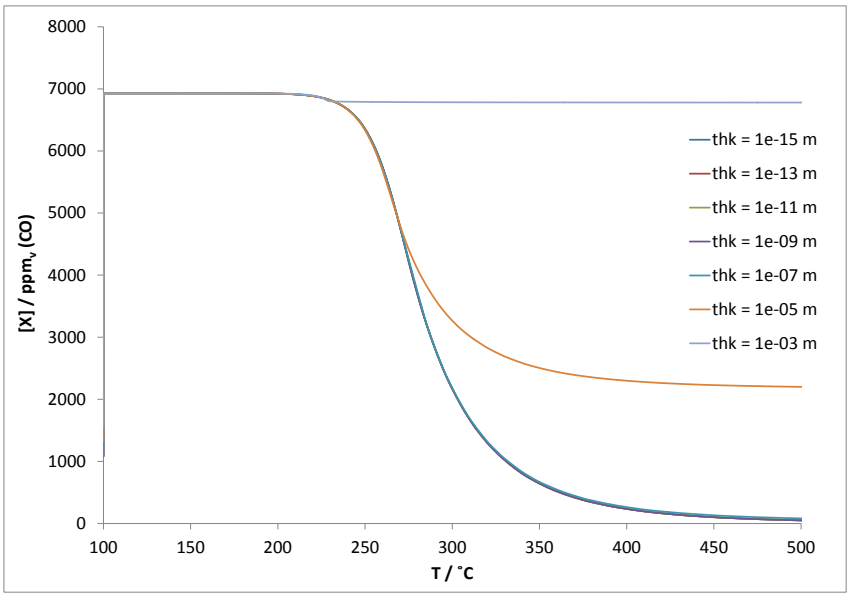

Figure 4.16: Impact of a thickness sensitivity analysis on the CO outlet concentration.

In Figure 4.16, a sensitivity analysis is performed to the thickness of the washcoat, using only one node to model the full washcoat. It is clear that the increase of thickness has an impact on the outlet concentration of CO. When the thickness is increased the mass and heat resistance increases with it. However the model has a limitation since the increase in the washcoat has no direct impact on the reaction rate. This should be addressed in future work. With a higher thickness of washcoat, it is visible that the amount of CO in the outlet is bigger and that the reaction is hindered by mass transfer resistance, which at least proves that the model reproduces (even if not with the perfect degree) the most basic feature of these type of problems.

In Figure 4.17, the impact of the washcoat discretization is shown. With 4 washcoat nodes, the reaction starts earlier than with 1 washcoat node. This is easily explained by the balance equations. In Table 4.10 it can be seen that if Δr is bigger, the mass flow inside the washcoat will be smaller which

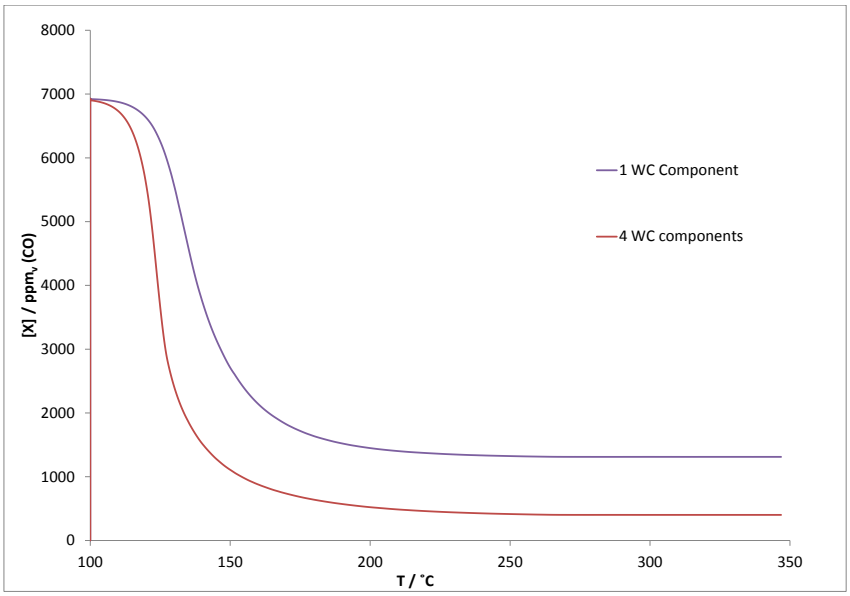

Figure 4.17: Impact of the discretization of the washcoat. Overall thickness: 5×10^{-6} m.

will result in a lowering of the reaction rate, due to the lack of species inside the washcoat node volume.

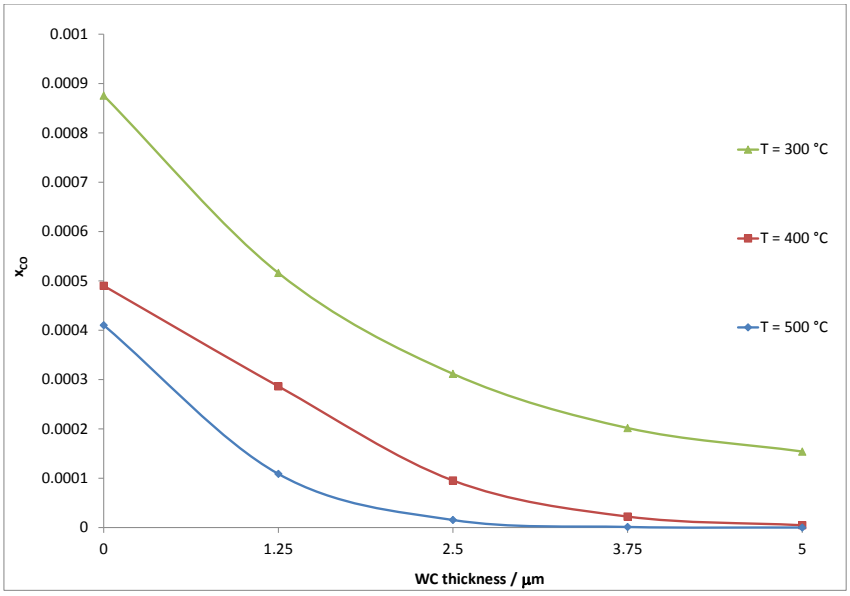

Figure 4.18: CO concentration profile along the waschoat thickness.

To analyse if the impact of the reaction rate in the diffusion problem was correct, the concentrations profile was analysed along the washcoat thickness, for three different temperatures as exposed in Figure 4.18. At lower temperatures, the reaction rate is slower and the full conversion is not possible due to the reaction's activation energy. However, at higher temperatures, one can see that the full conversion of the CO is no more hindered by thermodynamic reasons and instead is due to phenomena resistance, which constrains the access of CO to the catalyst sites in a way fast enough to enable full conversion. This type of assessment of the washcoat performance, is one clear feature that was impossible to have with the previous model, that, with this new one, is now available.

4.2.2 Homogeneous Layer

The model results for the homogeneous layer simulation are graphed against experimental data obtained in Test 1, in Figure 4.19 and Figure 4.20.

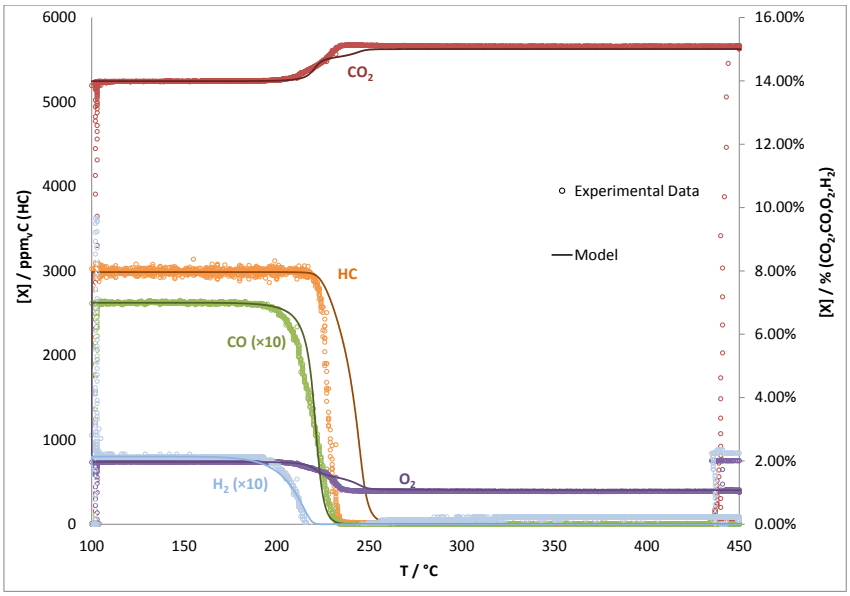

Figure 4.19: Homogeneous layer washcoat model results for lean conditions (λ = 0.95) with the outlet concentrations of CO, HC, CO_2, O_2 and H_2.

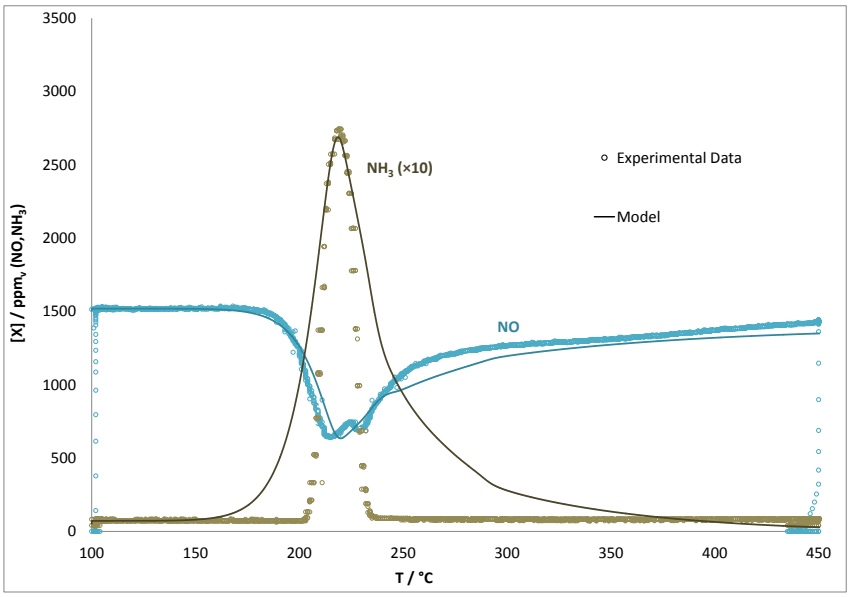

Figure 4.20: Washcoat diffusion model results for lean conditions (λ = 0.95) with the outlet concentrations of NO and NH_3.

The catalyst's outlet overall results seem to change little, with the added washcoat description. This indicates that, the lumped parameters used in the previous model represent a good compromise, in obtaining reliable results, while decreasing the complexity of the model. There are some slight changes, specially on the curves slopes and some sharp phenomena seem to have been smoothed with the model's upgrade. With some fitting work a smaller deviation would be seen, but, as a first try, these

results show a good promise.

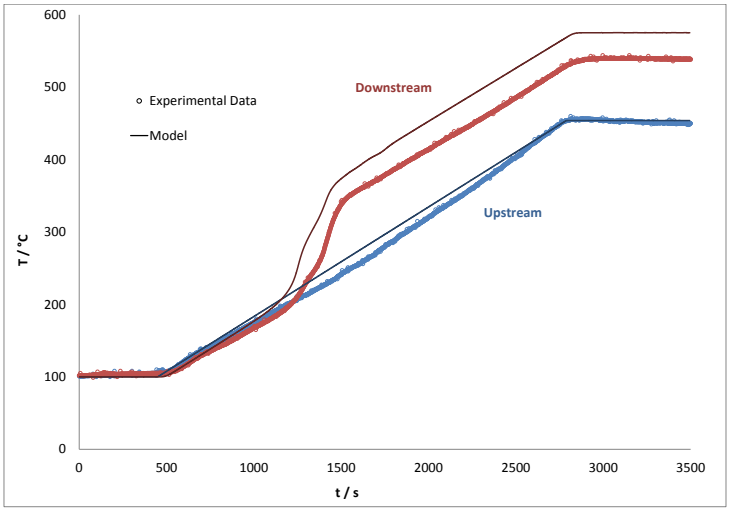

Figure 4.21: Homogeneous layer washcoat model results for lean conditions (λ = 0.95) with the temperature upstream and downstream of the catalyst.

In Figure 4.21 no relevant changes are perceived, in comparison with the temperature results obtained in the section 4.1 “Approach 1: Control Model”.

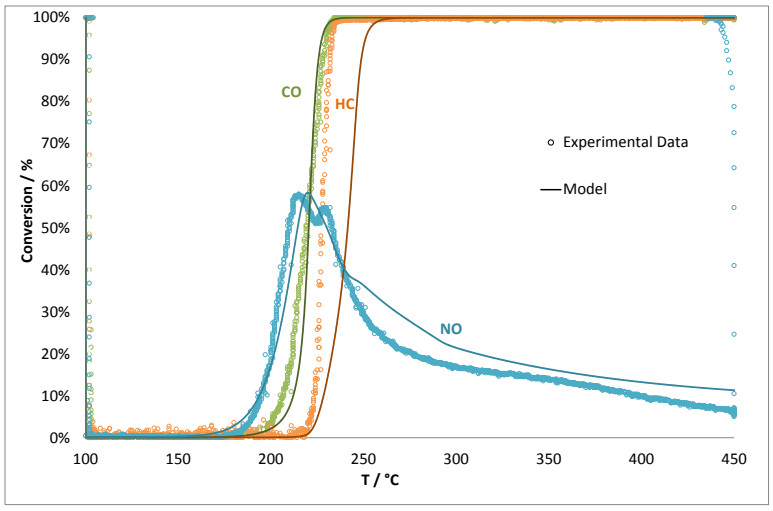

Figure 4.22: Homogeneous layer washcoat model results for lean conditions (λ = 0.95) with the conversion of the three main pollutants in function of the temperature.

The conversion of the three main pollutants in function of the temperature are graphed in the Figure 4.22. The light-off temperatures for these pollutants, experimentally obtained and predicted by the model, are in Table 4.11.

The CPU time needed to compute these results was 50.932 seconds.

Table 4.11: Homogeneous layer washcoat model and experimental light-off temperature results in lean conditions (λ = 0.95).

Components	CO	HC	NO_x
Experimental Data	219 ℃	227 ℃	210 ℃
Model	220.4 ℃	241.4 ℃	214.3 ℃
Error	0.64 %	6.36 %	2.03 %

4.2.3 Double Layer

An heterogeneous layer was also considered with a double layer set-up. The design proposed was with a layer, where the oxidation reactions were promoted, closer to the bulk gas phase, and with another layer closer to the substrate wall, where the reduction reactions where to happen. The summary of this design is given in Table 4.12.

Table 4.12: Oxidation and reduction layer reaction's summary.

Oxidation Layer Reactions
$CO + 0.5O_2 \longrightarrow CO_2$
$C_3H_6 + 4.5O_2 \longrightarrow 3CO_2 + 3H_2O$
$C_3H_6 + 3\,H_2O \longrightarrow 3\,CO + 6\,H_2$
$CO + H_2O \rightleftharpoons CO_2 + H_2$
$H_2 + 0.5O_2 \longrightarrow H_2O$
Reduction Layer Reactions
$CO + NO \longrightarrow CO_2 + 0.5N_2$
$C_3H_6 + 9\,NO \longrightarrow 3\,CO_2 + 3\,H_2O + 4.5\,N_2$
$NO + H_2 \longrightarrow 0.5\,N_2 + H_2O$
$NH_3 + 1.25O_2 \longrightarrow NO + 1.5\,H_2O$
$NO + 2.5\,H_2 \longrightarrow NH_3 + H_2O$
$NH_3 + 1.5\,NO \longrightarrow 1.25\,N_2 + 1.5\,H_2O$

The catalyst outlet results for the heterogeneous layer simulation are graphed against experimental data obtained in Test 1, in Figure 4.23 and Figure 4.24.

No particular differences are visualized in Figure 4.23. On the other hand, is quite curious the profile that arose in the Figure 4.24. With a double layer simulation one can see the rise of the NH_3 formation at a certain point, even though the global formation of NO seems to diminish in comparison with the homogeneous layer simulation. The probable explanation for that is, since the oxidation layer is considered to be the closest to the bulk gas phase, the CO and HC fully oxide first in this layer, due to the excess of oxygen in lean operation, and never reach the layer where the reduction reactions occur. Since no CO and HC reach the reduction layer, this leads to a diminution of the overall NO that reduces and, since more NO is available to react with H_2, it is possible to visualize little rise in the selectivity of the NH_3 formation. From Figure 4.14(e) one can support this theory with the fact that the existence of

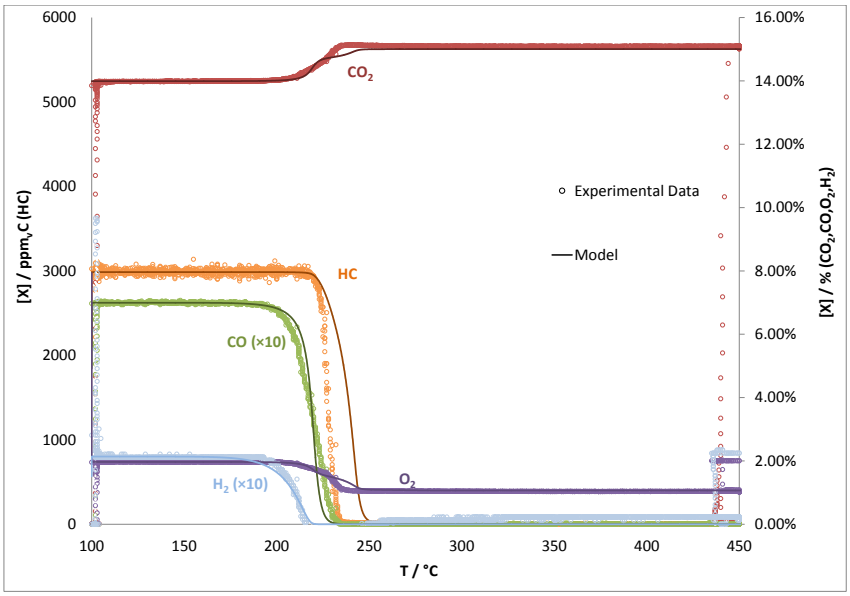

Figure 4.23: Double layer washcoat model results for lean conditions (λ = 0.95) with the outlet concentrations of CO, HC, CO_2, O_2 and H_2.

CO_2 formation suggests that, in lean operation, exists an impact of CO and HC on the reduction of NO. As so, if this impact is diminished, as in this particular scenario, the amount of NO reduced will suffer an impact.

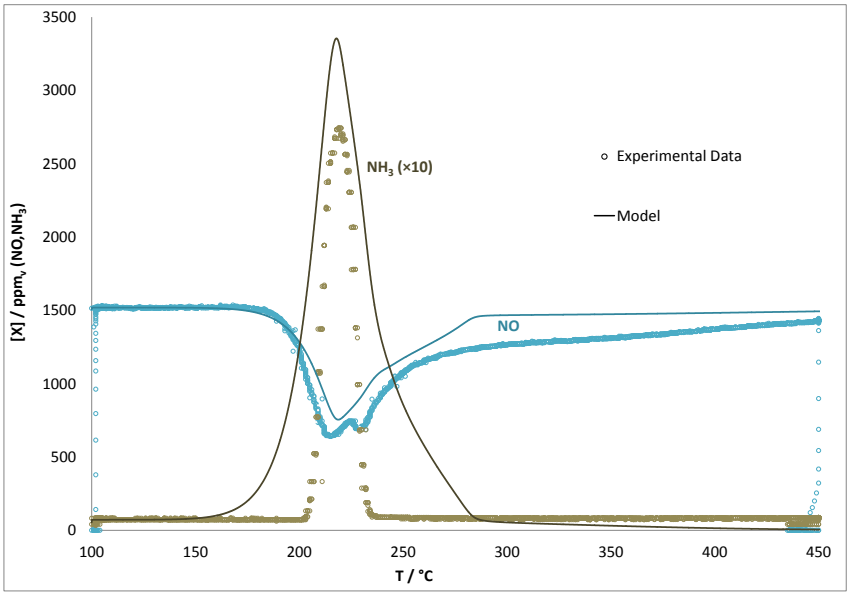

Figure 4.24: Double layer washcoat model results for lean conditions (λ = 0.95) with the outlet concentrations of NO and NH_3.

In Figure 4.25 no relevant changes are perceived.

The conversion of the three main pollutants in function of the temperature are graphed in the Figure 4.26. The light-off temperatures for these pollutants, experimentally obtained and predicted by the model, are in Table 4.13.

The CPU time needed to compute these results was 44.376 seconds.

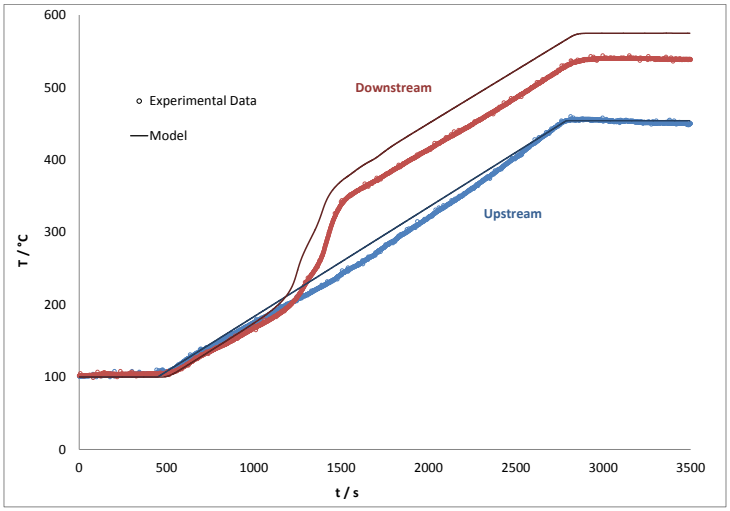

Figure 4.25: Double layer washcoat model results for lean conditions (λ = 0.95) with the temperature upstream and downstream of the catalyst.

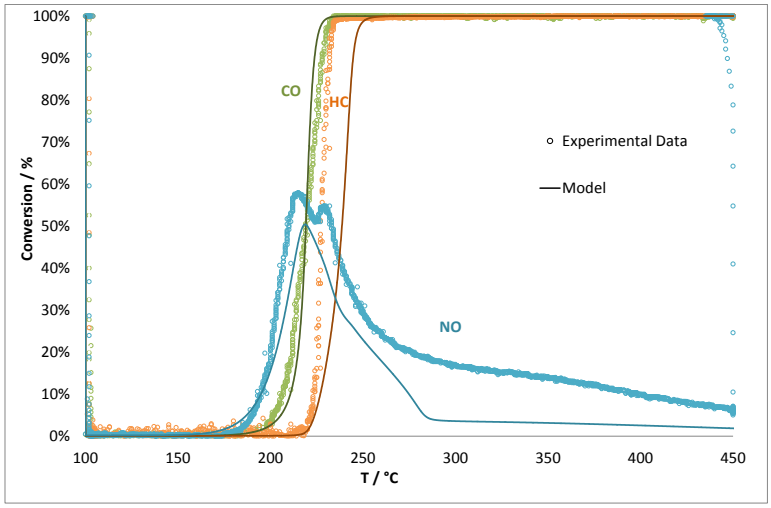

Figure 4.26: Double layer washcoat model results results for lean conditions (λ = 0.95) with the conversion of the three main pollutants in function of the temperature.

Table 4.13: Double layer washcoat model and experimental light-off temperature results in lean conditions (λ = 0.95).

Components	CO	HC	NO_x
Experimental Data	219 ℃	227 ℃	210 ℃
Model	219.1 ℃	238.6 ℃	215.7 ℃
Error	0.05 %	5.09 %	2.72 %

Chapter 5

Conclusions and Future Work

5.1 Conclusions

The aim of this work was to provide insight into the phenomena of monolithic catalysts, specially the particular case of the three-way catalyst, and translate some of that phenomena into a mathematical model. The work was divided into two different approaches, one more directed to control applications and another with more usefulness to design applications.

Regarding the model designed for control applications, the main work was to improve the kinetic scheme, that already existed, through the addition of the NH_3 reactions. The overall result shows that, with some basic tuning work, the model can give a well adjusted response. However, the validity of the model outside the tuning point was not proved in all conditions. The computational time was also satisfactory, due to the low time required, and the fact that it was needed similar times to simulate both conditions (rich and lean) proves that the model can cover several range of conditions, with a satisfactory result and have reliable computational time, which was desired for “control” applications and real time simulation.

The model, conceived for the washcoats’ design, was mainly focused on the mass and heat diffusion treatment. This approach is different from what is usually performed, in this type of studies, since it is a commonplace to consider a steady-state scenario between the reaction rate and the mass diffusion rate. The approach developed in this work differs from it since it takes into account the transient operation. Due to the lack of experimental data, the validation of this model was not possible and was left undone. However, the model displayed the basic functionalities for the diffusion/reaction problems and, when calibrated, it was able to predict the overall performance of the TWC. Taking a look into the computational times, the added complexity is reflected by resulting in a computational time 5 times bigger than the first model developed.

5.2 Future Work

The problematic present at this work is a quite actual one and a lot of research is being conducted to achieve a future lean burn gasoline vehicle. As so, some further work to enhance and capitalise the one performed here is suggested.

The addition of N_2O kinetic pathway is an important feature to be taken into account, in the reaction scheme, since it has been proved that N_2O formation is propitiated in cyclic lean and rich operations, which is nowadays being considered as a viable way to operate SIDI engines. Also, ceria reactions need to be coupled with this new kinetic scheme. With these modifications and additions to the kinetic scheme, possibly, the validation of the model outside the tuning point will achieve a better result than the one obtained in this work.

One improvement that can be performed, specifically in the “control” model, is the computational effort. Instead of a macrokinetic model, it can be used the empirical data to predict the light-off temperatures of the pollutants and use a switch to calculate the reactions’ products. Through this mechanism, a good deal of calculations can be neglected and the computational effort reduced.

Concerning specifically the model of the washcoat diffusion, the kinetic treatment used was exactly the same obtained for the “control” model, which can be lacklustre, and some more detailed analysis may be performed. Specially regarding the inhibition of competitive adsorption, since some studies date back from the 70s and are still in use. Another important feature that needs to be improved is the spatial discretization of the washcoat, as no studies were performed to estimate the appropriate radial-step that leads to having a good phenomena description but does not compromises too much the computational effort. An alternative interesting approach to the diffusion/reaction problem and one not performed during this work, but that was considered during its development, is the modelling of the mass resistance of the species to reach the macro, meso and micro volumes of the washcoat. This would replace the the spatial description of the washcoat performed here. This different approach might give an unique and useful insight regarding the phenomena in the washcoat, that might be valuable for producers to optimize their process.

Bibliography

[1] R. M. Heck, R. J. Farrauto, and S. T. Gulati. *Catalytic Air Pollution Control: Commercial Technology*. John Wiley & Sons, 3rd edition, 2009.

[2] J. B. Heywood. *Internal Combustion Engine Fundamentals*. McGraw-Hill, Inc., 3rd edition, 1988.

[3] *Railway Handbook 2012 (Energy Consumption and CO_2 Emissions)*. International Energy Agency & International Union of Railways, 2012.

[4] J. Hochmuth, K. Wassermann, and R. Farrauto. 7.19 - Car Exhaust Cleaning. In K. Poeppelmeier and J. Reedijk, editors, *Comprehensive Inorganic Chemistry II (Second Edition)*, pages 505 – 523. Elsevier, 2nd edition, 2013.

[5] *Worldwide Emissions Standards (Passenger Cars & Light Duty Vehicles)*. Delphi Automotive PLC, 2015/2016.

[6] `https://www.dieselnet.com`, . Accessed November 2, 2015.

[7] V. Y. Prikhodko, J. E. Parks, J. A. Pihl, and T. J. Toops. Ammonia generation over TWC for passive SCR NO_x control for lean gasoline engines. *SAE International Journal of Engines*, 7(2014-01-1505):1235–1243, 2014.

[8] C. Depcik and D. Assanis. One-dimensional automotive catalyst modeling. *Progress in Energy and Combustion Science*, 31(4):308–369, 2005.

[9] K. Ramanathan, C. S. Sharma, and C. H. Kim. Global kinetics for ammonia formation and oxidation reactions in a commercial three-way catalyst. *Industrial & Engineering Chemistry Research*, 51(3): 1198–1208, 2012.

[10] J. Wang, Y. Ji, G. Jacobs, S. Jones, D. J. Kim, and M. Crocker. Effect of aging on NO_x reduction in coupled LNT–SCR systems. *Applied Catalysis B: Environmental*, 148:51–61, 2014.

[11] Y. Ji, V. Easterling, U. Graham, C. Fisk, M. Crocker, and J.-S. Choi. Effect of aging on the NO_x storage and regeneration characteristics of fully formulated lean NO_x trap catalysts. *Applied Catalysis B: Environmental*, 103(3):413–427, 2011.

[12] C. D. DiGiulio, J. A. Pihl, J. E. Parks II, M. D. Amiridis, and T. J. Toops. Passive-ammonia selective catalytic reduction (SCR): Understanding NH_3 formation over close-coupled three way catalysts (TWC). *Catalysis Today*, 231:33–45, 2014.

[13] S. Y. Joshi, M. P. Harold, and V. Balakotaiah. Low-dimensional models for real time simulations of catalytic monoliths. *AIChE journal*, 55(7):1771–1783, 2009.

[14] A. K. Sharma, E. Birgersson, and M. Vynnycky. Towards computationally-efficient modeling of transport phenomena in three-dimensional monolithic channels. *Applied Mathematics and Computation*, 254:392–407, 2015.

[15] S. B. Kang, H. J. Kwon, I.-S. Nam, Y. I. Song, and S. H. Oh. Activity function for describing alteration of three-way catalyst performance over palladium-only three-way catalysts by catalyst mileage. *Industrial & Engineering Chemistry Research*, 50(9):5499–5509, 2011.

[16] J. H. Baik, H. J. Kwon, Y. T. Kwon, I.-S. Nam, and S. H. Oh. Effects of catalyst aging on the activity and selectivity of commercial three-way catalysts. *Topics in Catalysis*, 42(1-4):337–340, 2007.

[17] T. C. Watling and J. P. Cox. Factors affecting three-way catalyst light-off: A simulation study. *SAE International Journal of Engines*, 7(2014-01-1564):1311–1325, 2014.

[18] M. Braja Gopal et al. Structural, redox and catalytic chemistry of ceria based materials. *Bulletin of the Catalysis Society of India*, 2:122–134, 2003.

[19] S. Salasc, M. Skoglundh, and E. Fridell. A comparison between Pt and Pd in NO_x storage catalysts. *Applied Catalysis B: Environmental*, 36(2):145–160, 2002.

[20] Z.-s. Zhang, B.-b. Chen, X.-k. Wang, L. Xu, C. Au, C. Shi, and M. Crocker. NO_x storage and reduction properties of model manganese-based lean NO_x trap catalysts. *Applied Catalysis B: Environmental*, 165:232–244, 2015.

[21] J. Gong and C. Rutland. Three way catalyst modeling with ammonia and nitrous oxide kinetics for a lean burn spark ignition direct injection (SIDI) gasoline engine. Technical report, SAE Technical Paper, 2013.

[22] C. H. Kim, K. Perry, M. Viola, W. Li, and K. Narayanaswamy. Three-way catalyst design for urealess passive ammonia SCR: Lean-burn SIDI aftertreatment system. Technical report, SAE Technical Paper, 2011.

[23] W. Li, K. L. Perry, K. Narayanaswamy, C. H. Kim, and P. Najt. Passive ammonia SCR system for lean-burn SIDI engines. Technical report, SAE Technical Paper, 2010.

[24] M. Iwasaki and H. Shinjoh. A comparative study of ”standard”, ”fast” and ”NO_2” SCR reactions over Fe/zeolite catalyst. *Applied Catalysis A: General*, 390(1):71–77, 2010.

[25] J. A. Pihl, J. E. Parks, C. S. Daw, and T. W. Root. Product selectivity during regeneration of lean NO_x trap catalysts. Technical report, SAE Technical Paper, 2006.

[26] R. D. Clayton, M. P. Harold, and V. Balakotaiah. NO_x storage and reduction with H_2 on $Pt/BaO/Al_2O_3$ monolith: Spatio-temporal resolution of product distribution. *Applied Catalysis B: Environmental*, 84(3):616–630, 2008.

[27] A. Lindholm, N. W. Currier, A. Yezerets, and L. Olsson. A kinetic study of NO_x reduction over Pt/SiO_2 model catalysts with hydrogen as the reducing agent. *Topics in Catalysis*, 42(1-4):83–89, 2007.

[28] R. Hayes and S. Kolaczkowski. *Introduction to Catalytic Combustion*. Taylor & Francis, 1998.

[29] N. Mladenov, J. Koop, S. Tischer, and O. Deutschmann. Modeling of transport and chemistry in channel flows of automotive catalytic converters. *Chemical Engineering Science*, 65(2):812–826, 2010.

[30] S. Y. Joshi, M. P. Harold, and V. Balakotaiah. On the use of internal mass transfer coefficients in modeling of diffusion and reaction in catalytic monoliths. *Chemical Engineering Science*, 64(23): 4976–4991, 2009.

[31] K. Ramanathan and C. S. Sharma. Kinetic parameters estimation for three way catalyst modeling. *Industrial & Engineering Chemistry Research*, 50(17):9960–9979, 2011.

[32] R. Holder, M. Bollig, D. Anderson, and J. Hochmuth. A discussion on transport phenomena and three-way kinetics of monolithic converters. *Chemical Engineering Science*, 61(24):8010–8027, 2006.

[33] L. Mukadi and R. Hayes. Modelling the three-way catalytic converter with mechanistic kinetics using the Newton–Krylov method on a parallel computer. *Computers & chemical engineering*, 26 (3):439–455, 2002.

[34] H. J. Kwon, J. H. Baik, Y. T. Kwon, I.-S. Nam, and S. H. Oh. Detailed reaction kinetics over commercial three-way catalysts. *Chemical Engineering Science*, 62(18):5042–5047, 2007.

[35] L.-P. Ma, H.-J. Bart, P. Ning, A. Zhang, G. Wu, and Z. Zengzang. Kinetic study of three-way catalyst of automotive exhaust gas: Modeling and application. *Chemical Engineering Journal*, 155(1):241–247, 2009.

[36] N. Matthess, D. Schweich, B. Martin, and F. Castagna. From light-off curves to kinetic rate expressions for three-way catalysts. *Topics in Catalysis*, 16(1-4):119–124, 2001.

[37] S. E. Voltz, C. R. Morgan, D. Liederman, and S. M. Jacob. Kinetic study of carbon monoxide and propylene oxidation on platinum catalysts. *Industrial & Engineering Chemistry Product Research and Development*, 12(4):294–301, 1973.

[38] B. Subramaniam and A. Varma. Reaction kinetics on a commercial three-way catalyst: the carbon monoxide-nitrogen monoxide-oxygen-water system. *Industrial & engineering chemistry product research and development*, 24(4):512–516, 1985.

[39] G. Koltsakis, P. Konstantinidis, and A. Stamatelos. Development and application range of mathematical models for 3-way catalytic converters. *Applied Catalysis B: Environmental*, 12(2):161–191, 1997.

[40] P. Kočí, M. Kubíček, and M. Marek. Modeling of three-way-catalyst monolith converters with microkinetics and diffusion in the washcoat. *Industrial & Engineering Chemistry Research*, 43(16): 4503–4510, 2004.

[41] `https://www.grc.nasa.gov/www/BGH/nseqs.html`, . Accessed November 2, 2015.

[42] B. W. Riyandwita and M.-W. Bae. Three-dimensional simulation with porous medium as the washcoat layer for an SCR monolith reactor. Technical report, SAE Technical Paper, 2011.

[43] `https://www.grc.nasa.gov/www/k-12/airplane/eulereqs.html`, . Accessed November 2, 2015.

[44] V. Balakotaiah and R. R. Ratnakar. On the use of transfer and dispersion coefficient concepts in low-dimensional diffusion–convection-reaction models. *Chemical Engineering Research and Design*, 88(3):342–361, 2010.

[45] E. J. Bissett. An asymptotic solution for washcoat pore diffusion in catalytic monoliths. *Emission Control Science and Technology*, 1(1):3–16, 2015.

[46] R. Hayes and S. Kolaczkowski. A study of Nusselt and Sherwood numbers in a monolith reactor. *Catalysis Today*, 47(1):295–303, 1999.

[47] F. Lemos, J. M. Lopes, and F. R. Ribeiro. *Reactores Químicos*. IST Press, 2nd edition, 2013.

[48] N. Rankovic, A. Nicolle, and P. Da Costa. Detailed kinetic modeling study of NO_x oxidation and storage and their interactions over $Pt/Ba/Al_2O_3$ monolith catalysts. *The Journal of Physical Chemistry C*, 114(15):7102–7111, 2010.

Appendix A

Experimental Results for Tests 5, 6 and 7

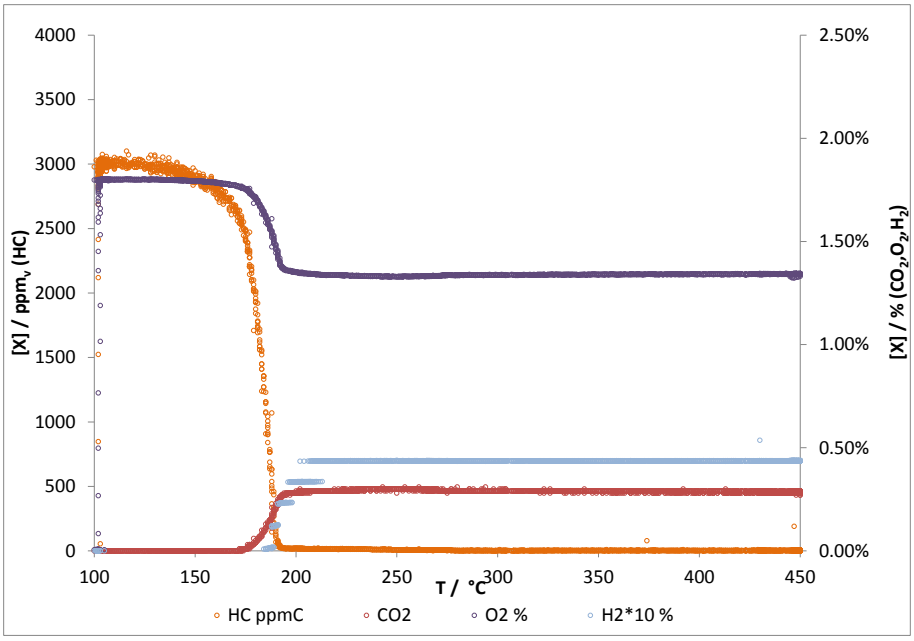

Figure A.1: Experimental results of Test 5 with the outlet concentrations of HC, CO_2, O_2 and H_2.

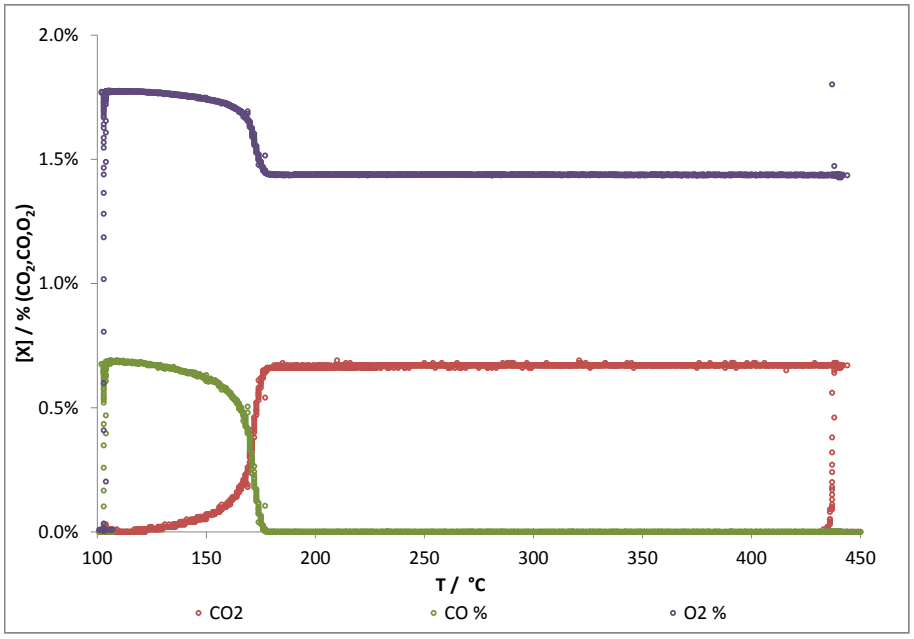

Figure A.2: Experimental results of Test 6 with the outlet concentrations of CO, CO_2 and O_2.

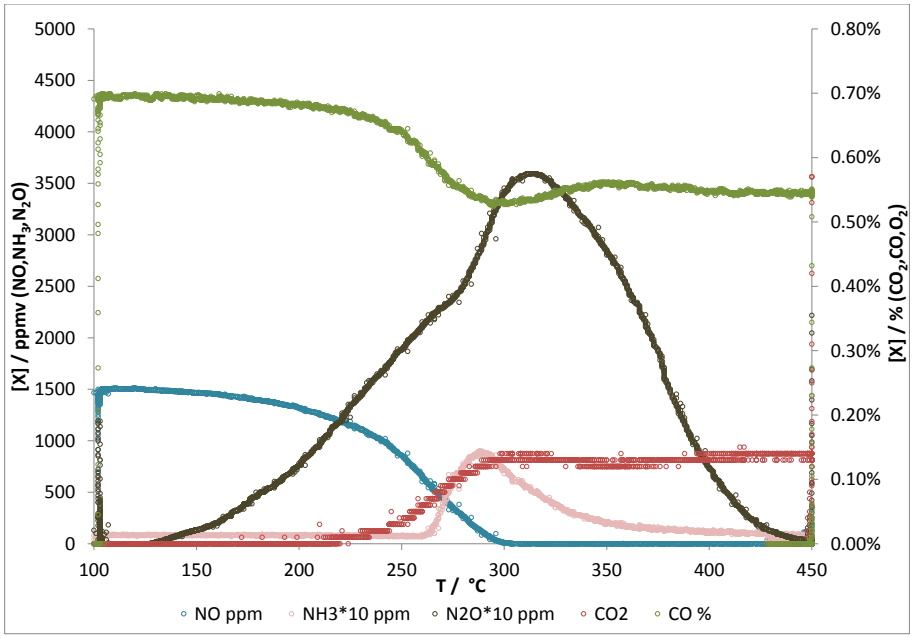

Figure A.3: Experimental results of Test 7 with the outlet concentrations of NO, CO, CO_2, NH_3 and N_2O.